EPISODIC SIERRAN ARC MAGMATISM EXPRESSED IN MESOZOIC ROCKS OF THE MOUNT MORRISON PENDANT, EAST-CENTRAL SIERRA NEVADA, CALIFORNIA

by Derek M. Field

A thesis

submitted in partial fulfillment

of the requirements for the degree of

Master of Science in Geology

Northern Arizona University

May 2018

Nancy R. Riggs, Chair

Andrew P. Barth, Co-chair

Michael H. Ort, Co-chair

EPISODIC SIERRAN ARC MAGMATISM EXPRESSED IN
MESOZOIC ROCKS OF THE MOUNT MORRISON PENDANT,
EAST-CENTRAL SIERRA NEVADA, CALIFORNIA

ABSTRACT

The Mount Morrison pendant contains approximately 40 km^2 of exposed Mesozoic volcanic rocks. Triassic strata include a 1.2-km-thick intra-caldera ignimbrite; 1.5 km of dacitic rocks including a large hypabyssal sill, tuff, breccia, and sedimentary rocks; and two local deposits of subaqueous volcanic breccia. Jurassic rocks include 1.3 km of intercalated dacitic to rhyolitic tuff and breccia that are highly deformed. The Cretaceous section contains subaqueous, finely laminated sedimentary strata interlayered with rhyolite tuffs and flows, and a >400-m-thick mass of andesite porphyry. U-Pb geochronology shows that these rocks were emplaced during periods of high magmatic flux beneath the Sierran arc prior to juxtaposition by faulting. The ages of Triassic rocks range from 217 to 213 ± 2 Ma, which corresponds to the first pulse of Sierran volcanism. Rhyolite tuff in the Jurassic block was dated at 170 ± 2 Ma and thus corresponds to the second high-flux episode. Volcanic rocks of the Cretaceous block were dated at 101 ± 2 Ma, and so were sourced from the final magmatic pulse. Six major volcanic units have geochemical signatures of arc magmas sourced from evolved crust. Structural patterns show that Triassic and Jurassic rocks underwent at least one period of deformation prior to emplacement of Cretaceous rocks, providing evidence for crustal contraction between the Middle Jurassic and latest Early Cretaceous. All rocks were contact metamorphosed by Cretaceous plutons emplaced during the final pulse of arc magmatism, and then likely translated by the Sierra Crest shear

zone. Dextral shear indicators are consistent with Sierra Crest shear zone transpressional tectonics. The Mesozoic Mount Morrison pendant records the major stages of development of the Sierran arc as it was built on the continental crust of southwest Laurentia, offering insight into eruption style, paleogeography, and arc tempo.

© Derek Field, 2018

TABLE OF CONTENTS

LIST OF FIGURES ……. xii

LIST OF TABLES ……...…….. xiii

ACKNOWLEDGEMENTS ……...……..... xiv

1. INTRODUCTION ..…….. 1

2. BACKGROUND …..…….. 5

2.1 GEOLOGIC HISTORY ……... 5

2.2 METHODS ….…… 7

3. ROCK DESCRIPTIONS ……... 8

3.1 TRIASSIC ROCKS ……. 8

3.1.1 BRECCIA OF MAMMOTH ROCK …….. 10

3.1.2 DACITE OF ARROWHEAD LAKE ……..... 21

3.1.3 TUFF OF SKELTON LAKE …….…. 33

3.1.4 BRECCIA OF PIKA LAKE ……... 37

3.2 JURASSIC ROCKS ……... 39

3.3 CRETACEOUS ROCKS ……... 42

3.3.1 RHYOLITE OF PURPLE LAKE ……... 44

3.3.2 ANDESITE OF MAMMOTH CREST ……... 45

3.3.3 DUCK LAKE SUCCESSION …… 47

4. GEOCHRONOLOGY …… 51

4.1 GEOCHRONOLOGY OF TRIASSIC ROCKS …… 52

4.2 GEOCHRONOLOGY OF JURASSIC ROCKS …….…….. 56

4.3 GEOCHRONOLOGY OF CRETACEOUS ROCKS …… 57

5. GEOCHEMISTRY …….. 59

5.1 GEOCHEMISTRY OF TRIASSIC ROCKS ……..…… 60

5.2 GEOCHEMISTRY OF JURASSIC ROCKS …… 61

5.3 GEOCHEMISTRY OF CRETACEOUS ROCKS …… 61

6. STRUCTURAL GEOLOGY ……... 68

7. DISCUSSION & INTERPRETATIONS ……. 74

7.1 FACIES INTERPRETATIONS …… 75

7.2 GEOCHEMISTRY INTERPRETATIONS ……..….. 79

7.3 STRUCTURAL INTERPRETATIONS ……..…... 84

7.4 IMPLICATIONS FOR SIERRAN ARC TEMPO ……..…… 86

8. CONCLUSIONS ……..……... 88

REFERENCES …… 90

APPENDIX A ……. 95

APPENDIX B ……..…….. 113

LIST OF FIGURES

Figure 1: Generalized geologic map of the east-central Sierra Nevada showing the location of Mesozoic volcanic rocks in the Ritter Range pendant (RRP), Saddlebag Lake pendant (SLP), and Mount Morrison pendant (MMP). Modified from Barth et al. (2011).

Figure 2: Geologic map of Mesozoic volcanic rocks of the Mount Morrison pendant and environs. Mesozoic rocks and their bounding contacts are shown according to mapping done in this study. Intrusive contacts between Paleozoic sedimentary rocks and Cretaceous granites are based on Rinehart and Ross (1964). Samples were used for both U-Pb zircon geochronology and whole-rock bulk geochemistry analyses. Sample abbreviations: MRB = breccia of Mammoth Rock, ALD = dacite of Arrowhead Lake, SLT = tuff of Skelton Lake, PLB = breccia of Pika Lake, DLT = tuff of Deer Lakes, PLR = rhyolite of Purple Lake, MCA = andesite of Mammoth Crest.

Figure 3: Schematic cross-section of Mesozoic rocks in the Mount Morrison pendant with tilting and maximum thickness restored.

Figure 4: Stratigraphic section of the breccia of Mammoth Rock at Mammoth Rock.

Figure 5: Outcrop of the polymictic facies of the breccia of Mammoth Rock, showing clast variety: volcanic (V), sandstone (ss), limestone (L), and shale (sh). Hammer is 33 cm long.

Figure 6: Photomicrographs of the polymictic facies of the breccia of Mammoth Rock in cross-polarized light and 10x magnification. C = quartzite clast. M = matrix.

Figure 7: Photomicrographs of monomictic facies of the breccia of Mammoth Rock in cross-polarized light and 10x magnification. C = clast, M = matrix.

Figure 8: Clast textures in the monomictic facies of the breccia of Mammoth Rock. (a) Cuspate clasts. (b) Jigsaw clasts with cuspate margins. Pencil is 14.5 cm long.

Figure 9: Angular, ragged sandstone clasts of in the upper monomictic breccia of Mammoth Lake. Pencil is 14 cm long.

Figure 10: Photomicrograph of the sandstone facies (lower bed) of the breccia of Mammoth Rock under cross-polarized light and 10x magnification. V = volcanic clast.

Figure 11: Sandstone facies of the breccia of Mammoth Rock. Red lines are laminations. (a) Lower bed, showing the interface (bold line) between cross-sets. Pencil is 14 cm long. (b) Upper bed, with planar, slightly wavy laminations. Hammer is 33 cm long.

Figure 12: Sharp, irregular contact between heavily oxidized, planar-laminated sandstone and monomictic breccia of Mammoth Rock. Dashed black line is the contact. Red lines are sandstone laminations. Hammer is 33 cm long.

Figure 13: Facies map of Triassic rocks in the southeast Mount Morrison pendant (North Fork Fisk Creek area, Fig. 2) with selected cleavage measurements for tuffaceous facies of the dacite of Arrowhead Lake shown for orientation. Red lines correspond to stratigraphic sections (Fig. 14).

Figure 14: Stratigraphic sections of Triassic rocks in the southeast Mount Morrison pendant (North Fork, Fish Creek area). Locations correspond to the North Fork Fish Creek area map (Fig. 13). ALD = dacite of Arrowhead Lake, SLT = tuff of Skelton Lake.

Figure 15: Typical outcrops of the breccia facies of the dacite of Arrowhead Lake, showing range of clast sizes. Hammer is 33 cm long.

Figure 16: Clast textures in the breccia facies of the dacite of Arrowhead Lake. (a) Cuspate clast margins. (b) Jigsaw clasts (circled). Pencil is 14 cm long. (Location: SW Ridge, Red Slate Mountain; Fig. 13).

Figure 17: Tuffaceous sedimentary rocks associated with the dacite of Arrowhead Lake. (a) Coarse-grained sandstone with two conglomerate lenses outlined in black line. Hammer is 33 cm long. (b) Irregular layers of reworked fine-grained tuffaceous material with black lines for bedding. Pencil is 14 cm long. (Location: SW Ridge, Red Slate Mountain, Fig. 13).

Figure 18: Typical outcrop of Arrowhead Lake tuff with white feldspar phenocrysts and dark, wispy pumice fragments (faint). Pen is 14 cm long. (Location: North Fork Fish Creek; Fig. 13).

Figure 19: Looking northeast at the irregular, intrusive contact between the dacite of Arrowhead Lake (dark grey) and the tuff of Skelton Lake (white) in the central part of the pendant, northwest of Duck Lake.

Figure 20: (a) Looking east-southeast at the Triassic sequence on Red and White Spur, showing a large intrusion of dacite of Arrowhead Lake. (b) Looking northeast across the Triassic-Jurassic fault at the same dacite intrusion within the tuff of Skelton Lake.

Figure 21: Typical outcrop of the massive, porphyritic lava facies of the dacite of Arrowhead Lake, showing abundance of plagioclase phenocrysts. Pencil is 14 cm long. (Location: SW Ridge, Red Slate Mountain; Fig. 13).

Figure 22: Photomicrograph of porphyritic facies of the dacite of Arrowhead Lake in cross-polarized light and 25x magnification. P = plagioclase phenocryst.

Figure 23: Typical outcrops of the tuff of Skelton Lake showing size range of pumice fragments. Pencil is 14 cm long. (Location: North Fork Fish Creek; Fig. 13).

Figure 24: Photomicrographs of the tuff of Skelton Lake under cross-polarized light at 10x magnification. (a) Mica and epidote strands bent around quartz phenocrysts. (b, c) Ragged, wispy pumice fragments (P) pseudomorphically replaced by mica. Q = quartz phenocryst.

Figure 25: Breccia facies of the tuff of Skelton Lake in the North Fork Fish Creek area. (a) Tuff breccia lens. (b) Aphyric volcanic clast. (c) Andesite(?) tuff clast. Pencil is 14 cm long. (Location: Red and White Spur; Fig. 13).

Figure 26: Typical outcrop of the breccia of Pika Lake showing clast angularity. Hammer is 33 cm long. (Location: unnamed ridge east of Duck Lake; Fig. 2).

Figure 27: Jigsaw clasts in the breccia of Pika Lake. Pencil is 14 cm long. (Location: unnamed ridge east of Duck Lake; Fig. 2).

Figure 28: Facies of the Jurassic Deer Lakes sequence in Deer Lakes basin (Fig. 2). (a) Finely laminated facies. Black lines show bedding. Hammer is 33 cm long. (b) Rhyolite tuff with pumice and quartzite clasts stretched along regional foliation direction. Pink color is due to piemontite alteration. (c) Tuff breccia with clasts deformed along strike. (d) Poorly sorted dacite breccia with large, subrounded to rounded dacite porphyry clasts. Pencil is 14 cm long.

Figure 29: Outcrops of Duck Lake sequence showing stratigraphy. (a) Looking southwest at the lower part of the sequence exposed on the ridge immediately southeast of Purple Lake. (b) The lower part of the sequence exposed on the Mammoth Crest. Unit abbreviations: LLM = Lee Lake Mass, DLS = Duck Lake sequence (facies type in parentheses), PLR = rhyolite of Purple Lake, MCA = andesite of Mammoth Crest. Facies key for schematic cross-section according to Fig. 3.

Figure 30: Stratigraphy of the Cretaceous Duck Lake sequence. Locations correspond to Figure 2. Note that the andesite porphyry facies is greater than 400 meters thick in the northwest part of the pendant. Locations correspond to labels on Fig. 2.

Figure 31: Photomicrograph of the rhyolite of Purple Lake under cross-polarized light at 10x magnification. P = plagioclase phenocryst.

Figure 32: Photomicrograph under crossed-polarized light and 10x magnification of the andesite of Mammoth Crest showing abundance of albitic plagioclase. P = plagioclase phenocryst.

Figure 33: Laminated calc-silicate rocks of the Duck Lake succession (DLS) locally folded around the massive andesite of Mammoth Crest (MCA), south of Purple Lake. Trekking pole (yellow box) is 120 cm tall.

Figure 34: Alternating beds of sandstone (white) and shale (dark purple-grey) in the lower half of the Duck Lake sedimentary succession. Pencil is 14 cm long. (Location: Duck Lake).

Figure 35: Outcrops of finely laminated calc-silicate rocks of the upper Duck Lake sedimentary succession east of Purple Lake. Pencil is 14 cm long.

Figure 36: (a) Concordia diagram of all zircon data from a sample of the breccia of Mammoth Rock. (b) All Triassic zircon ages from a sample of the breccia of Mammoth Rock. (c) Weighted mean average of the youngest population of zircons from a sample of the breccia of Mammoth rock. MSWD = mean square of weighted deviates. n = number of crystals analyzed.

Figure 37: (a) Concordia diagram of all zircon data from a sample of the intrusive dacite of Arrowhead Lake. (b) Plot of all zircons from a sample of the intrusive dacite of Arrowhead Lake. (c) Weighted mean average of the youngest population of zircons from a sample of the intrusive dacite of Arrowhead Lake. MSWD = mean square of weighted deviates. n = number of crystals analyzed.

Figure 38: (a) Concordia diagram of all coherent zircons from a sample of the breccia of Pika Lake. (b) Plot of all zircons from a sample of the breccia of Pika Lake. (c) Weighted mean average of the youngest population of zircons from a sample of the breccia of Pika Lake. MSWD = mean square of weighted deviates. n = number of crystals analyzed.

Figure 39: (a) Concordia diagram of all zircons from a sample of the tuff of Deer Lakes. (b) Plot of all zircons from a sample of the tuff of Deer Lakes. (c) Weighted mean average of the youngest population of zircons from a sample of the tuff of Deer Lakes. MSWD = mean square of weighted deviates. n = number of crystals analyzed.

Figure 40: (a) Concordia diagram of all zircons from a sample of the rhyolite of Purple Lake. (b) Weighted mean average of the dominant population of zircons from a sample of the rhyolite of Purple Lake. MSWD = mean square of weighted deviates. n = number of crystals analyzed.

Figure 41: (a) Concordia diagram of all Cretaceous zircons from a sample of the andesite of Mammoth Crest. (b) Weighted mean average of Cretaceous zircons from a sample of the andesite of Mammoth Crest. MSWD = mean square of weighted deviates. n = number of crystals analyzed.

Figure 42: Plot of P_2O_5 against SiO2 for Mesozoic volcanic rocks of the Mount Morrison pendant. Data for the tuff of Skelton Lake from Barth (pers. comm., 2017).

Figure 43: Plot of TiO_2 against SiO_2 for Mesozoic volcanic rocks of the Mount Morrison pendant. Data for the tuff of Skelton Lake from Barth (pers. comm. 2017).

Figure 44: Plot of MnO against SiO_2 for Mesozoic volcanic rocks of the Mount Morrison pendant. Data for the tuff of Skelton Lake from Barth (pers. comm. 2017).

Figure 45: Plot of MgO against SiO_2 for Mesozoic volcanic rocks of the Mount Morrison pendant. Data for the tuff of Skelton Lake from Barth (pers. comm. 2017).

Figure 46: Plot of Fe_2O_3* against SiO_2 for Mesozoic volcanic rocks of the Mount Morrison pendant. Data for the tuff of Skelton Lake from Barth (pers. comm. 2017).

Figure 47: Plot of Al_2O_3 against SiO_2 for Mesozoic volcanic rocks of the Mount Morrison pendant. Data for the tuff of Skelton Lake from Barth (pers. comm. 2017).

Figure 48: Classification of Mount Morrison volcanic rocks by comparing Nb/Y against SiO_2 per Winchester and Floyd (1977).

Figure 49: Classification of Mount Morrison volcanic rocks by comparing Zr/Ti with SiO_2 per Winchester and Floyd (1977).

Figure 50: Classification of Mount Morrison volcanic rocks by comparing Nb/Y with Zr/Ti (Winchester and Floyd, 1977).

Figure 51: Spider diagram of rare earth elements for volcanic rocks of the Mount Morrison pendant normalized to primitive mantle (Sun and McDonough, 1989). Average upper crust composition from Rudnick (2003).

Figure 52: Spider diagram of selected trace elements normalized to primitive mantle (Sun and McDonough, 1989) for volcanic rocks of the Mount Morrison pendant. Average upper crust composition from Rudnick (2003).

Figure 53: Stereographic projection of poles to cleavage planes for Triassic, Jurassic, and Cretaceous rocks in the Mount Morrison pendant.

Figure 54: Saussuritized dacite breccia of the Jurassic Deer Lakes sequence with highly strained and saussuritized clasts due to proximity to fault zone with the Cretaceous block. Compare with Figure 24d. Hammer is 33 cm long.

Figure 55: Quartz boudins in the Jurassic Deer Lakes sequence indicating dextral shear motion. Photo was taken within 100 meters of the contact with the Cretaceous Mono Creek Granite. Hammer is 33 cm long.

Figure 56: Looking northeast at the Jurassic-Cretaceous fault zone in Deer Lakes basin, showing of boudins of quartz-epidote-piemontite rocks (white dashed outline) within highly sheared rocks of the Jurassic Deer Lakes sequence. Thicker white dashed lines show the extent of the fault zone.

Figure 57: Looking northeast at a block of anomalously shallow-dipping sedimentary rocks of Duck Lake succession (center) on the ridgeline south of Pika Lake. Red lines show bedding.

Figure 58: Summary diagram comparing volcanic and structural patterns in the Mount Morrison pendant (MMP) against overall Sierran arc trends from Cao and Paterson (2016). Blue circles are MMP rocks; red circles are other Sierran arc rocks from Paterson et al. (2014). The paleo-elevation curves are based on MMP facies (purple line) and Sierran facies (orange line) from Paterson et al. (2014).

Figure 59: Areal extent of Mount Morrison pendant volcanic material according to age.

Figure 60: Discrimination of tectonic setting for volcanic rocks of the Mount Morrison pendant using Th/Yb against Ta/Yb (Pearce, 1983).

Figure 61: Discrimination of arc type for volcanic rocks of the Mount Morrison pendant using Zr/Y against Zr (Pearce, 1983).

Figure 62: Discrimination of tectonic setting for volcanic rocks of the Mount Morrison pendant using Ti against Zr (Pearce, 1983).

Figure 63: Discrimination of tectonic setting for volcanic rocks of the Mount Morrison pendant using Nb against Y (Pearce et al., 1984).

Figure 64: Discrimination of tectonic setting for volcanic rocks of the Mount Morrison pendant using Ta against Yb (Pearce et al., 1984).

Figure 65: Ternary diagram for discrimination of tectonic setting for Mesozoic volcanic rocks of the Mount Morrison pendant using Hf, Th, and Ta (Wood, 1980).

LIST OF TABLES

Table 1: List of samples collected and analyzed in this study. The same samples were used for U-Pb zircon geochronology and whole-rock geochemistry.

Table 2a: U-Pb analytical data for 49 zircon samples of the breccia of Mammoth Rock (MRB).

Table 2b: U-Pb age data for 49 zircon samples of the breccia of Mammoth Rock (MRB).

Table 3a: U-Pb analytical data for 49 zircon samples of the dacite of Arrowhead Lake (ALD).

Table 3b: U-Pb age data for 49 zircon samples of the dacite of Arrowhead Lake (ALD).

Table 4a: U-Pb analytical data for 49 zircon samples of the breccia of Pika Lake (PLB).

Table 4b: U-Pb age data for 49 zircon samples of the breccia of Pika Lake (PLB).

Table 5a: U-Pb analytical data for 49 zircon samples of the tuff of Deer Lakes (DLT).

Table 5b: U-Pb age data for 49 zircon samples of the tuff of Deer Lakes (DLT).

Table 6a: U-Pb analytical data for 49 zircon samples of the rhyolite of Purple Lake (PLR).

Table 6b: U-Pb age data for 49 zircon samples of the rhyolite of Purple Lake (PLR).

Table 7a: U-Pb analytical data for 14 zircon samples of the andesite of Mammoth Crest (MCA).

Table 7b: U-Pb age data for 49 zircon samples of the andesite of Mammoth Crest (MCA).

Table 8: Analytical data for bulk-rock major element oxide geochemistry of Mount Morrison samples. Unit abbreviations: ALD = dacite of Arrowhead Lake, DLT = tuff of Deer Lakes, PLR = rhyolite of Purple Lake, MCA = andesite of Mammoth Crest, PLB = breccia of Pika Lake, MRB = breccia of Mammoth Rock.

Table 9 (continued on next page): Analytical data for bulk-rock trace element geochemistry of Jurassic and Cretaceous samples. Unit abbreviations: ALD = dacite of Arrowhead Lake, DLT = tuff of Deer Lakes, PLR = rhyolite of Purple Lake, MCA = andesite of Mammoth Crest, PLB = breccia of Pika Lake, MRB = breccia of Mammoth Rock.

ACKNOWLEDGEMENTS

This project would not have been possible without support from friends, family, colleagues, and mentors. Firstly, I owe this opportunity to my advisor Nancy Riggs, who entrusted me with a rather large, rugged, backcountry field area, knowing that was precisely what I wanted. Her guidance and wisdom directed my intellectual explorations throughout the journey, and I feel that I am a more well-rounded and meticulous geologist because of it. I was fortunate to have Andrew Barth and Michael Ort as members of my committee, for they stimulated ideas and taught me the craft of observation and interpretation from microscopic to continental scale. I am indebted to my field assistants (Ray Eckland, Stephen Dobbs, and Emma Lodes), with whom I spent many wonderful weeks roaming the High Sierra. I am especially grateful to Ray, whose keen participation and innate curiosity throughout the process proved highly beneficial and greatly enhanced the entire experience. I also thank my lab assistant, Alan Ponce, who made fun the long shifts in the rock-crushing laboratory. For invaluable help with GIS programs, I thank Lisa Skinner and Bob Lenegan. I am ever grateful for my mother and father in continuing to support my pursuits in the Earth Sciences and beyond. Finally, I acknowledge my partner Giselle Fernandez. In addition to spending several weeks as my field assistant, she provided much-needed emotional support in difficult times.

1. INTRODUCTION

Mesozoic pendants of the east-central Sierra Nevada (Fig. 1) record the development of the Sierran arc as it was being built on the western margin of Laurentia. Volcanic units within these pendants are together recognized as the surface manifestation of episodic Sierran arc magmatism (Barth et al., 2011; 2012), a process largely controlled by internal arc dynamics (Ducea, 2001; Paterson et al., 2014). The pattern of magmatic flux, referred to as the "arc tempo", is recorded in U-Pb zircon data throughout the range (Paterson et al., 2014; de Silva et al., 2015; Paterson and Ducea, 2015). Periods of minimal magmatic addition, termed "lulls", were interposed with high-flux "pulses", in which volumetric magma addition rates increased by one to three orders of magnitude (Paterson and Ducea, 2015). Arc volcanism entailed construction of local volcanic fields (Fiske and Tobisch, 1978) and was punctuated by caldera-forming eruptions (Fiske and Tobisch, 1994; Schweickert and Lahren, 1999). A thick volcanic carapace probably covered the entire range during Late Cretaceous time (Fiske and Tobisch, 1994). Post-Cretaceous erosion and exhumation of the underlying batholith destroyed most of these rocks, except those preserved as roof pendants. In the east-central part of the range, along the axial crest, volcanic successions are best preserved in the Ritter Range, Saddlebag Lake, and Mount Morrison pendants (Fig. 1). Similarities in age and geochemistry argue that extrusive pendant rocks and nearby intrusive units were coeval (e.g. McNulty et al., 1996; Barth et al., 2012), suggesting that volcanic flare-ups were roughly contemporaneous with major stages of plutonism and thus invoking a close link between the two processes.

Volcanic sections in the Ritter Range and Saddlebag Lake pendants have been comprehensively described (Huber and Rinehart, 1965; Brook, 1977; Fiske and Tobisch, 1978; Fiske and Tobisch, 1994; Schweickert and Lahren, 1999; Barth et al., 2012; Paterson et al.,

2014), leading to an increasing understanding of their roles in Sierran history. The stratigraphy of Mesozoic rocks in the Mount Morrison pendant, in contrast, has not been revisited since the initial USGS survey (Rinehart and Ross, 1964). This pendant provides a rare opportunity to analyze and compare all three stages of Sierran arc growth with respect to eruptive patterns and paleogeography, as ages of the rocks correspond to each stage of high magmatic flux along the arc.

Despite the fact that rocks of the east-central Sierran pendants have undergone hornfels- to greenschist-grade contact metamorphism due to intrusion of granite bodies (Hanson et al., 1993; Jones and Rougvie, 2004), this study follows previous workers (e.g. Fiske and Tobisch, 1978; Busby-Spera, 1985; Schweickert and Lahren, 1999; Barth et al., 2012) by using protolith names (i.e. the prefix "meta" is omitted) for the sake of concision and emphasis on original facies relations. Both volcanic and sedimentary rocks are referred to according to their inferred original rock type, and elements of structural deformation and metamorphism are described independently.

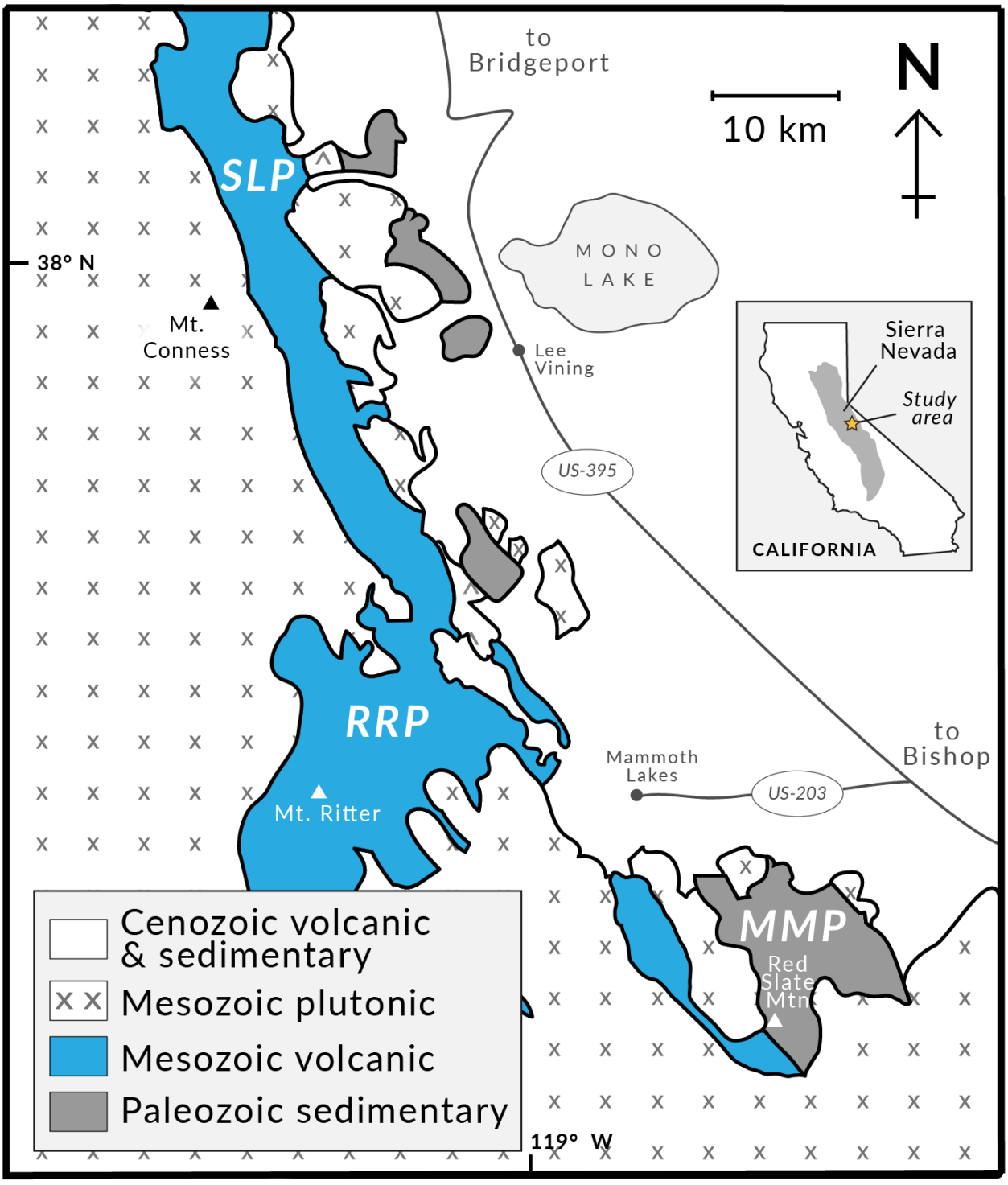

Figure 1: Generalized geologic map of the east-central Sierra Nevada showing the location of Mesozoic volcanic rocks in the Ritter Range pendant (RRP), Saddlebag Lake pendant (SLP), and Mount Morrison pendant (MMP). Modified from Barth et al. (2011).

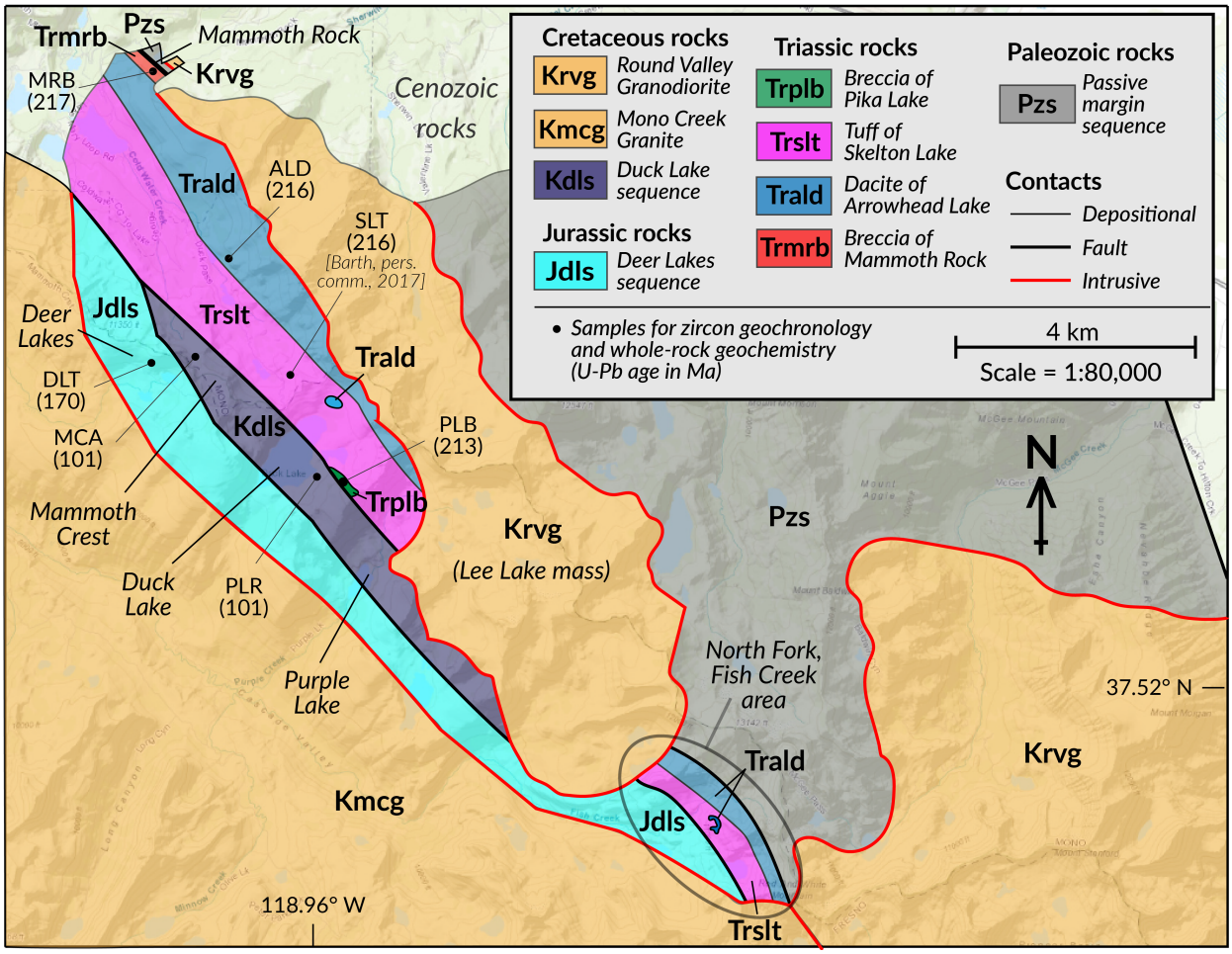

Figure 2: Geologic map of Mesozoic volcanic rocks of the Mount Morrison pendant and environs. Mesozoic rocks and their bounding contacts are shown according to mapping done in this study. Intrusive contacts between Paleozoic sedimentary rocks and Cretaceous granites are based on Rinehart and Ross (1964). Samples were used for both U-Pb zircon geochronology and whole-rock bulk geochemistry analyses. Sample abbreviations: MRB = breccia of Mammoth Rock, ALD = dacite of Arrowhead Lake, SLT = tuff of Skelton Lake, PLB = breccia of Pika Lake, DLT = tuff of Deer Lakes, PLR = rhyolite of Purple Lake, MCA = andesite of Mammoth Crest.

2. BACKGROUND

2.1 GEOLOGIC HISTORY

The western margin of Laurentia was originally formed by Neoproterozoic rifting (Stevens et al., 1997). A southwest-trending continental shelf was established by ~560 Ma, and subsidence of the passive margin allowed sedimentation that continued through Late Devonian time (Stevens et al., 1997). Initiation of the Devonian Antler orogeny resulted in the thrusting of the Roberts Mountain allochthon onto the Laurentian margin, while a subsequent thrust event during the Permian-Triassic Sonoma orogeny emplaced the Golconda allochthon and created a range-wide unconformity (Morgan and Rankin, 1972; Russel and Nokleberg, 1977; Miller et al., 1992). The southwest-trending passive margin of Laurentia became a transform boundary that eventually collapsed due to gravitational instability in the Late Permian epoch (Miller et al., 1992; Saleeby and Dunne, 2015). A subduction zone was established through spontaneous nucleation (Stern, 2004; Roberts, 2013), and the ensuing Sierran arc was emplaced into progressively thicker and more geochemically evolved continental crust (Barth et al., 2013). The change from passive to convergent margin is recorded as a tectonically overprinted angular unconformity that divides Paleozoic sedimentary rocks from Mesozoic volcanic rocks in the Ritter Range, Saddlebag Lake, and Mount Morrison pendants (Nokleberg and Kistler, 1980).

After its inception around 250-260 Ma (Paterson et al., 2014; Saleeby and Dunne, 2015), the Mesozoic Sierran arc experienced three pulses of high-flux magmatism: (1) Late Triassic, (2) Middle Jurassic, and (3) Late Cretaceous (Barth et al., 2013; Paterson and Ducea, 2015). This tempo is recorded in U-Pb zircon age data from a broad range of plutonic, volcanic, and sedimentary rocks (Stern et al., 1981; Barth et al., 2012; Paterson et al., 2014; Barth et al., in press). The Late Triassic pulse experienced its peak around 210-220 Ma (Paterson et al., 2014),

producing rhyolitic arc-type ignimbrites between ~224 Ma (Barth et al., 2012) and ~207 Ma (Barth et al., in press). Thick volcanic successions are preserved in all three pendants, indicating that Late Triassic volcanism was voluminous in the east-central Sierra Nevada. The Late Triassic arc was in a shallow marine setting (Rinehart and Ross, 1964; Fiske and Tobisch, 1978; Douglas et al., 2010; Saleeby and Dunne, 2015). Following a magmatic lull, a second high-flux pulse during the Middle to Late Jurassic epoch (centered at 165 Ma) coincided with a Cordillera-wide transgression emplacing dominantly marine rocks in the east-central Sierra Nevada (Fiske and Tobisch, 1978; Sorensen et al., 1998; Barth et al., 2015). The third and final pulse was the arc's most voluminous (Paterson et al., 2011), with volcanic rates peaking in latest Early Cretaceous time (ca. 102 Ma) and pluton input peaking in earliest Late Cretaceous time (91 Ma; Paterson et al., 2014). This event accounts for most plutons in the Sierra Nevada (Stern et al., 1981; Cao and Paterson, 2016), as well as a laterally continuous belt of volcanic rocks including two large calderas in the Ritter Range and Merced Peak pendants (Fiske and Tobisch, 1994; Paterson et al., 2014). Pluton emplacement resulted in greenschist-grade contact metamorphism of the volcanic rocks (Hanson et al., 1993; Jones and Rougvie, 2004) Thermochronologic (McPhillips and Brandon, 2012) and paleoisotopic (Poage and Chamberlain, 2002; Cassel et al., 2012) models place the Sierran arc at a high-elevation (3-5 km) setting by the end of Late Cretaceous time, although the precise timing of uplift has yet to be determined. Emplacement of Late Cretaceous plutons was accommodated mostly by dextral transpressive motion along the Sierra Crest shear zone, and partly by crustal contraction and wall-rock return flow (Tobisch et al., 2000). Transpressional tectonics continued for ~20 m.y. (Bentley, 2004). Total displacement along the shear zone is estimated to be 20 km (Greene and Schweickert, 1995).

2.2 METHODS

This study is based on mapping, stratigraphy, facies analysis, petrography, geochronology, and geochemistry. Field work was carried out during the summers of 2016 and 2017, with laboratory work between and after those periods. Standard techniques were used throughout. Maps were generated at scales of 1:12,000 to 1:80,000. Petrographic thin sections were prepared by Quality Thin Sections (Tucson, AZ) from billet samples cut at Northern Arizona University. The objective is to provide a detailed description of the Mesozoic volcanic rocks of the Mount Morrison pendant, including the breccia of Mammoth Rock, the dacite of Arrowhead Lake, the tuff of Skelton Lake, the breccia of Pika Lake, the Duck Lake sequence, and the Deer Lakes sequence, and thereby an interpretation of its role in the geologic evolution of the Sierra Nevada.

Five-kilogram bulk-rock samples were collected from six major volcanic units selected for U-Pb zircon geochronology analysis. Rock crushing, mineral separation, and zircon extraction were performed at Northern Arizona University using standard methods (Gehrels, 2000). All rocks contain euhedral zircon crystals that show little to no sign of detrital transport. All samples were analyzed for U and Pb isotopes and trace element concentrations at the University of California at Santa Barbara (UCSB) Laser Ablation Split Stream (LASS) facility. The LASS facility includes a Nu Plasma HR MC-ICPMS (high resolution multi-collector inductively coupled plasma mass spectrometer), a Nu AttoM single collector ICPMS (Nu Instruments Ltd., Wrexham, UK), and an Analyte 193 excimer ArF laser-ablation system equipped with a HeLex sample cell (Photon Machines, San Diego, USA). Analyses were normalized against the GJ1, 91500, and Plesovice zircon reference standards (Wiedenbeck et al.,

1995). Data were reduced using Iolite 2.5 software in Igor Pro 6.3. Error was assessed according to Kylander-Clark et al. (2013).

Major and trace element geochemistry analyses were performed on bulk-rock samples crushed in steel and tungsten carbide jaw crushers and ground in a tungsten carbide mixer mill. X-ray fluorescence (XRF) analyses for major elements as well as Rb, Sr, and Zr were completed on fused glass disks at Michigan State University using a Bruker spectrometer. Trace element analyses were performed with a Micromass inductively coupled plasma–mass spectrometer (ICP-MS) at Michigan State University. The following major element oxides were measured: SiO_2, TiO_2, AlO_2, Fe_2O_3, MnO, MgO, CaO, Na_2O, K_2O, and P_2O_5. Trace elements included in the analysis were Sc, V, Cr, Co, Ni, Rb, Sr, Y, Zr, Nb, Cs, Ba, La, Ce, Pr, Nd, Sm, Eu, Gd, Tb, Dy, Ho, Er, Tm, Yb, Lu, Hf, Ta, Pb, Th, and U. Precision was monitored according to USGS and GSJ rock standards. For XRF analysis, precision is better than 1% for most major elements and trace elements present in abundances >100 ppm. For ICP-MS analysis, precision is 2%–5% for trace elements analyzed by ICP-MS.

3. ROCK DESCRIPTIONS

3.1 TRIASSIC ROCKS

Triassic rocks make up more than half the volcanic material in the Mount Morrison pendant (Fig. 3), with a maximum thickness of 3 km in the northwestern part of the pendant (Fig. 2). Within this structural block, a regionally extensive, 1.2-km-thick rhyolite ignimbrite (the tuff of Skelton Lake) stratigraphically overlies a 1.5-km-thick suite of dacitic tuffs, tuff breccias, hypabyssal lavas, and minor sedimentary lenses (the dacite of Arrowhead Lake). The oldest and

youngest units in this section (the breccia of Mammoth Rock and the breccia of Pika Lake) are localized masses of low-silica lava breccia.

Along much of its eastern margin, the Triassic block is bounded by an intrusive contact with the Cretaceous Lee Lake Mass of the Round Valley Peak Granodiorite (Fig. 2; Bateman, 1992). At two locations (Mammoth Rock and North Fork Fish Creek) along the eastern boundary, the section is truncated by a fault contact with highly folded Paleozoic passive-margin sedimentary rocks (Morgan and Rankin, 1972). On the west, the section is truncated by a broad intra-pendant shear zone, juxtaposed against the Cretaceous block in the central part of the pendant, and against the Jurassic block in the northern and southern extremities (Fig. 2).

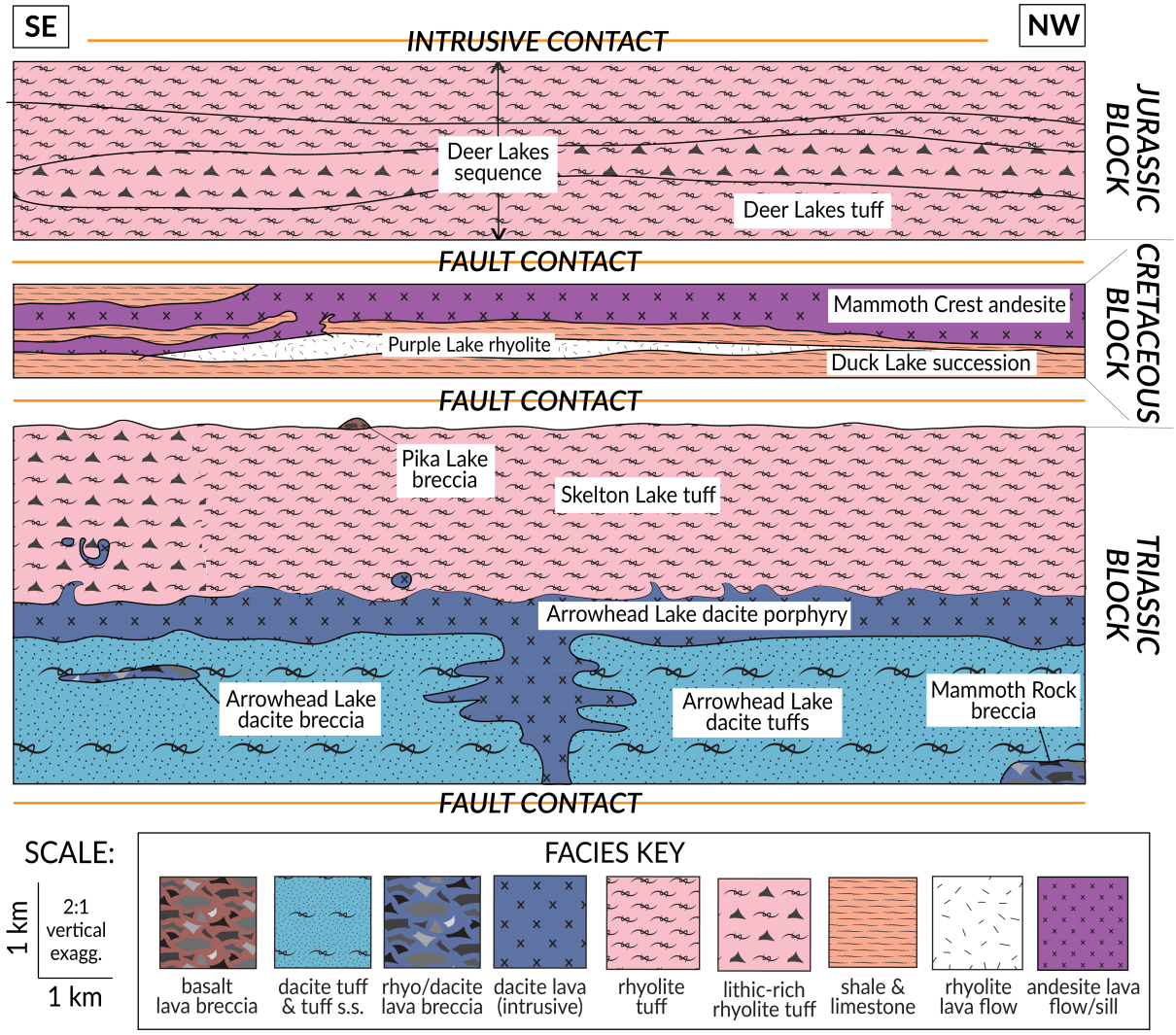

Figure 3: Schematic cross-section of Mesozoic rocks in the Mount Morrison pendant with tilting and maximum thickness restored.

3.1.1 BRECCIA OF MAMMOTH ROCK

The lowermost unit in the pendant is the breccia of Mammoth Rock, a local mafic deposit in the far northwest corner of the pendant (Trmrb, Fig. 2). More than 300 stratigraphic meters of pyroclastic and epiclastic rocks are exposed on the slope immediately southwest of Mammoth

Rock, a prominent topographic feature composed of Paleozoic Mount Baldwin Marble. The three dominant facies are polymictic breccia, monomictic breccia, and sandstone (Fig. 4).

The basal polymictic breccia facies is juxtaposed against the Paleozoic Mount Baldwin Marble along a fault contact. The polymictic facies is 140 meters thick (Fig. 4), including a 15-m-thick zone of severe bleaching adjacent to the fault. The typical outcrop (Fig. 5) weathers medium grey and is speckled with a variety of white, grey, brown, and black clasts averaging 1-10 cm in diameter. The rock hosts a poorly sorted, approximately equal-parts mixture of subrounded sedimentary clasts and subangular volcanic clasts that together make up 25-30% of the rock. Clasts are largely undeformed, but fine-grained sedimentary varieties have been altered to a reddish-brown color. Rinehart and Ross (1964) noted that the sedimentary clasts are almost exclusively composed of white to light grey quartzite with rare brown siliceous hornfels and grey marble. The subrounded texture of sedimentary clasts contrasts with their subangular volcanic counterparts, indicating that they may have undergone a comparatively higher degree of sedimentary transport prior to entrainment. The volcanic clasts are the same dark grey, aphyric type as the clasts of the overlying monomictic breccia. Sandstone clasts have been fully recrystallized to quartzite (Fig. 6), whereas volcanic clasts have been pseudomorphically replaced by dark microcrystalline aggregates too fine to identify under the microscope. The matrix is a microgranular mosaic of quartz, feldspar, chlorite, and epidote with trace amounts of amphibole, muscovite, biotite, and oxides (Fig. 6).

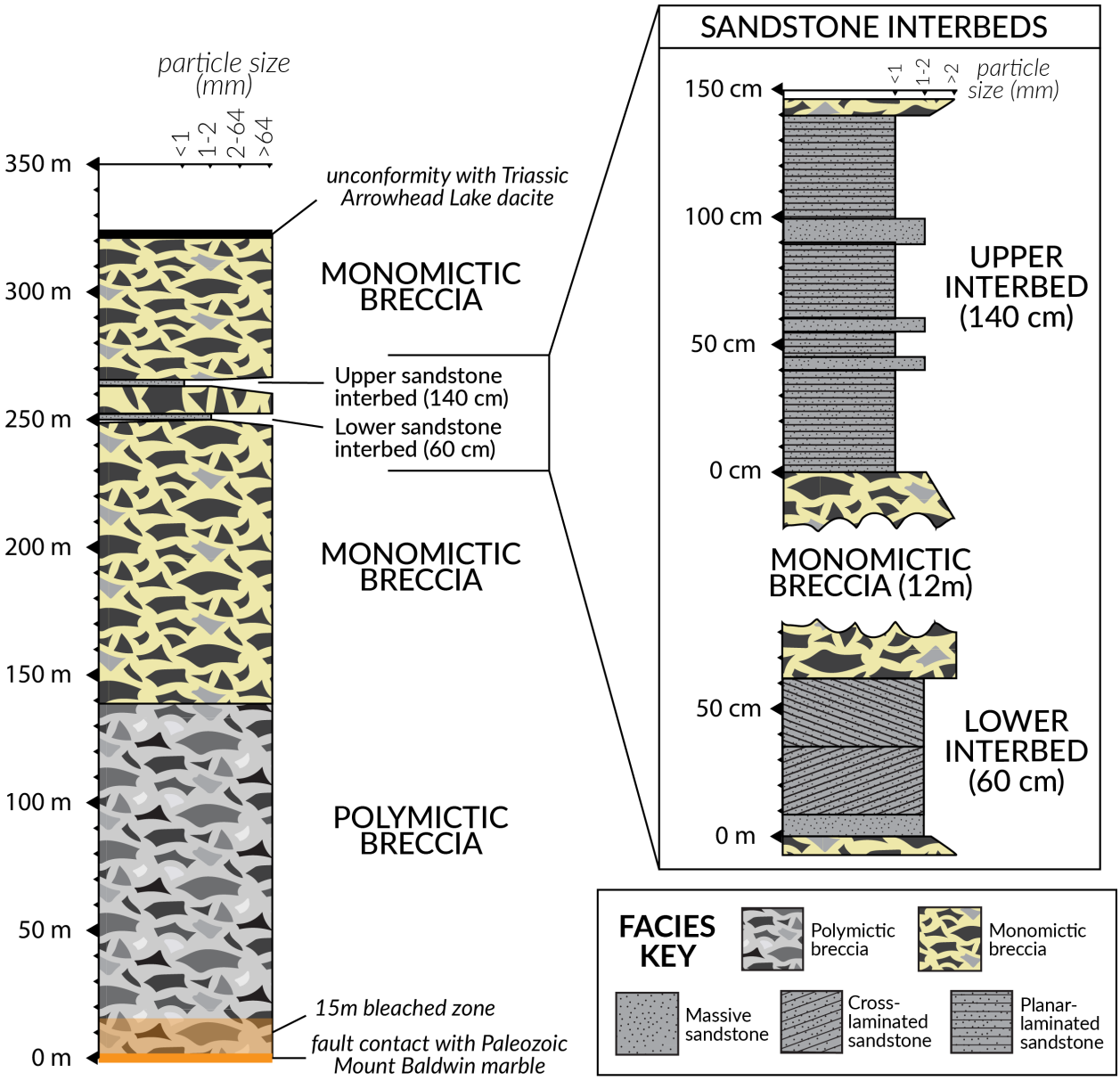

Figure 4: Stratigraphic section of the breccia of Mammoth Rock at Mammoth Rock.

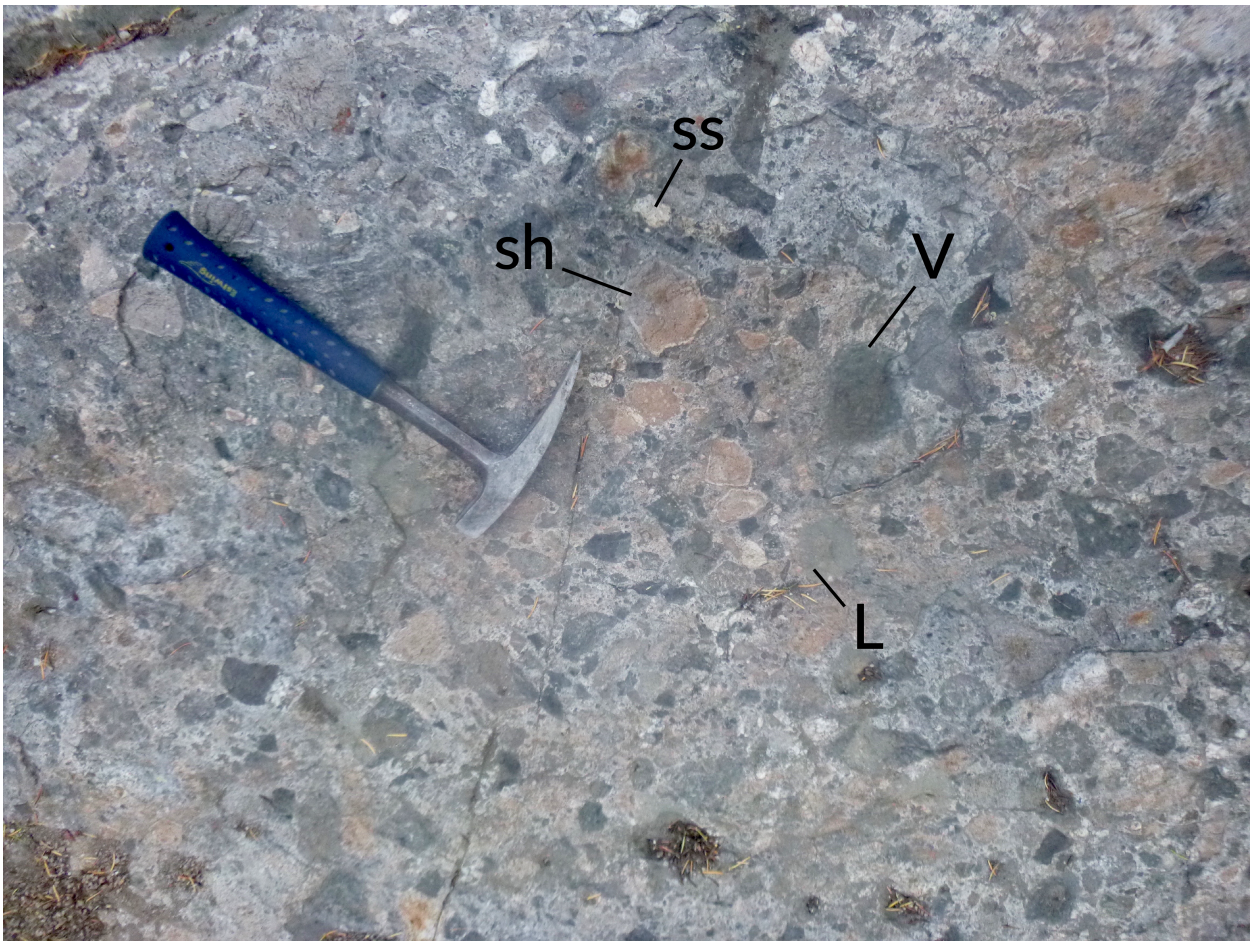

Figure 5: Outcrop of the polymictic facies of the breccia of Mammoth Rock, showing clast variety: volcanic (V), sandstone (ss), limestone (L), and shale (sh). Hammer is 33 cm long.

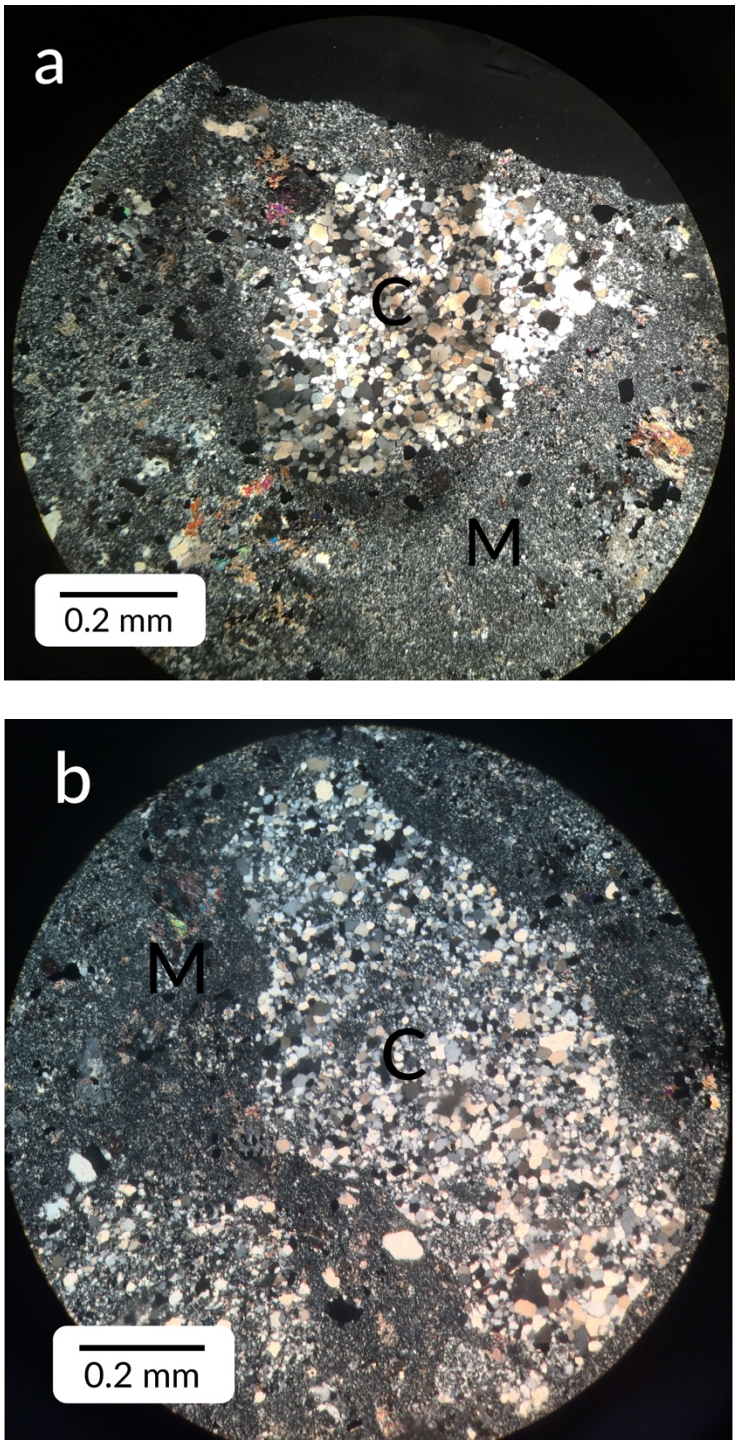

Figure 6: Photomicrographs of the polymictic facies of the breccia of Mammoth Rock in cross-polarized light and 10x magnification. C = quartzite clast. M = matrix.

The monomictic breccia overlies the polymictic breccia along a sharp contact and is almost 200 meters thick (Fig. 4). The mass of monomictic breccia is largely structureless except for two southwest-dipping sandstone interbeds. This facies contains 20-30% angular, dark, aphyric basalt clasts in a bleached white to tan matrix. Between and immediately above the sandstone beds, volcanic clasts make up 30-40% of the breccia and angular fragments of laminated sandstone (Fig. 9) up to one meter in diameter account for an additional 5%. The rock is poorly sorted, with clast sizes ranging from 1-30 cm. Volcanic clasts have cuspate margins and jigsaw fractures (Fig. 8). (Fig. 7). Clasts are composed of dark microcrystalline material unresolvable under the microscope, with varying degrees of overprinting by secondary mica and epidote. The petrographic texture of the clasts is suggestive of devitrified glass. The matrix is composed of recrystallized quartz, mica, and minor feldspar. Thin-section petrography shows that the rock has undergone complete mineralization.

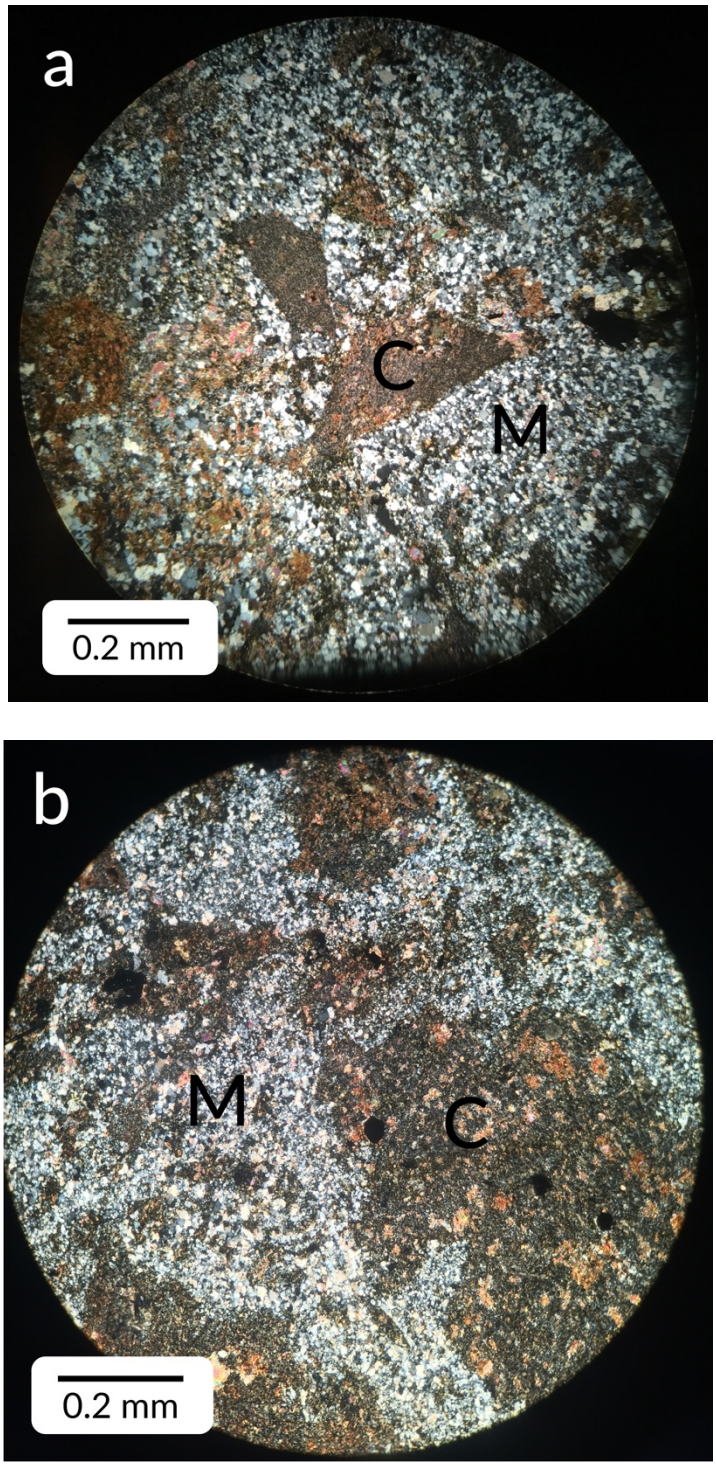

Figure 7: Photomicrographs of monomictic facies of the breccia of Mammoth Rock in cross-polarized light and 10x magnification. C = clast, M = matrix.

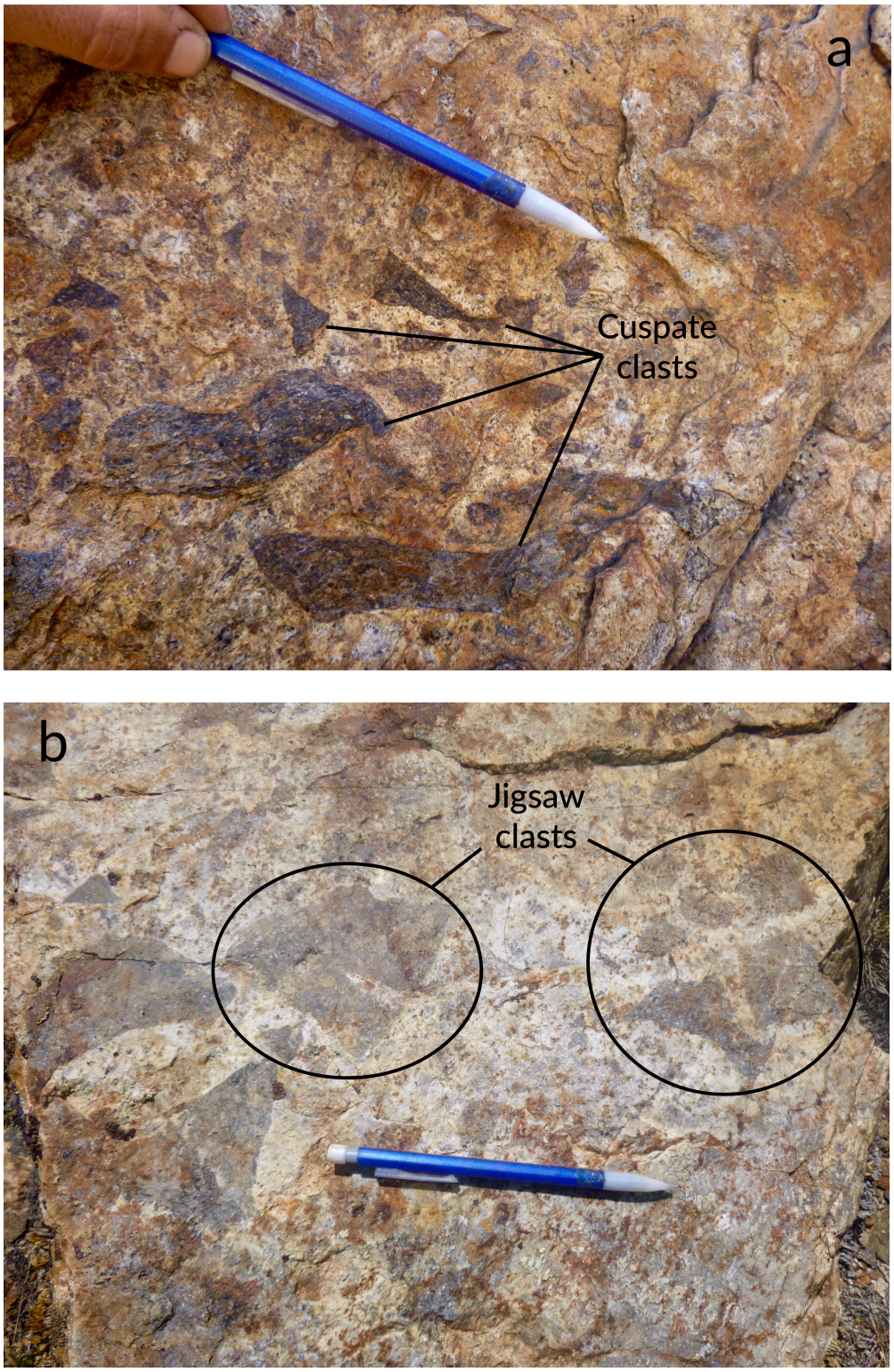

Figure 8: Clast textures in the monomictic facies of the breccia of Mammoth Rock. (a) Cuspate clasts. (b) Jigsaw clasts with cuspate margins. Pencil is 14.5 cm long.

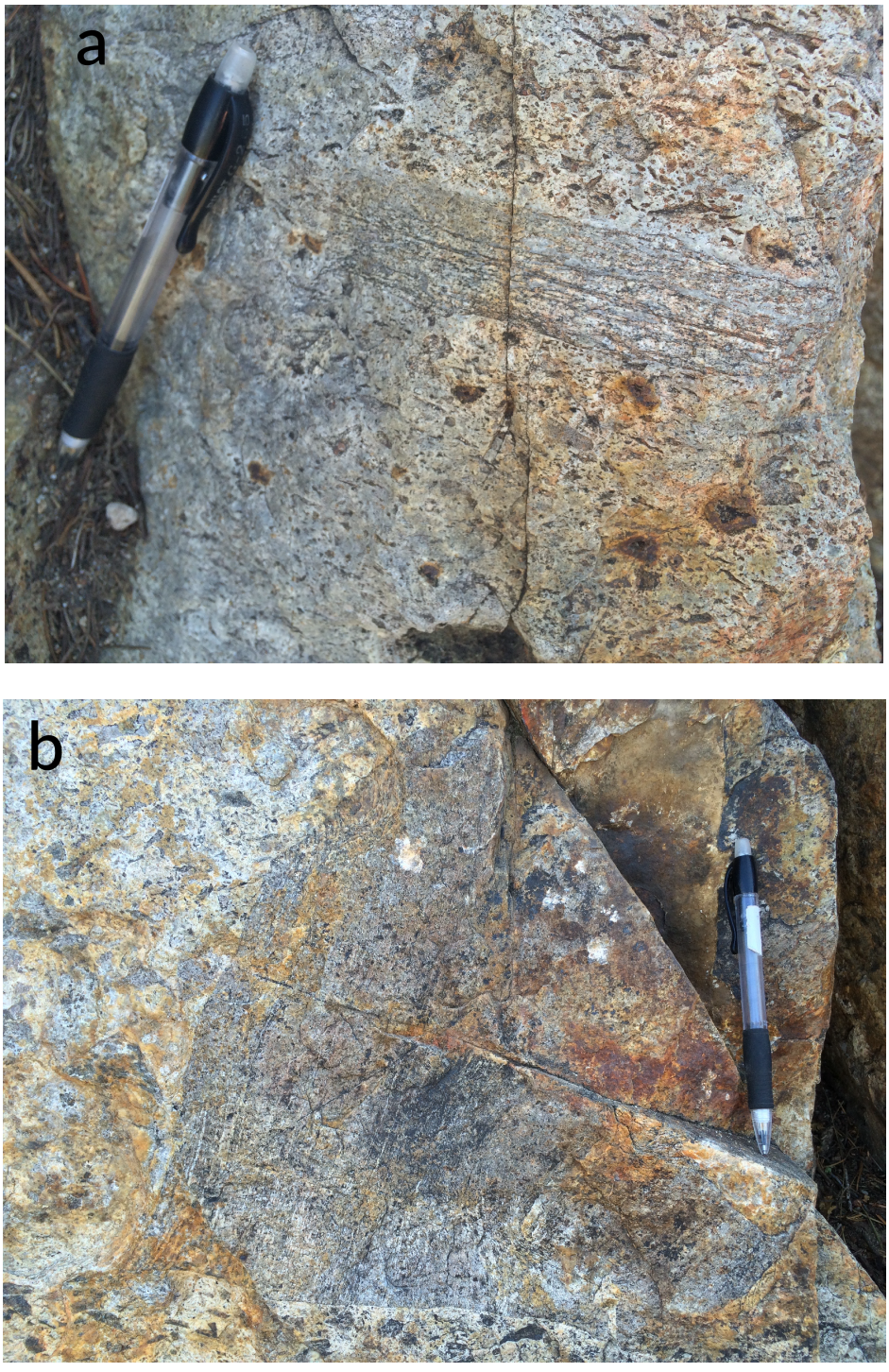

Figure 9: Angular, ragged sandstone clasts of in the upper monomictic breccia of Mammoth Lake. Pencil is 14 cm long.

Two conspicuous volcaniclastic sandstone beds punctuate the otherwise structureless monomictic facies in its upper half (Fig. 4). Both interbeds display highly irregular contacts with the monomictic breccia (Fig. 12). The two beds are separated by 12 meters of monomictic breccia (Fig. 4). The lower sandstone bed is 60 cm thick and contains two 30-cm cross-beds separated by a sharp interface (Fig. 11a) The lower cross-set is truncated at the interface whereas the upper set has an asymptotic base, indicating the unit is oriented upright. Average grain size of the lower sandstone bed is 0.5-1 mm. The upper sandstone bed is 140 cm thick, and is planar-laminated (Fig. 11b). Laminations are 1-10 mm thick and wavy. For both sandstone beds, bedding is well defined by alternating light and dark laminations. Average grain size of the upper sandstone bed is 1-2 mm. These two sandstones have the same mineral assemblage: 70% 0.5-2-mm recrystallized quartz grains, 20-25% subangular to subrounded pseudomorphic volcanic grains, and minor amounts of feldspar, mica, epidote, and oxide minerals (Fig. 10).

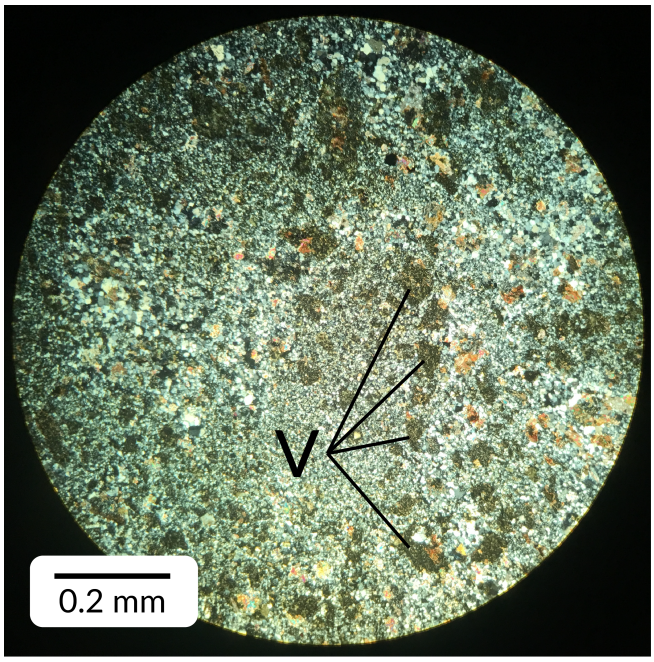

Figure 10: Photomicrograph of the sandstone facies (lower bed) of the breccia of Mammoth Rock under cross-polarized light and 10x magnification. V = volcanic clast.

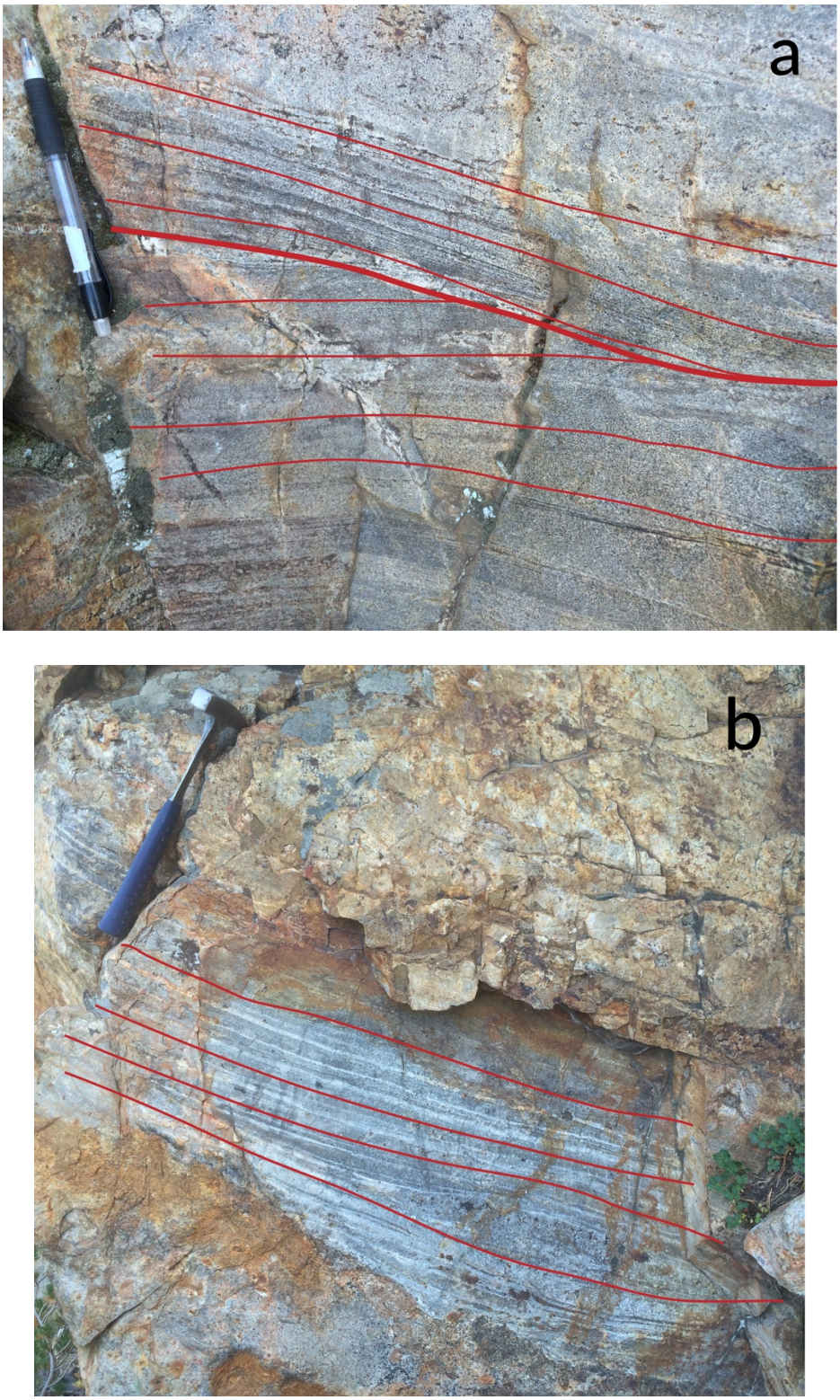

Figure 11: Sandstone facies of the breccia of Mammoth Rock. Red lines are laminations. (a) Lower bed, showing the interface (bold line) between cross-sets. Pencil is 14 cm long. (b) Upper bed, with planar, slightly wavy laminations. Hammer is 33 cm long.

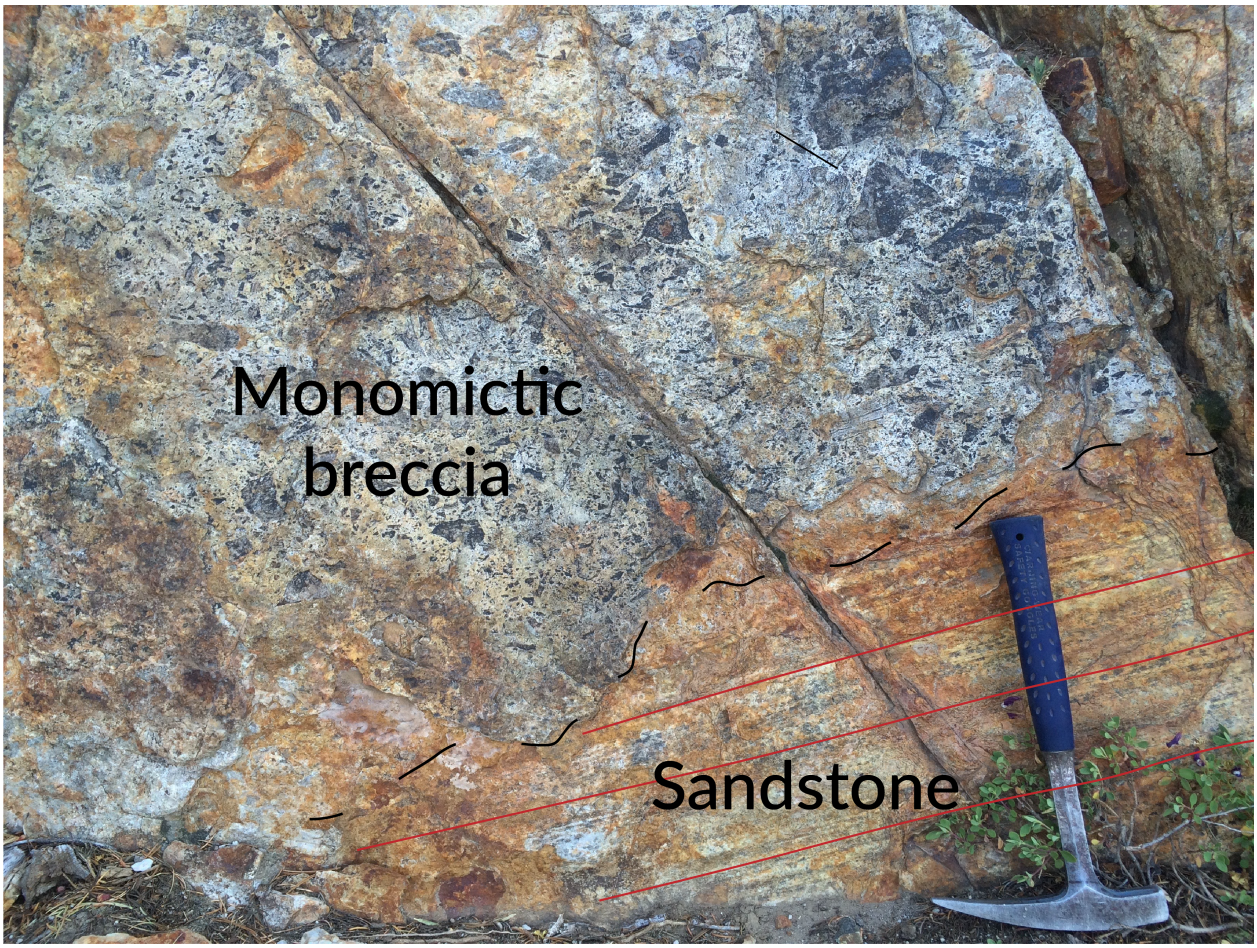

Figure 12: Sharp, irregular contact between heavily oxidized, planar-laminated sandstone and monomictic breccia of Mammoth Rock. Dashed black line is the contact. Red lines are sandstone laminations. Hammer is 33 cm long.

3.1.2 DACITE OF ARROWHEAD LAKE

The dacite of Arrowhead Lake (Trald, Fig. 2; "latite of Arrowhead Lake" of Rinehart and Ross, 1964) comprises a diverse suite of dacitic rocks including breccia, tuff, tuffaceous sandstone, and porphyritic lava. Tuffaceous strata unconformably overlie the breccia of Mammoth Rock at Mammoth Rock (Fig. 2). The dacite also extends 10 km along strike to the southeast corner of the pendant where it is truncated on its east side by a fault, with Pennsylvanian sedimentary rocks to the west. The suite has a maximum thickness of 1.5 km

northeast of Arrowhead Lake. The porphyritic lava cuts through the tuffaceous rocks and intrudes the tuff of Skelton Lake. Because intrusive facies grade laterally into extrusive facies (Rinehart and Ross, 1964) it is difficult to map them as wholly separate units. In the far northwest corner of the pendant, the dacite of Arrowhead Lake is severely altered to a pyritic hornfels composition (Rinehart and Ross, 1964) and weathers to a bright red color. Stratigraphic observations were made in the North Fork Fish Creek area (Figs. 13, 14) where alteration is minimal and facies are well exposed.

The lowermost strata of the dacite of Arrowhead Lake includes intercalated breccia, tuff, and tuffaceous sandstone of dacitic composition. The breccia has a maximum thickness of 60 meters on the southwest ridge of Red Slate Mountain (Fig. 14) and pinches abruptly to the southwest (Fig. 13). This unit contains 20-30% light to dark grey, subangular to subrounded dacite porphyry clasts in a grey to purple tuffaceous matrix (Fig. 15). The clasts are identical in texture and composition to the intrusive dacite porphyry higher in the section. Clast diameter ranges from 5-50 cm, with some up to one meter. Many clasts have cuspate edges and some are jigsaw fractured similar to hyaloclastite (Fig. 16). The tuffaceous matrix contains 10-15% subhedral feldspar phenocrysts and 5-10% wispy, ragged pumice fragments.

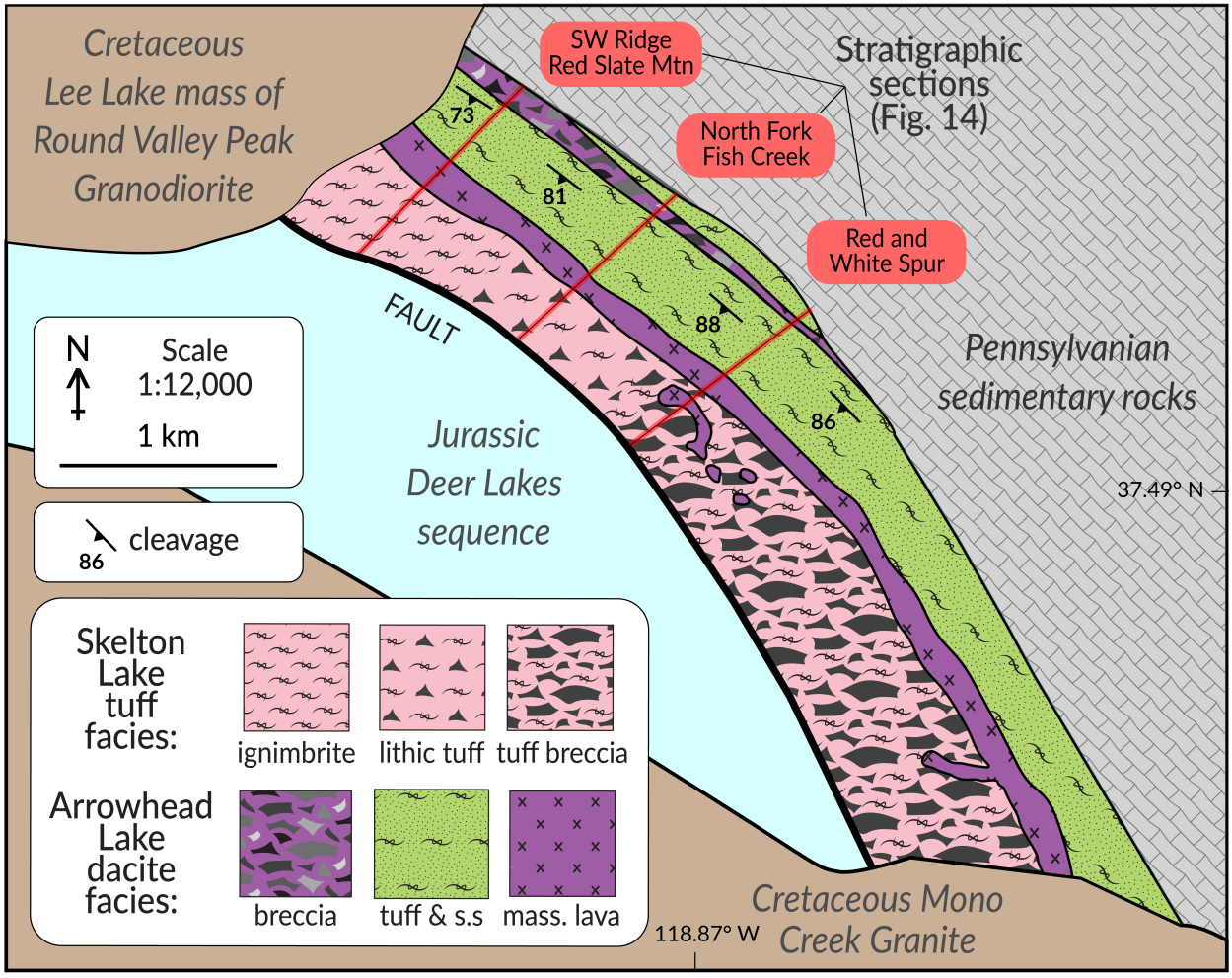

Figure 13: Facies map of Triassic rocks in the southeast Mount Morrison pendant (North Fork Fisk Creek area, Fig. 2) with selected cleavage measurements for tuffaceous facies of the dacite of Arrowhead Lake shown for orientation. Red lines correspond to stratigraphic sections (Fig. 14).

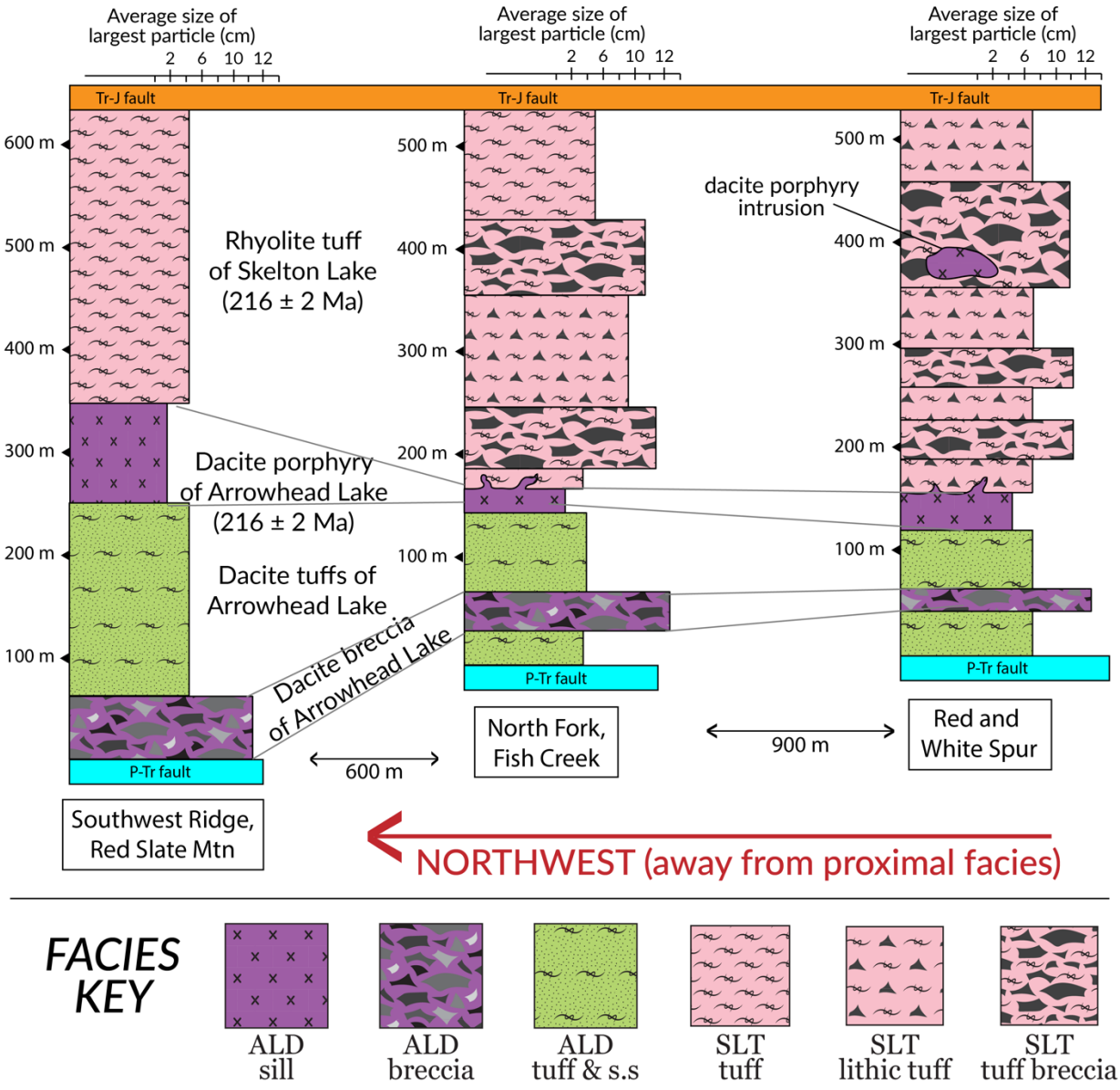

Figure 14: Stratigraphic sections of Triassic rocks in the southeast Mount Morrison pendant (North Fork, Fish Creek area). Locations correspond to the North Fork Fish Creek area map (Fig. 13). ALD = dacite of Arrowhead Lake, SLT = tuff of Skelton Lake.



Figure 15: Typical outcrops of the breccia facies of the dacite of Arrowhead Lake, showing range of clast sizes. Hammer is 33 cm long.

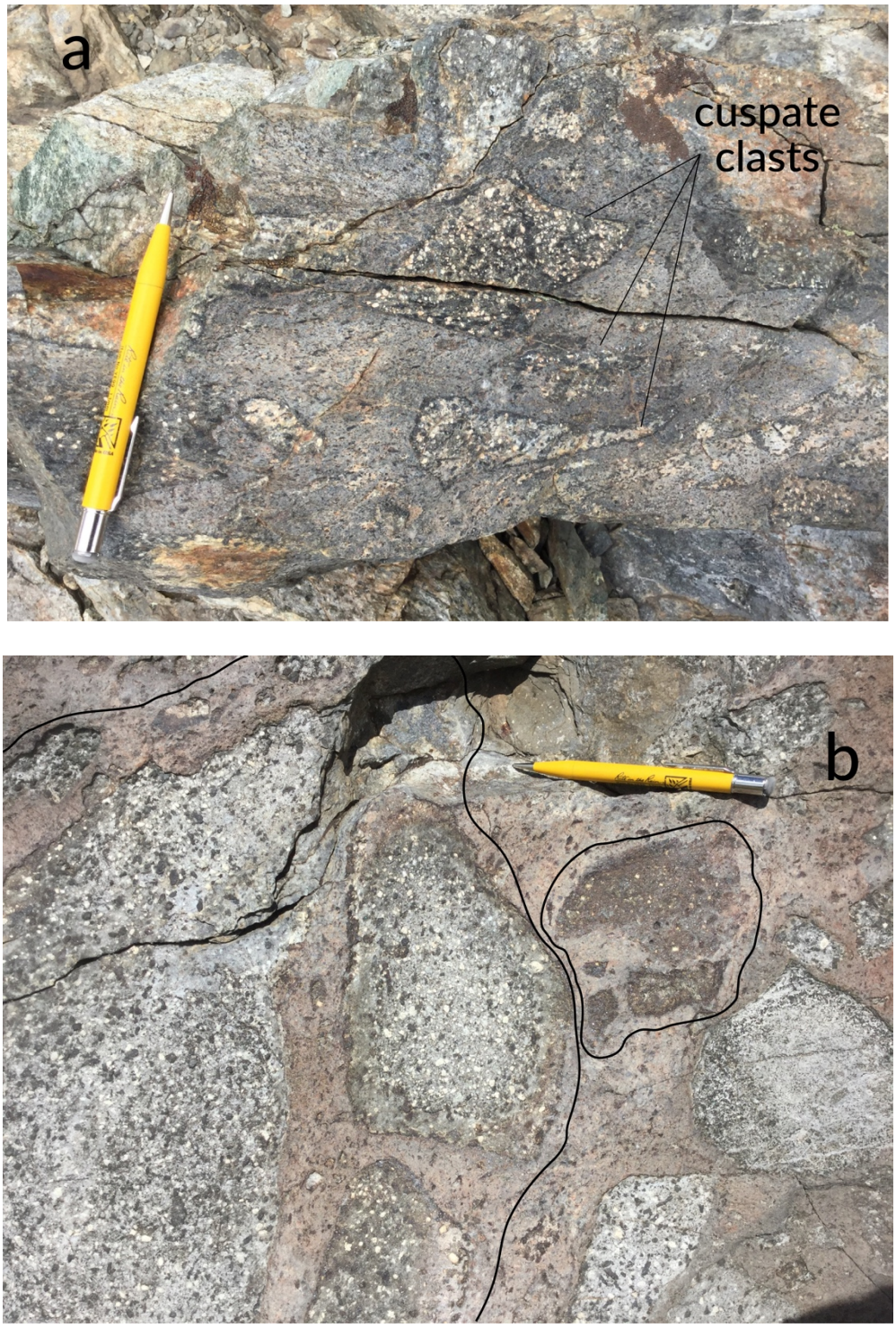

Figure 16: Clast textures in the breccia facies of the dacite of Arrowhead Lake. (a) Cuspate clast margins. (b) Jigsaw clasts (circled). Pencil is 14 cm long. (Location: SW Ridge, Red Slate Mountain; Fig. 13).

Interlayered tuffaceous sedimentary facies in the dacite of Arrowhead Lake (Fig. 17) include finely laminated siltstone, coarse-grained sandstone, and conglomerate. The rocks are interlayered, have the general texture of reworked dacite tuff, and grade laterally into the compositionally similar intrusive facies of the dacite of the Arrowhead Lake. Contacts between tuffaceous strata are generally wavy, and beds are commonly lenticular. Conglomerate (Fig. 17a) occurs as 3-5-meter-wide, 1-2-meter-thick lenses within 5-10-meter-thick layers of sandstone. Conglomerate beds have 5-10-cm dacite clasts aligned along regional foliation. Finer-grained reworked pyroclastic strata (primarily siltstones and coarse sandstones) have very well defined cm- to dm-scale beds (Fig. 17b). Sandstone facies are poorly sorted and have 60-70% recrystallized quartz grains with 30-40% metamorphic mica and epidote and 5-10% albitic plagioclase.

Tuffs associated with the dacite of Arrowhead Lake are interlayered with the tuffaceous sandstones and intruded by the porphyritic lava. The typical sample (Fig. 18) contains 15% angular pumice fragments (up to 2 cm long, flattened 10:1 along strike), and 10% white, subhedral plagioclase crystals (up to 1 cm) and 2-3% subhedral, broken quartz phenocrysts (up to 1 cm) in a light grey ash matrix. Some outcrops have a vesicular texture due to plucked-out pumice fragments.

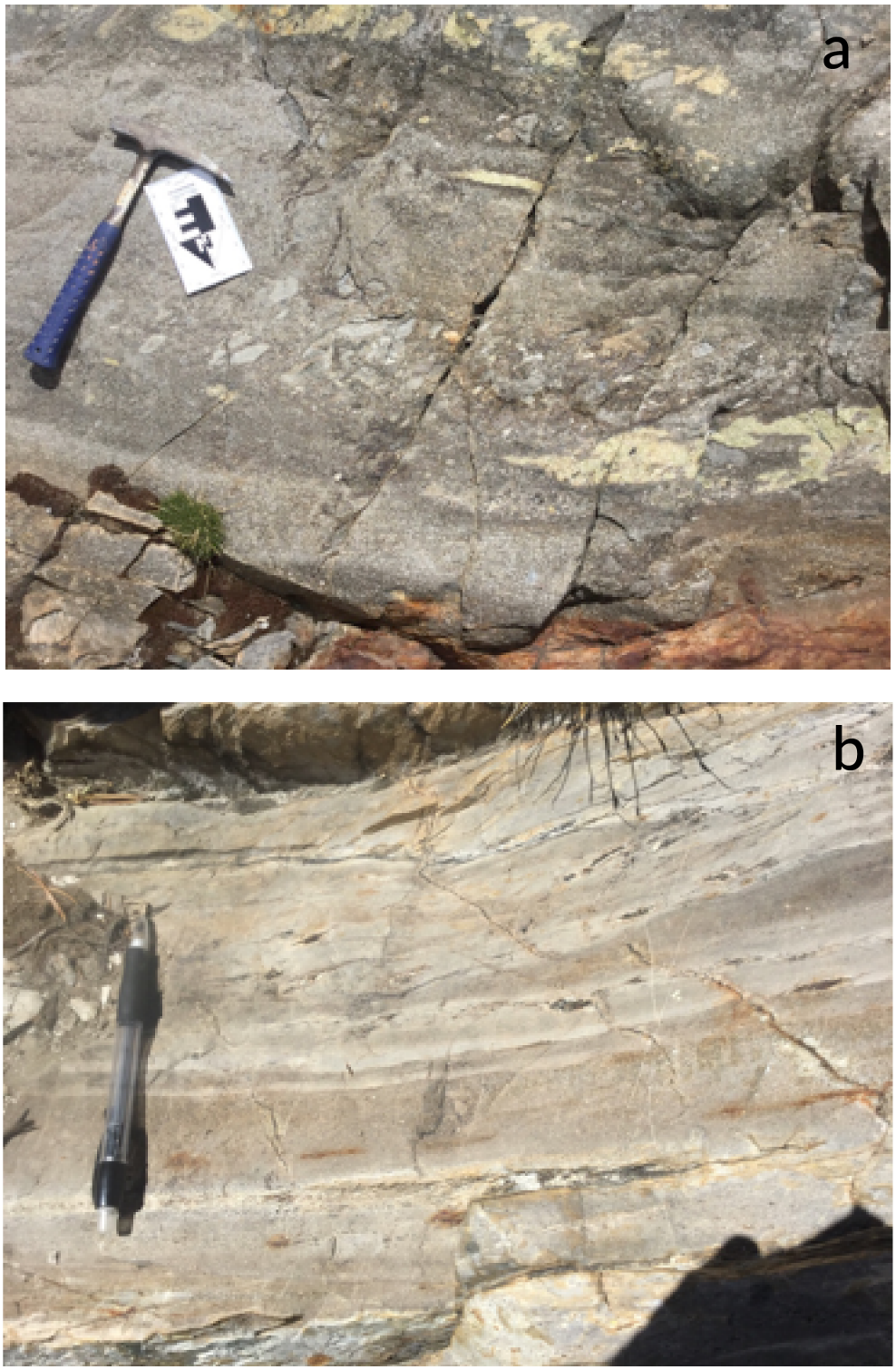

Figure 17: Tuffaceous sedimentary rocks associated with the dacite of Arrowhead Lake. (a) Coarse-grained sandstone with two conglomerate lenses outlined in black line. Hammer is 33 cm long. (b) Irregular layers of reworked fine-grained tuffaceous material with black lines for bedding. Pencil is 14 cm long. (Location: SW Ridge, Red Slate Mountain, Fig. 13).



Figure 18: Typical outcrop of Arrowhead Lake tuff with white feldspar phenocrysts and dark, wispy pumice fragments (faint). Pen is 14 cm long. (Location: North Fork Fish Creek; Fig. 13).

The most prominent unit in the dacite of Arrowhead Lake is a laterally continuous, regionally concordant mass of massive, dacitic, porphyritic lava that intrudes the tuffaceous rocks as well as the tuff of Skelton Lake at several localities (Figs. 2, 3). Dikes and sills of the dacite lava intrude the tuff of Skelton Lake in the Duck Lake area (Fig. 19) and in the North Fork Fish Creek area (Fig. 20). It has an approximate maximum thickness along strike of 100 meters. A typical sample (Fig. 21) contains 25-30% euhedral, round, white feldspar phenocrysts in a dark grey groundmass. The intact, unbroken nature of phenocrysts suggests emplacement by effusive flow instead of explosive. Mafic minerals are replaced by chlorite-epidote aggregates. The groundmass is a dense microcrystalline mosaic of quartz, feldspar, and mica with abundant (40%) feldspar microlites (Fig 22).

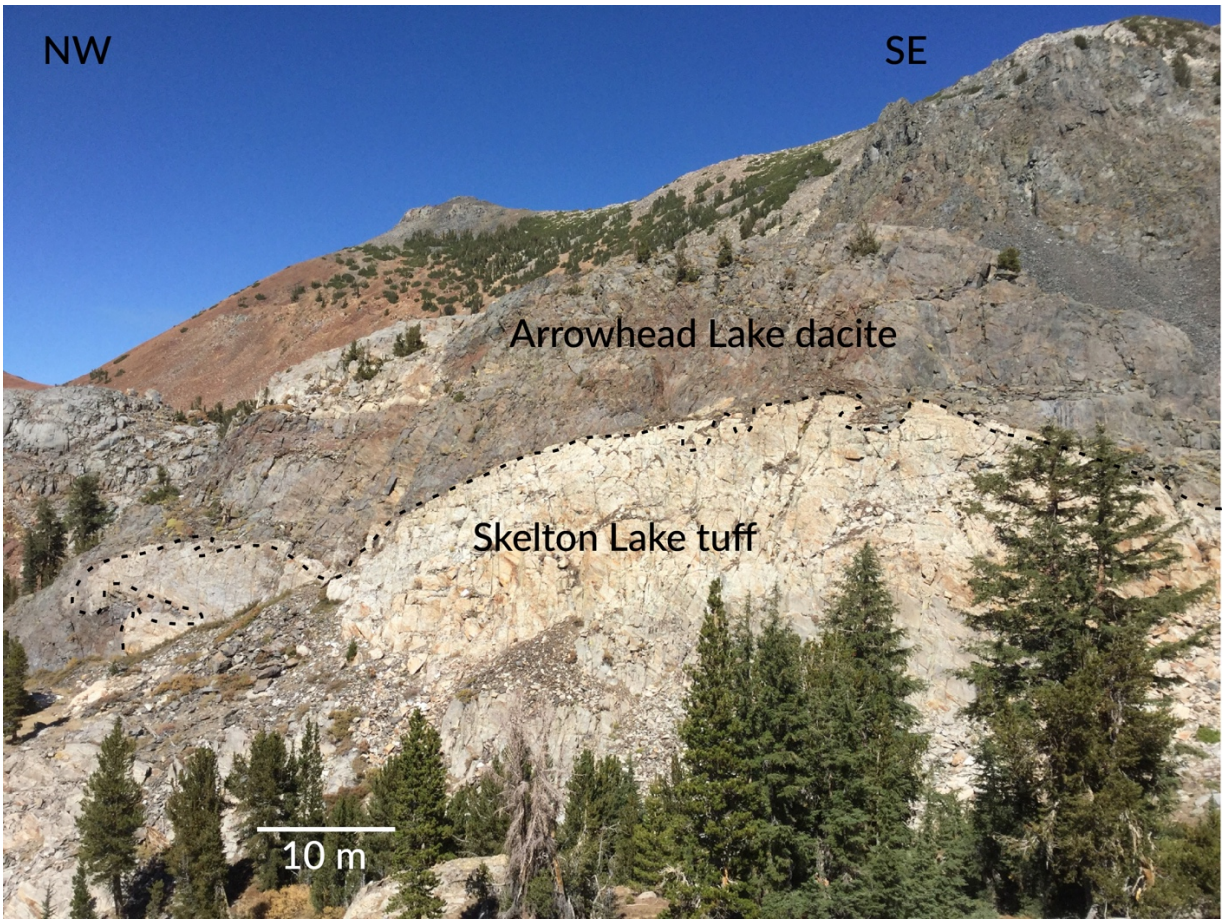

Figure 19: Looking northeast at the irregular, intrusive contact between the dacite of Arrowhead Lake (dark grey) and the tuff of Skelton Lake (white) in the central part of the pendant, northwest of Duck Lake.

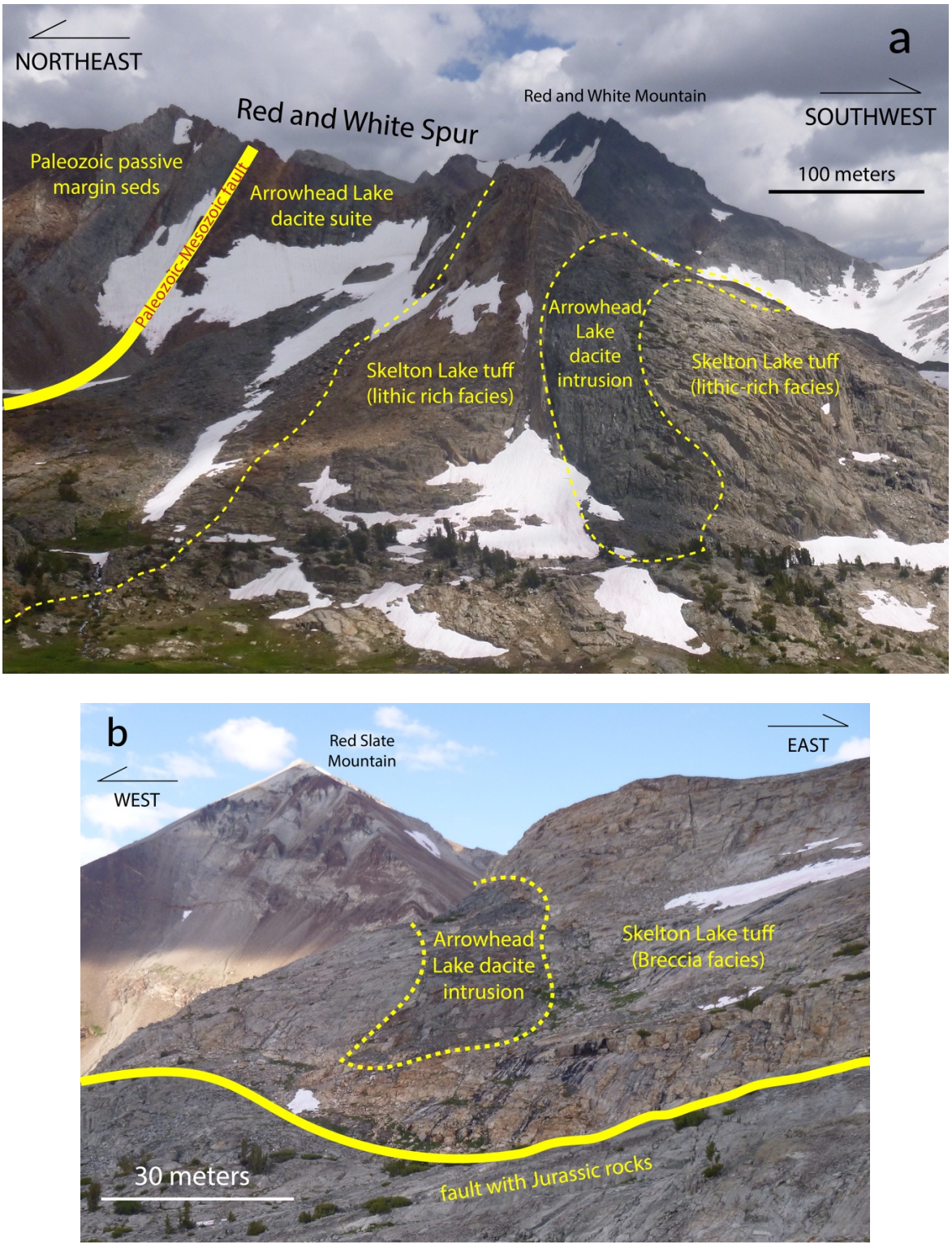

Figure 20: (a) Looking east-southeast at the Triassic sequence on Red and White Spur, showing a large intrusion of dacite of Arrowhead Lake. (b) Looking northeast across the Triassic-Jurassic fault at the same dacite intrusion within the tuff of Skelton Lake.



Figure 21: Typical outcrop of the massive, porphyritic lava facies of the dacite of Arrowhead Lake, showing abundance of plagioclase phenocrysts. Pencil is 14 cm long. (Location: SW Ridge, Red Slate Mountain; Fig. 13).

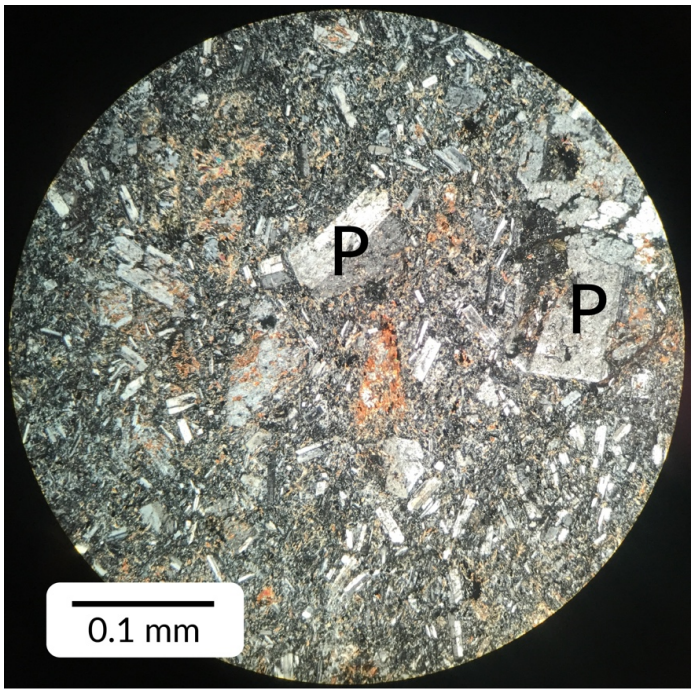

Figure 22: Photomicrograph of porphyritic facies of the dacite of Arrowhead Lake in cross-polarized light and 25x magnification. P = plagioclase phenocryst.

3.1.3 TUFF OF SKELTON LAKE

The tuff of Skelton Lake (Trslt, Fig. 2; "quartz latite tuff of Skelton Lake" of Rinehart and Ross, 1964) is the most voluminous unit in the pendant, with a maximum thickness of 1.2 km. This unit is divided in two by the Lee Lake mass of the Round Valley Peak Granodiorite, with tuff and tuff breccia in the southeast corner of the pendant and a regionally extensive tuff exposed to the northwest continuously 10 km along strike.

The tuff is easily recognized by abundant (up to 25%) quartz phenocrysts, 10% feldspar phenocrysts and 10-15% pumice fragments in a light to medium grey, quartzose matrix (Fig. 23). Quartz phenocrysts (Fig. 24a) are globular, subhedral, and 2-5 mm in diameter. Feldspar phenocrysts are slightly smaller (1-2 mm) and variably albitized and corroded by the groundmass to produce indistinct grain boundaries. Pumice fragments (Figs. 24b, 24c) are pseudomorphically replaced by birefringent mica containing small inclusions of microcrystalline quartzofeldspathic aggregates. These wispy, ragged clasts are commonly 1-5 cm long and flattened 10:1 along regional strike. Smaller (1-2 mm) pumice fragments appear stretched and sinuous, and viscous attenuation is observed locally between phenocrysts (Fig. 24c). Rinehart and Ross (1964) inferred that these textures represent relict welding of the tuff. Strains of mica and epidote are commonly bent around angular quartz and feldspar phenocrysts (Fig. 24b).



Figure 23: Typical outcrops of the tuff of Skelton Lake showing size range of pumice fragments. Pencil is 14 cm long. (Location: North Fork Fish Creek; Fig. 13).

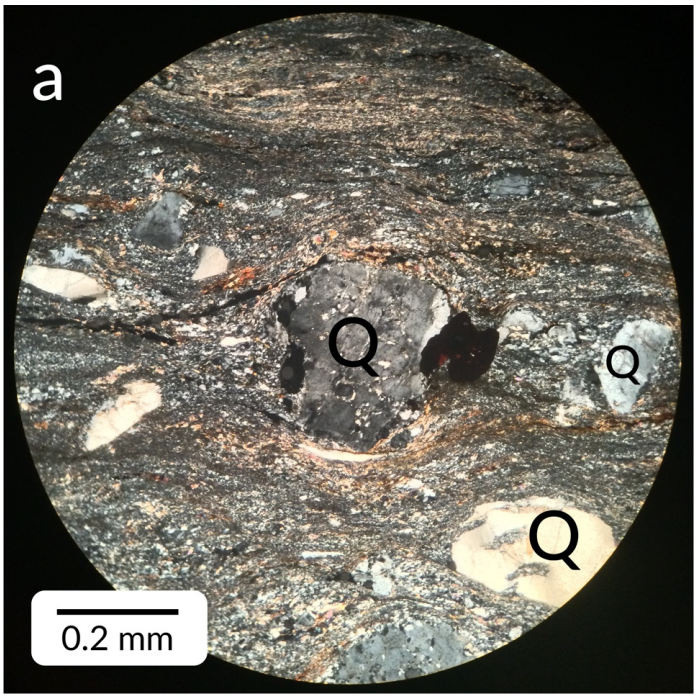

Figure 24 (continued on next page): Photomicrographs of the tuff of Skelton Lake under cross-polarized light at 10x magnification. (a) Mica and epidote strands bent around quartz phenocrysts. (b, c) Ragged, wispy pumice fragments (P) pseudomorphically replaced by mica. Q = quartz phenocryst.

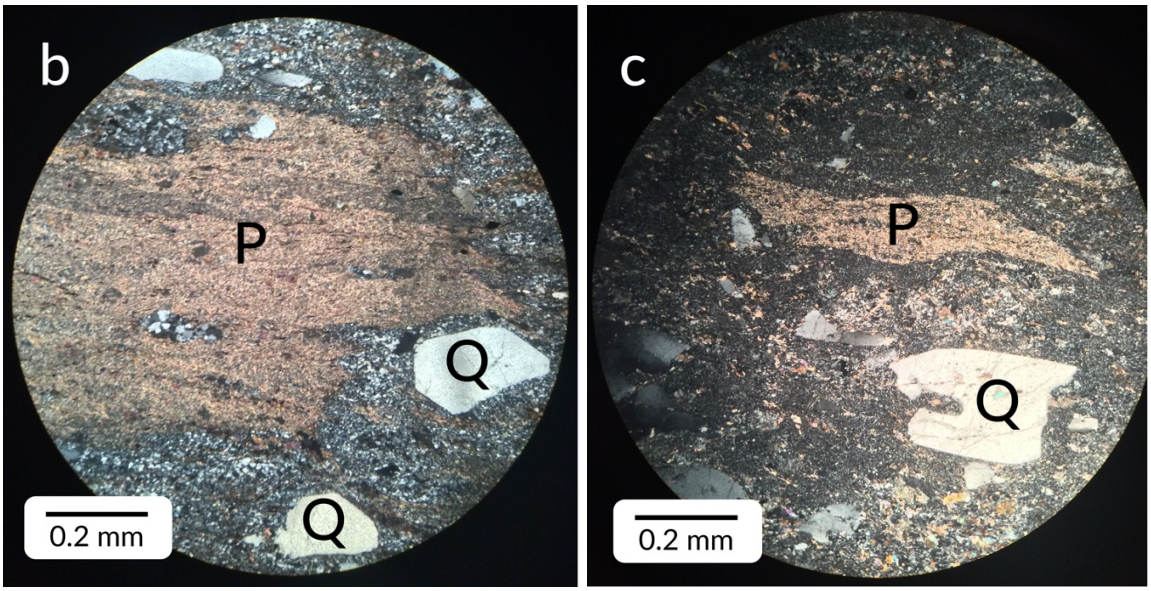

Figure 24 (continued from previous page): Photomicrographs of the tuff of Skelton Lake under cross-polarized light at 10x magnification. (a) Mica and epidote strands bent around quartz phenocrysts. (b, c) Ragged, wispy pumice fragments (P) pseudomorphically replaced by mica. Q = quartz phenocryst.

The tuff of Skelton Lake is monotonous everywhere except in the North Fork Fish Creek area (Fig. 13). Here, the usual crystal-rich tuff is interrupted by thick lenses of tuff breccia with 20-30% angular to subangular lithic clasts (up to one meter diameter) (Fig. 25a). The majority of these clasts are dark and aphyric (Fig. 25b), while others are grey dacite tuff (Fig. 25c). Breccia facies are only present in the southern half of North Fork Fish Creek area (Figs. 2, 13). Within the brecciated zone, clast size, angularity, and concentration increase to the southeast.

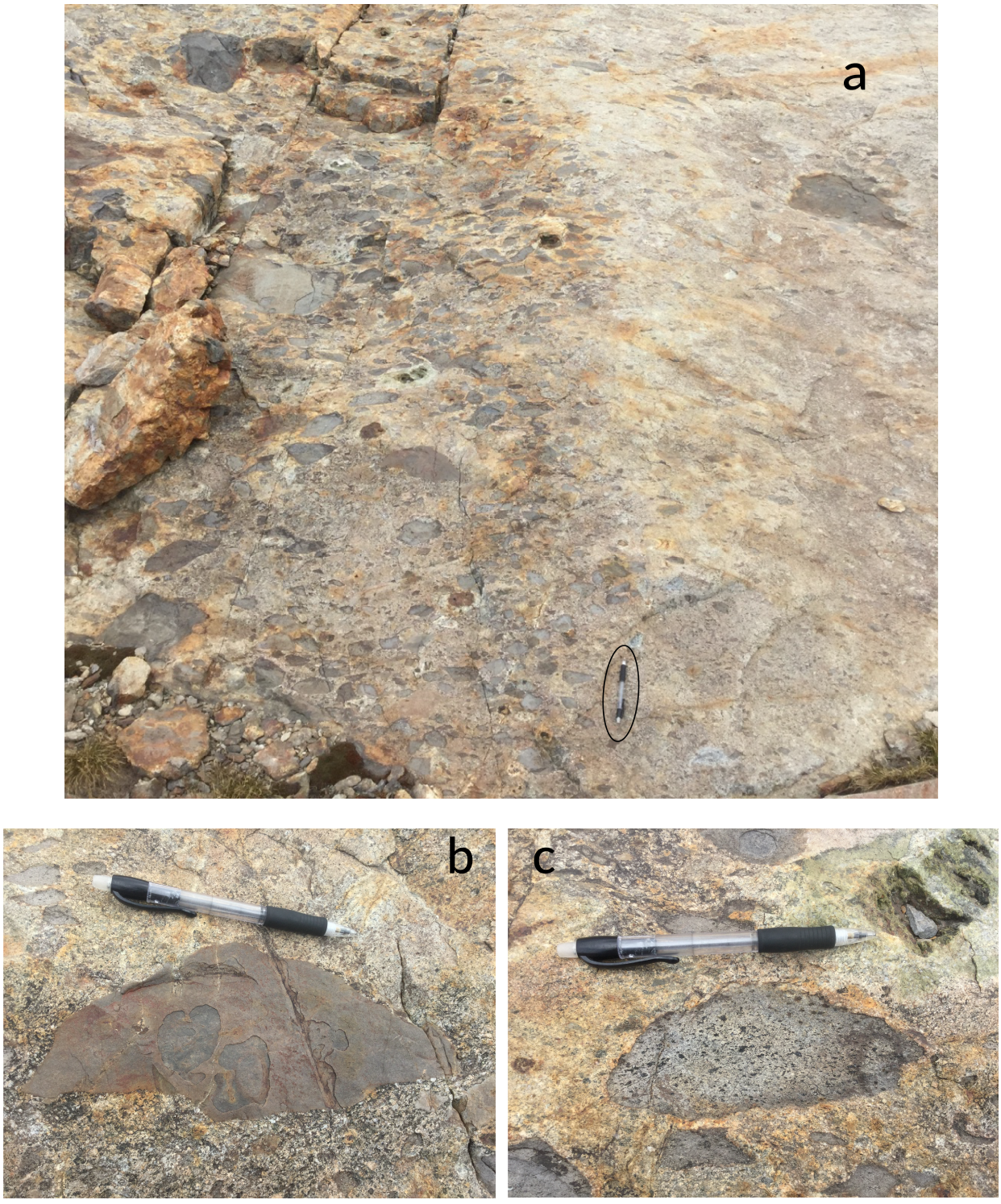

Figure 25: Breccia facies of the tuff of Skelton Lake in the North Fork Fish Creek area. (a) Tuff breccia lens. (b) Aphyric volcanic clast. (c) Andesite(?) tuff clast. Pencil is 14 cm long. (Location: Red and White Spur; Fig. 13).

3.1.4 BRECCIA OF PIKA LAKE

A localized (~0.02 km^2) mass of Triassic breccia crops out along the fault contact between the Triassic and Cretaceous structural blocks on the ridgeline southwest of Pika Lake (Fig. 2). The rock has a very distinctive appearance, with light-grey volcanic clasts set in a dark green matrix (Fig. 26). Clasts are roughly aligned along strike. Grain-size variations are commonly abrupt, with clast-supported and matrix-supported zones appearing adjacent to one another. Clasts account for 40-60% of the rock, are angular to subangular and poorly sorted, and range from 5 to 50 cm in diameter. All of the clasts are volcanic, with 5-10% dark phenocrysts in a light-grey matrix. Jigsaw clasts are common (Fig. 27).

Primary petrographic study of this unit is hindered by severe saussuritization, as the unit is composed almost entirely of metamorphic minerals. Both matrix and clast material have been overprinted by epidote, chlorite, biotite, and subhedral microcrystalline quartz. Clasts are slightly coarser grained and more quartzose than the matrix. Quartz and plagioclase phenocrysts, where present within the clasts, are deeply embayed. The matrix is aphyric and dominated by fine-grained chlorite and epidote overprinting microcrystalline quartz and feldspar.

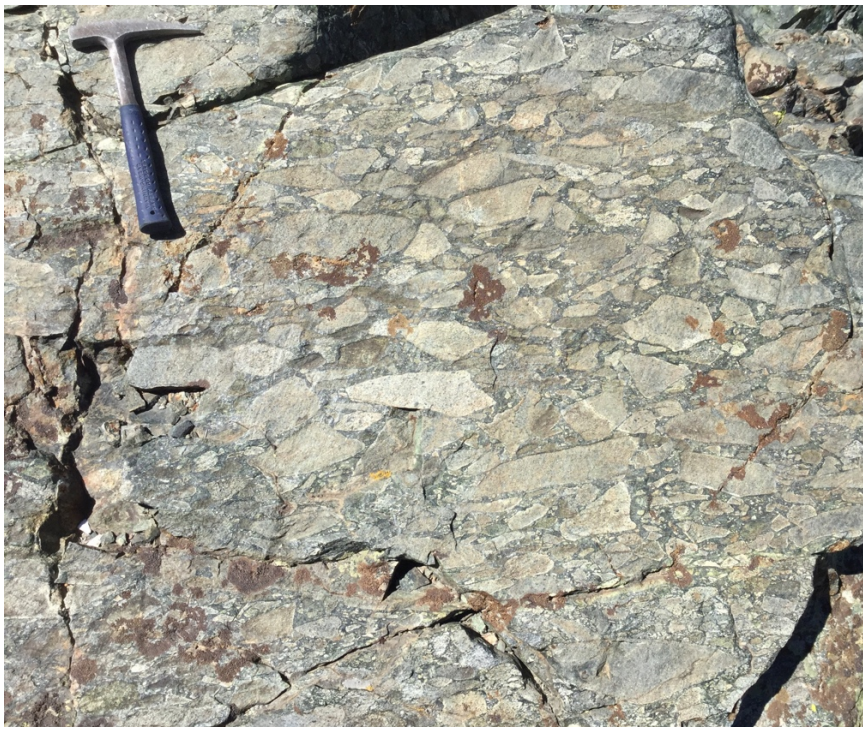

Figure 26: Typical outcrop of the breccia of Pika Lake showing clast angularity. Hammer is 33 cm long. (Location: unnamed ridge east of Duck Lake; Fig. 2).



Figure 27: Jigsaw clasts in the breccia of Pika Lake. Pencil is 14 cm long. (Location: unnamed ridge east of Duck Lake; Fig. 2).

3.2 JURASSIC ROCKS

The Deer Lakes sequence (Jdls, Fig. 2) is a ~1.5-km-thick succession of dominantly pyroclastic material bound on the east by a fault with Triassic rocks and on the west by an intrusive contact with the Cretaceous Mono Creek Granite (Fig. 2). Facies grade laterally and vertically into one another, making it very difficult to map separate units in the field. The units are rhyolitic to dacitic in composition. These Jurassic rocks have strongly developed phyllitic cleavage, and rocks closest to the intrusive contact grade from micaceous phyllites to quartz schist, to hornfels. Saussuritization is prevalent throughout the unit. Piemontite alteration extends from the fault with Cretaceous rocks, altering the lowermost tuffs to a brilliant pink color.

The Deer Lakes sequence is dominated by lenticular bodies of tuff and tuff breccia. Fine-grained tuffs (Fig. 28a) are well sorted and have 1-5 mm laminae. The rhyolite tuff facies is poorly sorted and contains 20-25% globular, subhedral quartz phenocrysts, 5-10% subhedral feldspar phenocrysts, 5-10% angular, ragged pumice fragments, and up to 5% quartzite clasts. These tuff facies are compositionally similar to the tuff of Skelton Lake, but have a highly sheared texture, with 3:1 to 6:1 clast elongation.

Two types of breccia facies are present in the Jurassic block. One variety of breccia (Fig. 28b) has 1-10-cm angular lithic fragments in a rhyolite tuff(?) matrix. Another breccia facies (Fig. 28c) contains 1-5-meter subrounded dacitic lava(?) clasts in a dacitic lava(?) groundmass. Although different facies are present throughout the Jurassic block, there is an overall grain-size increase northwestward as tuff breccia and dacite breccia grade into successively finer-grained tuffs.

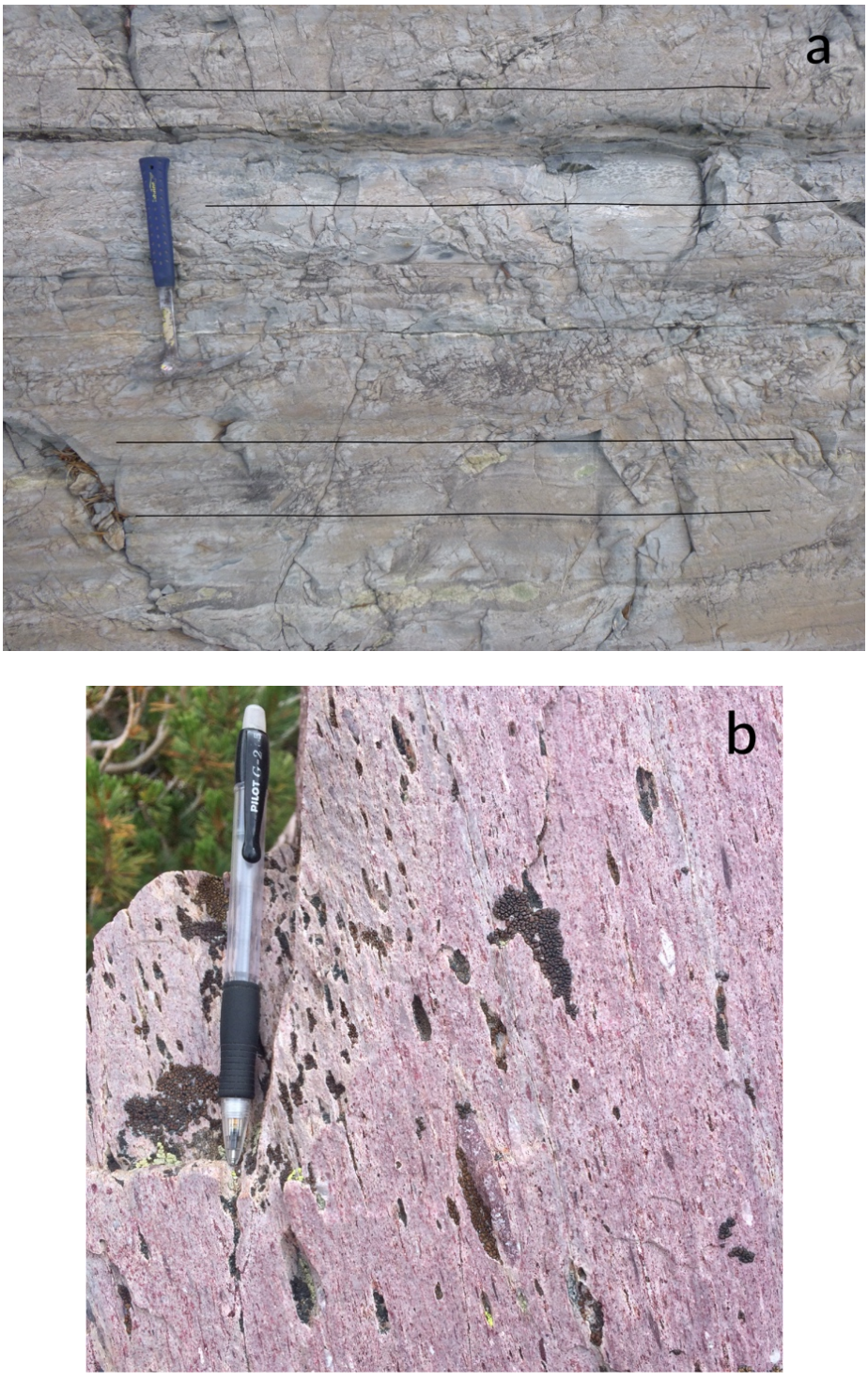

Figure 28 (continued on next page): Facies of the Jurassic Deer Lakes sequence in Deer Lakes basin (Fig. 2). (a) Finely laminated facies. Black lines show bedding. Hammer is 33 cm long. (b) Rhyolite tuff with pumice and quartzite clasts stretched along regional foliation direction. Pink color is due to piemontite alteration. (c) Tuff breccia with clasts deformed along strike. (d) Poorly sorted dacite breccia with large, subrounded to rounded dacite porphyry clasts. Pencil is 14 cm long.





Figure 28 (continued from previous page): Facies of the Jurassic Deer Lakes sequence in Deer Lakes basin (Fig. 2). (a) Finely laminated facies. Black lines show bedding. Hammer is 33 cm long. (b) Rhyolite tuff with pumice and quartzite clasts stretched along regional foliation direction. Pink color is due to piemontite alteration. (c) Tuff breccia with clasts deformed along strike. (d) Poorly sorted dacite breccia with large, subrounded to rounded dacite porphyry clasts. Pencil is 14 cm long.

3.3 CRETACEOUS ROCKS

Volcanic and sedimentary Cretaceous rocks in the Mount Morrison pendant are here collectively referred to as the Duck Lake sequence (Kdls, Fig. 2). The sequence is mapped as a lenticular tectonic slice, bound on the southwest by a fault with the Jurassic block, and on the northeast by a fault with the Triassic block (Fig. 2). The Duck Lake sequence includes rhyolite lava, andesite lava, rhyolite tuff and tuffaceous sandstone, shale, and limestone (Figs. 29, 30). The two thick marker units are the rhyolite of Purple Lake and the andesite of Mammoth Crest.

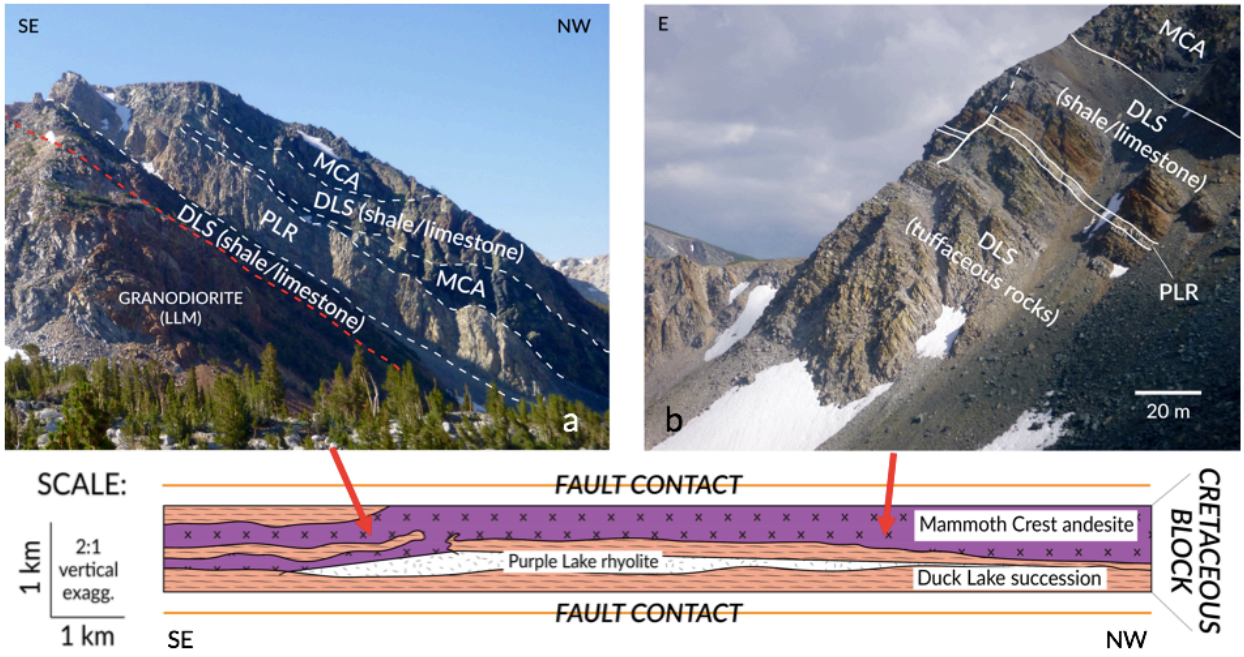

Figure 29: Outcrops of Duck Lake sequence showing stratigraphy. (a) Looking southwest at the lower part of the sequence exposed on the ridge immediately southeast of Purple Lake. (b) The lower part of the sequence exposed on the Mammoth Crest. Unit abbreviations: LLM = Lee Lake Mass, DLS = Duck Lake sequence (facies type in parentheses), PLR = rhyolite of Purple Lake, MCA = andesite of Mammoth Crest. Facies key for schematic cross-section according to Fig. 3.

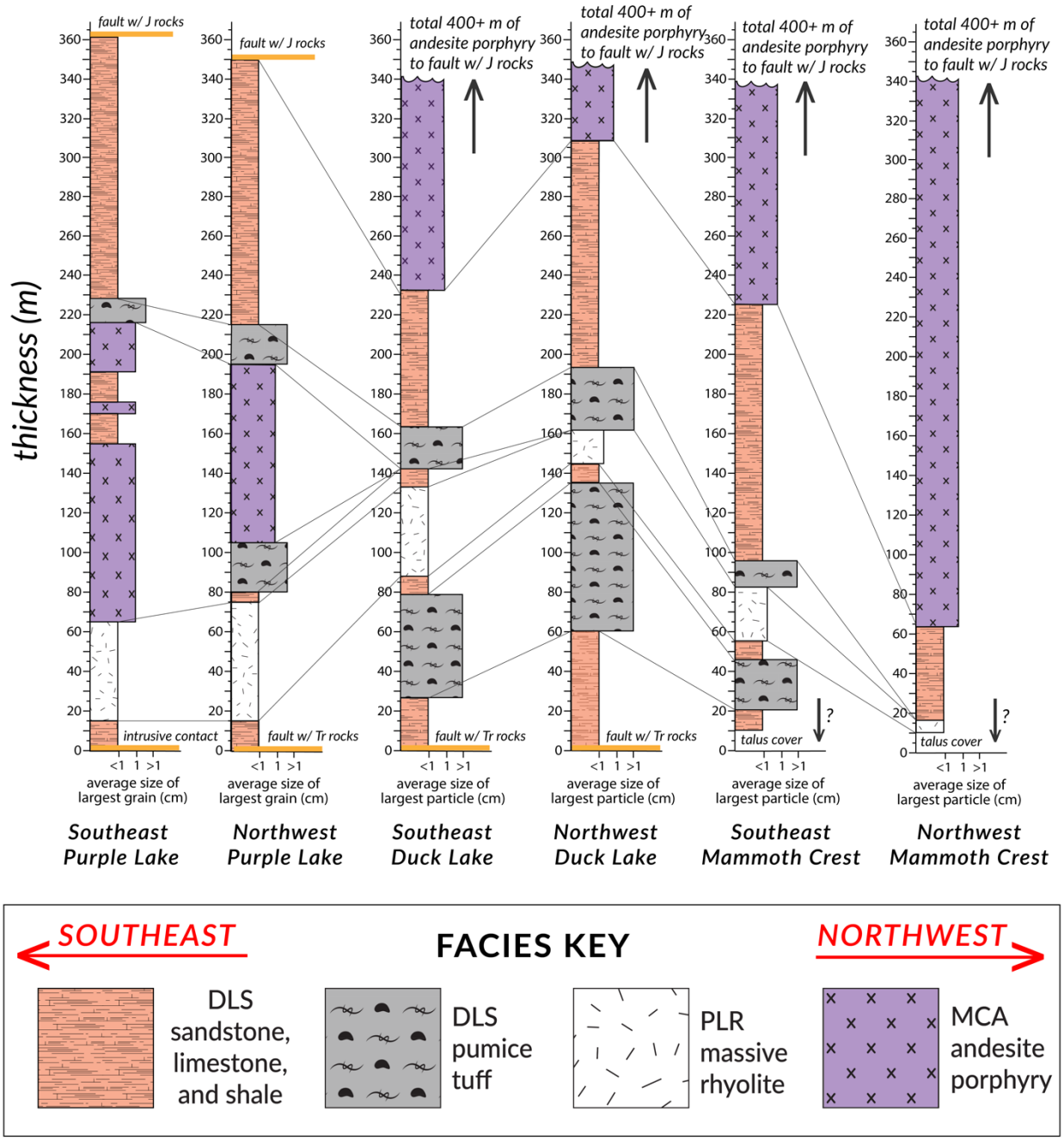

Figure 30: Stratigraphy of the Cretaceous Duck Lake sequence. Locations correspond to Figure 2. Note that the andesite porphyry facies is greater than 400 meters thick in the northwest part of the pendant. Locations correspond to labels on Fig. 2. Unit abbreviations: DLS = Duck Lake succession, PLR = rhyolite of Purple Lake, MCA = andesite of Mammoth Crest.

3.3.1 RHYOLITE OF PURPLE LAKE

The most distinct unit in the Duck Lake sequence is the rhyolite of Purple Lake, a northwest-tapering bed of massive rhyolite lava. The rock is light grey on a fresh surface, weathering to a brilliant white color that makes it easily identifiable from even a distance of several kilometers. Both the texture and the mineral assemblage are unique to the pendant. The hand-sample texture is massive, aphyric, and sugary. In thin section (Fig. 31), the rock has 2-3% 2-3 mm subhedral, partially resorbed feldspar phenocrysts in a fine-grained groundmass of recrystallized quartz, feldspar, mica, and epidote. The unit pinches sharply toward the northwest from a maximum thickness of 60 meters at Purple Lake to a minimum thickness of six meters in the northwest part of the pendant (Figs. 29, 30). In the southeast direction, it thins to 50 meters before being truncated by the Cretaceous Lee Lake mass of the Round Valley Peak Granodiorite.

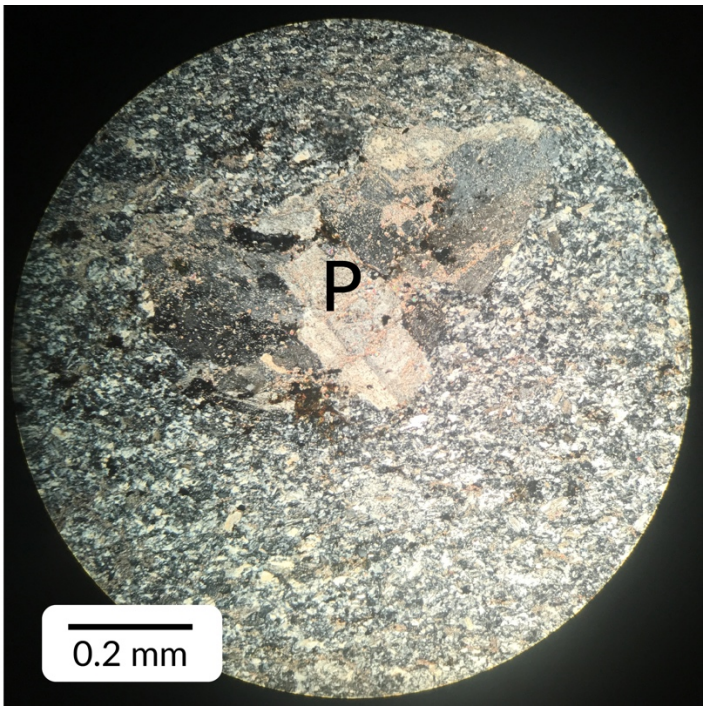

Figure 31: Photomicrograph of the rhyolite of Purple Lake under cross-polarized light at 10x magnification. P = plagioclase phenocryst.

3.3.2 ANDESITE OF MAMMOTH CREST

The most voluminous of the Cretaceous volcanic units is a dark purple, andesitic, porphyritic lava, more than 400 meters of exposed thickness in the northern half of the pendant (Figs. 29, 30). This unit forms high cliffs and ridges including the highest peaks (ca. 3,500 meters) of the Mammoth Crest. The andesite is intercalated with shales and limestones of the Duck Lake succession, which appear to have been either folded by the emplacement of the andesite or were slumped prior to emplacement of the andesite (Fig. 33). The andesite is massive and shows neither textural nor compositional variation. The rock is dark purple on both fresh and weathered surfaces but, in some places, it weathers grey. It commonly has a greenish tint due to abundance of secondary epidote. The andesite has a porphyritic texture, with 15-25% light grey to white feldspar phenocrysts up to 1-3 mm in diameter. In thin section (Fig. 32), these crystals are subhedral, intact, and albitized (Rinehart and Ross, 1964) due to metasomatism. Feldspar microlites, slightly larger than the matrix but not as large as the phenocrysts, make up an additional 20-30% of the rock. The matrix is a dense mosaic of recrystallized quartz, feldspar, mica, and mafic minerals.

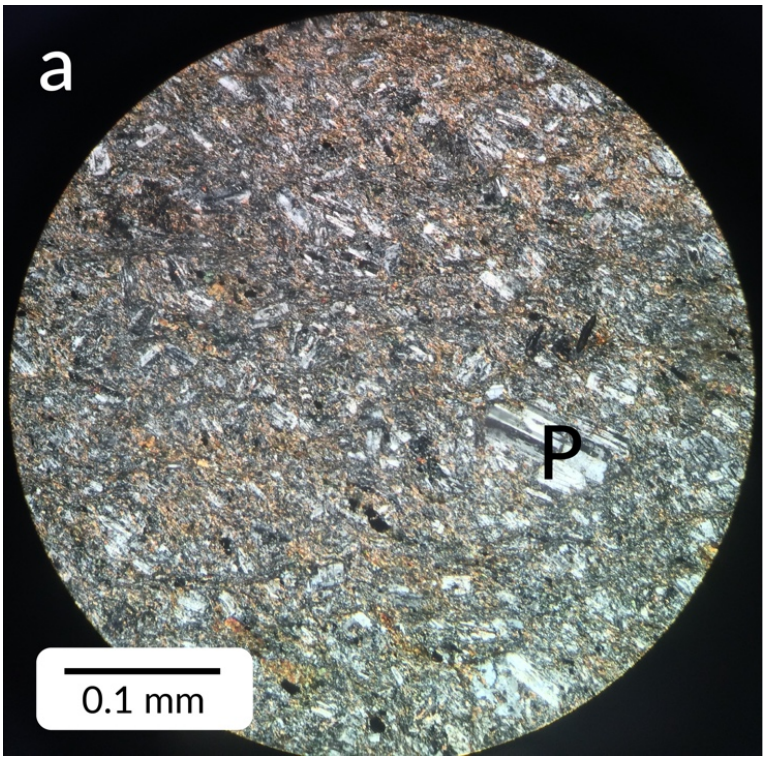

Figure 32: Photomicrograph under crossed-polarized light and 10x magnification of the andesite of Mammoth Crest showing abundance of albitic plagioclase. P = plagioclase phenocryst.

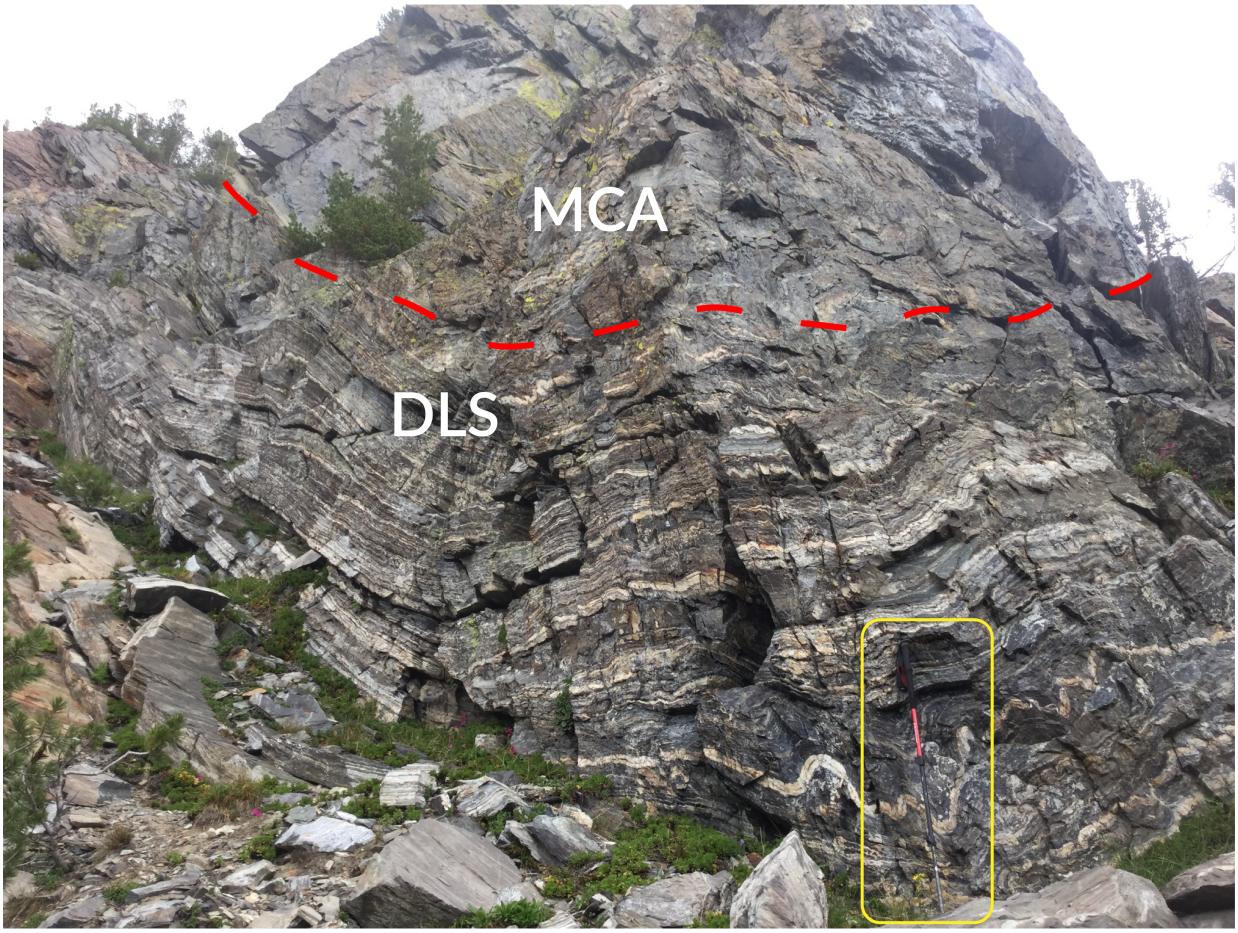

Figure 33: Laminated calc-silicate rocks of the Duck Lake succession (DLS) locally folded around the massive andesite of Mammoth Crest (MCA), south of Purple Lake. Trekking pole (yellow box) is 120 cm tall.

3.3.3 DUCK LAKE SUCCESSION

Calcareous, calc-silicate, and siliciclastic sedimentary rocks grouped as the Duck Lake sedimentary succession make up more than 200 m of the Cretaceous section in the Mount Morrison pendant. These multicolored strata are interlayered with the rhyolite of Purple Lake and the andesite of Mammoth Crest (Figs. 29, 30). The sedimentary succession displays a large-scale fining-upward sequence from coarse-grained sandstone to fine-grained shale and limestone. The lower part of the section contains 10-80-meter-thick beds of tuff and tuffaceous sandstone.

Light to medium grey rhyolite tuff is composed of 10-15% 2-5-mm, subhedral feldspar phenocrysts, 5% 2-5-mm, subhedral quartz phenocrysts, and less than 5% pumice fragments pseudomorphically replaced by mica aggregates, all in a microgranular quartzofeldspathic matrix. Sedimentary layers in the lower Duck Lake sedimentary succession (Fig. 34) include alternating bands of grey to green, coarse-grained volcaniclastic sandstone and dark grey siltstone. Sandstone beds are 10-20 cm thick whereas siltstone beds are 5-10 cm thick. Sandstone layers contain subangular to subrounded quartz and feldspar crystals that appear to have undergone minimal transportation as sedimentary grains. Siltstone beds are compacted, microcrystalline mats of mica with minor quartz and feldspar.

Calc-silicate rocks (Fig. 35) are most prevalent in the upper half of the Duck Lake sedimentary succession and are up to 140 meters thick at Purple Lake. These strata overlie the rhyolite of Purple Lake and appear to have been disrupted by the emplacement of the andesite of Mammoth Crest (Fig. 33). One of the layers disrupted by the andesite of Mammoth Crest is an 18-meter-thick layer of white to black limestone (Fig. 33) that is laterally continuous across the pendant. Extremely fine-grained calc-silicate minerals (dominantly quartz and calcite) are arranged in 1-2 mm-thick laminae.

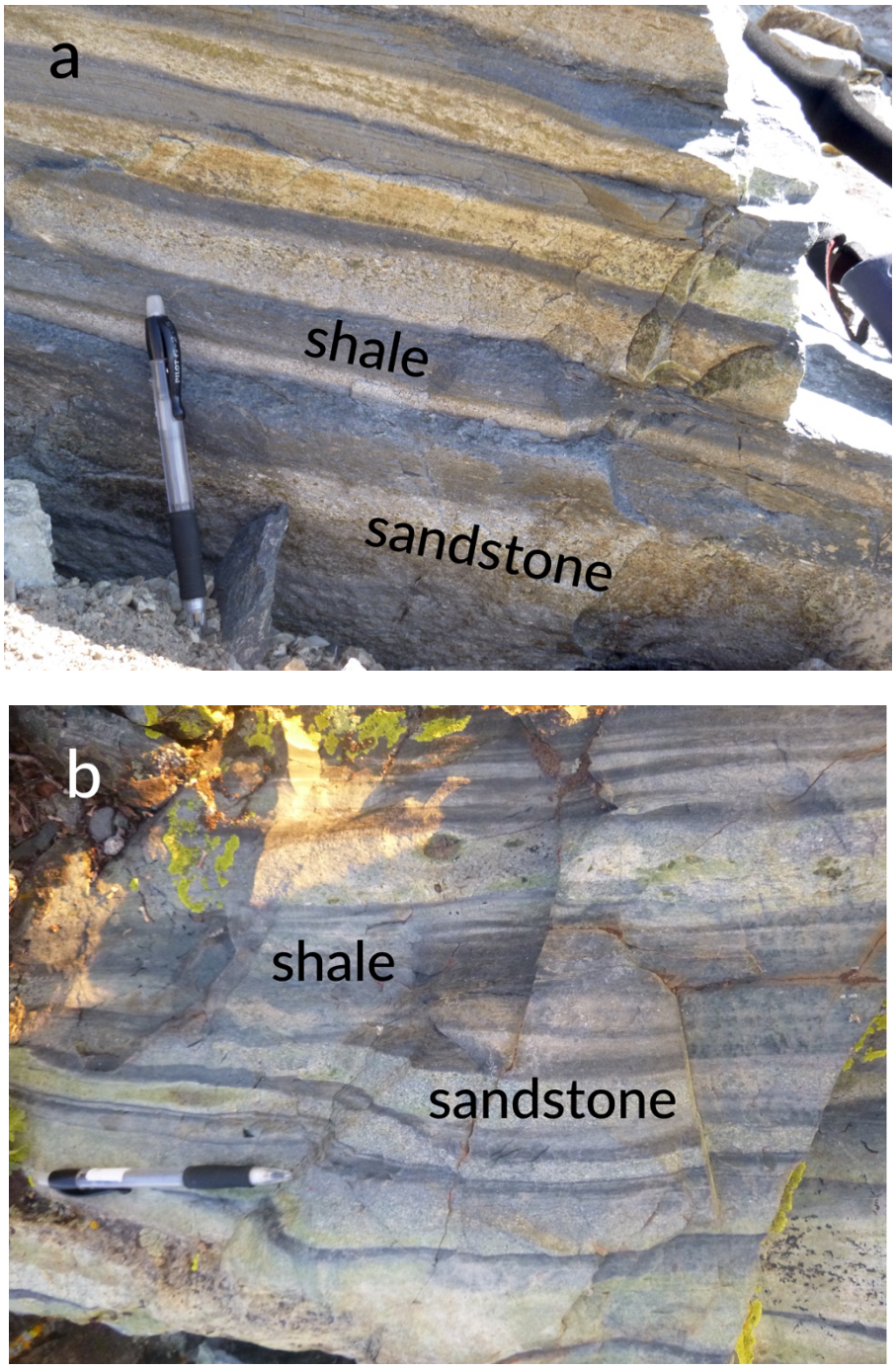

Figure 34: Alternating beds of sandstone (white) and shale (dark purple-grey) in the lower half of the Duck Lake sedimentary succession. Pencil is 14 cm long. (Location: Duck Lake).

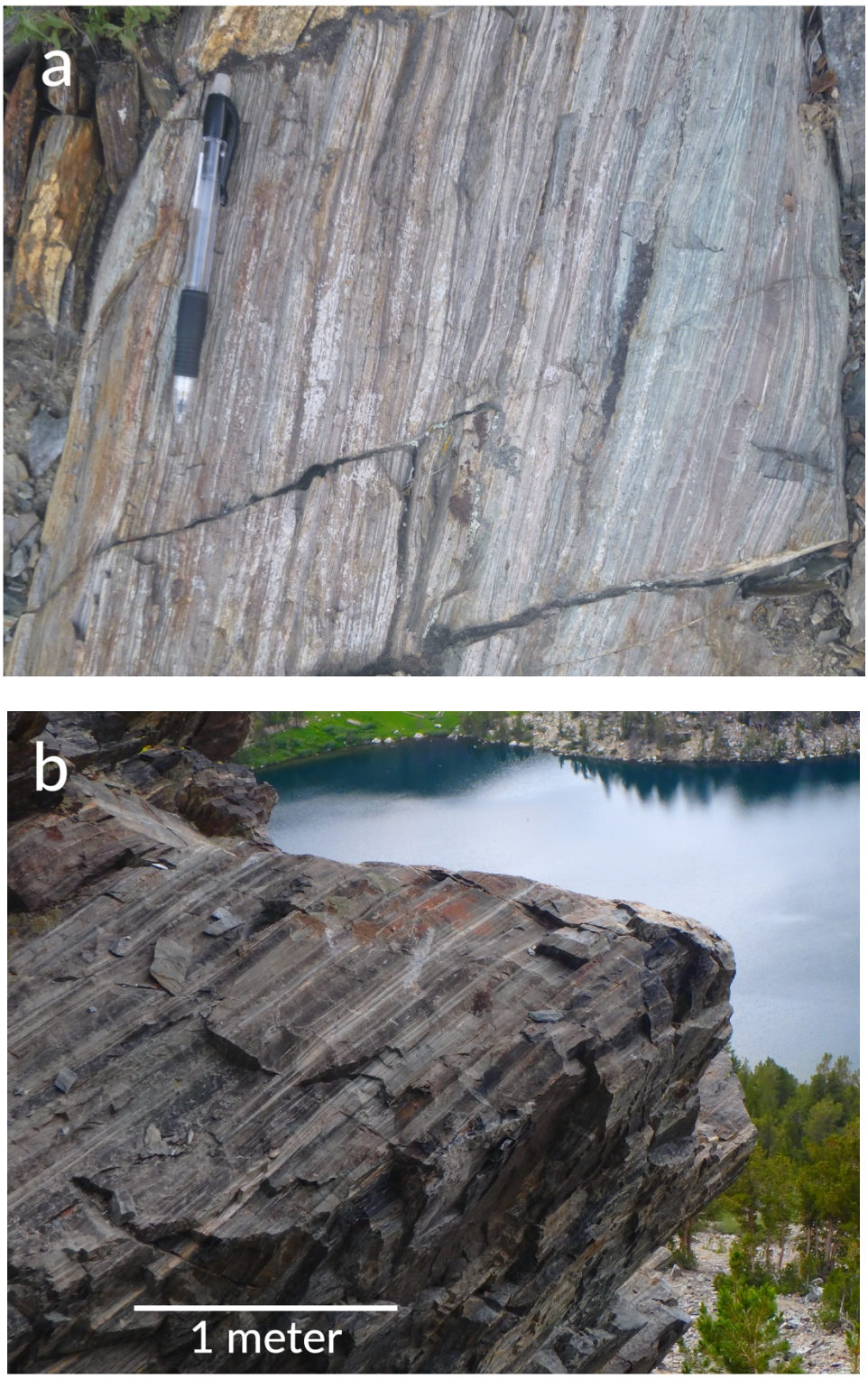

Figure 35: Outcrops of finely laminated calc-silicate rocks of the upper Duck Lake sedimentary succession east of Purple Lake. Pencil is 14 cm long.

4. GEOCHRONOLOGY

LA-ICP-MS U-Pb analysis on a suite of zircon crystals from six major units (Table 1) helps constrain the eruptive history of the Mesozoic Mount Morrison pendant rocks. Data are presented in Appendix A. Concordance was determined by comparing $^{206}Pb/^{238}U$ and $^{207}Pb/^{235}U$; only grains for which the two ages were within 10% normal discordance and 5% reverse discordance were used for interpretation. All samples returned a range of ages greater than the total analytical error, implying that radiogenic lead loss may have occurred, and/or that antecrysts as well as xenocrysts are likely present (Barth et al., 2011; Spencer et al., 2015) For each sample, the weighted mean age of the youngest population with the lowest mean square of weighted deviate (MSWD) value was taken as the best estimate of crystallization age.

Sample	Unit name	GPS location (latitude, longitude)
MRB	Breccia of Mammoth Rock	37.56359 N, 118.98130 W
ALD	Dacite of Arrowhead Lake	37.58451 N, 118.97565 W
PLB	Breccia of Pika Lake	37.54757 N, 118.95413 W
DLT	Tuff of Deer Lakes	37.56474 N, 118.98936 W
PLR	Rhyolite of Purple Lake	37.54722 N, 118.95806 W
MCA	Andesite of Mammoth Crest	37.56568 N, 118.98462 W

Table 1: List of samples collected and analyzed in this study. The same samples were used for U-Pb zircon geochronology and whole-rock geochemistry.

4.1 GEOCHRONOLOGY OF TRIASSIC ROCKS

The oldest block of Mesozoic volcanic rocks in the Mount Morrison pendant is Late Triassic in age. Barth (pers. comm., 2017) reports a U-Pb zircon age of 216 ± 2 Ma for a sample of the tuff of Skelton Lake from Duck Pass. Three additional samples from the Triassic block were analyzed in this study: the breccia of Mammoth Rock (MRB), the dacite of Arrowhead Lake (ALD), and the breccia of Pika Lake (PLB). All three units contained abundant zircon.

The oldest volcanic unit in the pendant is the breccia of Mammoth Rock (MRB, Table 2, Appendix A). A bulk-rock sample of the polymictic facies taken 20 meters up-section from the fault contact with Paleozoic Mount Baldwin marble at Mammoth Rock (Fig. 2) yielded a range of ages spanning 232 to 214 Ma (Table 2b, Appendix A). The youngest population has a weighted mean average age of 217 ± 2 Ma and an MSWD of 0.8 (Fig. 36). The presence of concordant grains as old as 232 Ma in the polymictic breccia suggests that volcanism commenced at this latitude as early as 232 Ma. The data include six grains of Proterozoic age. A single 1084 Ma grain is Grenville in age (Davidson, 1995; Whitmeyer and Karlstrom, 2007). A group of five grains from 1424-1322 Ma correlates with anorogenic magmatism in southern Laurentia (Nyman and Karlstrom, 1997).

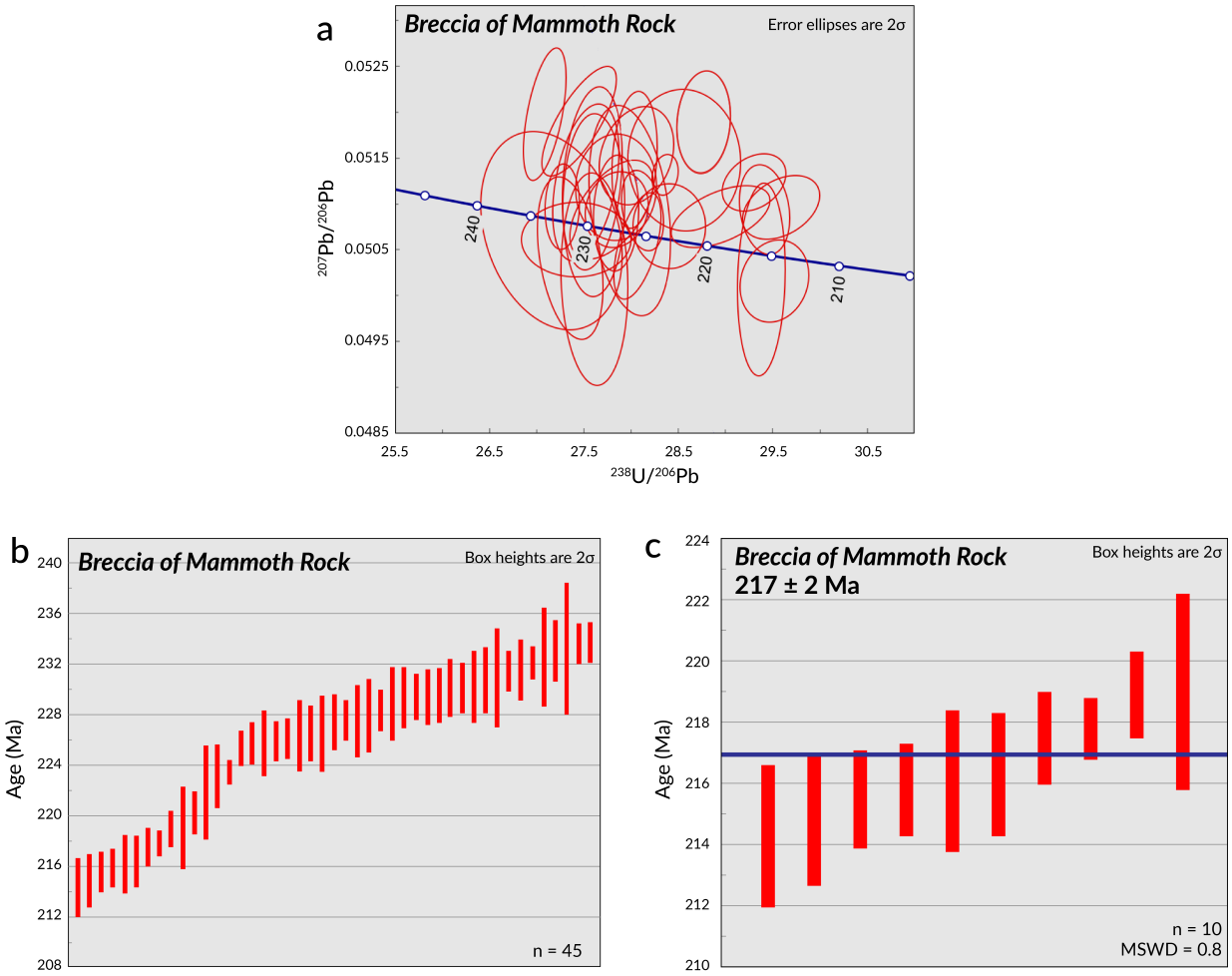

Figure 36: (a) Concordia diagram of all zircon data from a sample of the breccia of Mammoth Rock. (b) All Triassic zircon ages from a sample of the breccia of Mammoth Rock. (c) Weighted mean average of the youngest population of zircons from a sample of the breccia of Mammoth rock. MSWD = mean square of weighted deviates. n = number of crystals analyzed.

The dacite of Arrowhead Lake (ALD, Table 3, Appendix A) includes tuff, tuffaceous sandstone, breccia and a large sill. Tuffs overlie the breccia of Mammoth Rock along an angular unconformity. The sill intrudes the dacitic tuffs as well as the tuff of Skelton Lake in several locations (Fig. 2) and is therefore younger than 217 ± 2 Ma. A sample of the yielded a weighted mean average age of 216 ± 2 Ma for the youngest coherent population, with an MSWD of 2.1 (Fig. 37). The contact between the dacite porphyry and the tuff of Skelton Lake is highly irregular, and the units appear to intrude one another. This relation suggests that the tuff of

Skelton Lake was still fluid during emplacement of the dacite sill, and that the two eruptions were likely from the same volcanic system. Field relations show that the tuffaceous strata were emplaced prior to the porphyry sill as well as the overlying tuff of Skelton Lake. The age of the tuffs is well constrained by the underlying breccia of Mammoth Rock (217 ± 2 Ma) and the overlying tuff of Skelton Lake (216 ± 2 Ma).

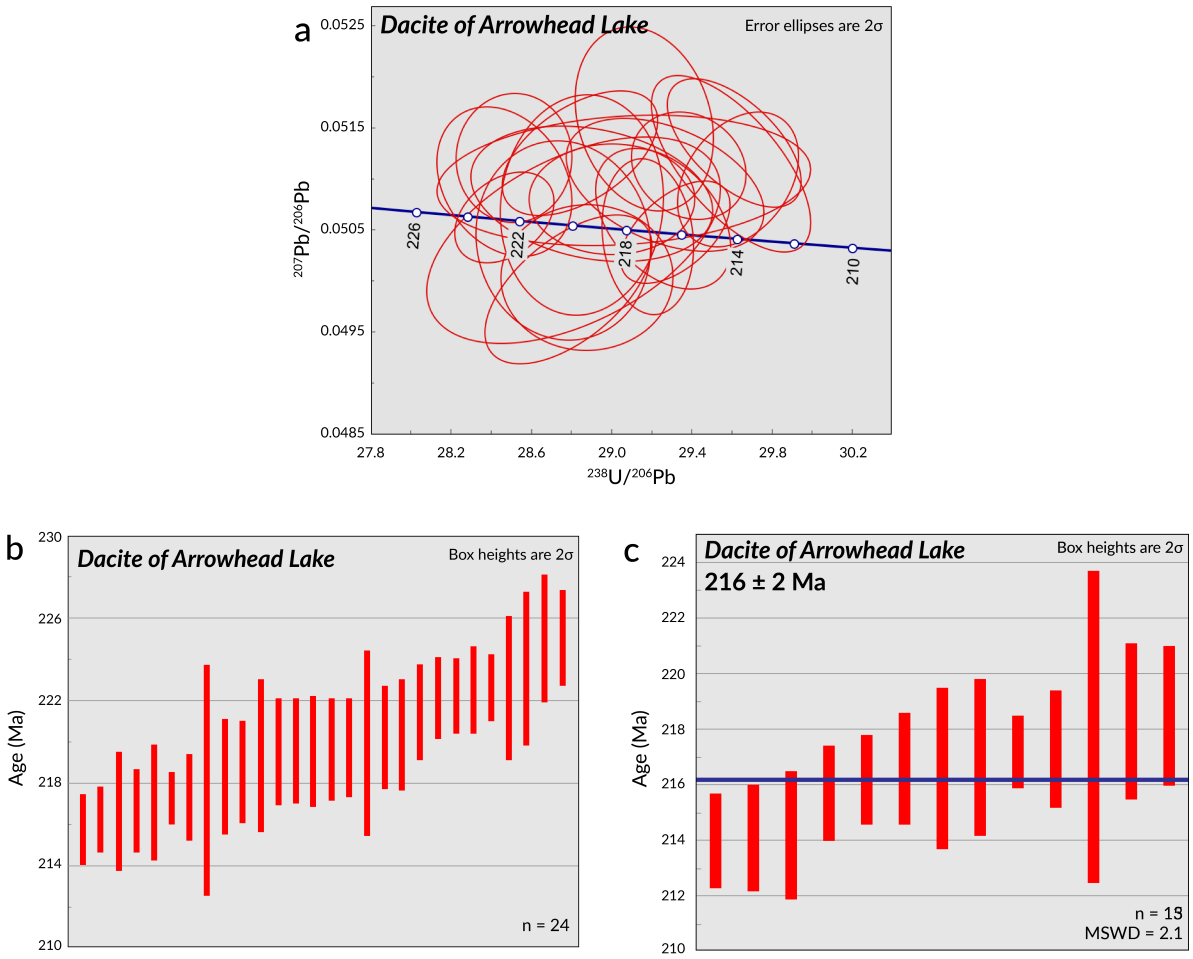

Figure 37: (a) Concordia diagram of all zircon data from a sample of the intrusive dacite of Arrowhead Lake. (b) Plot of all zircons from a sample of the intrusive dacite of Arrowhead Lake. (c) Weighted mean average of the youngest population of zircons from a sample of the intrusive dacite of Arrowhead Lake. MSWD = mean square of weighted deviates. n = number of crystals analyzed.

The breccia of Pika Lake (PLB, Table 4, Appendix A) is the stratigraphically highest unit in the Triassic block. The ages of zircon crystals from a bulk-rock sample range from 211 to 224 Ma. The most coherent group of 18 zircons, with an MSWD of 1.1, yielded a weighted mean average age of 213 ± 2 Ma (Fig. 38).

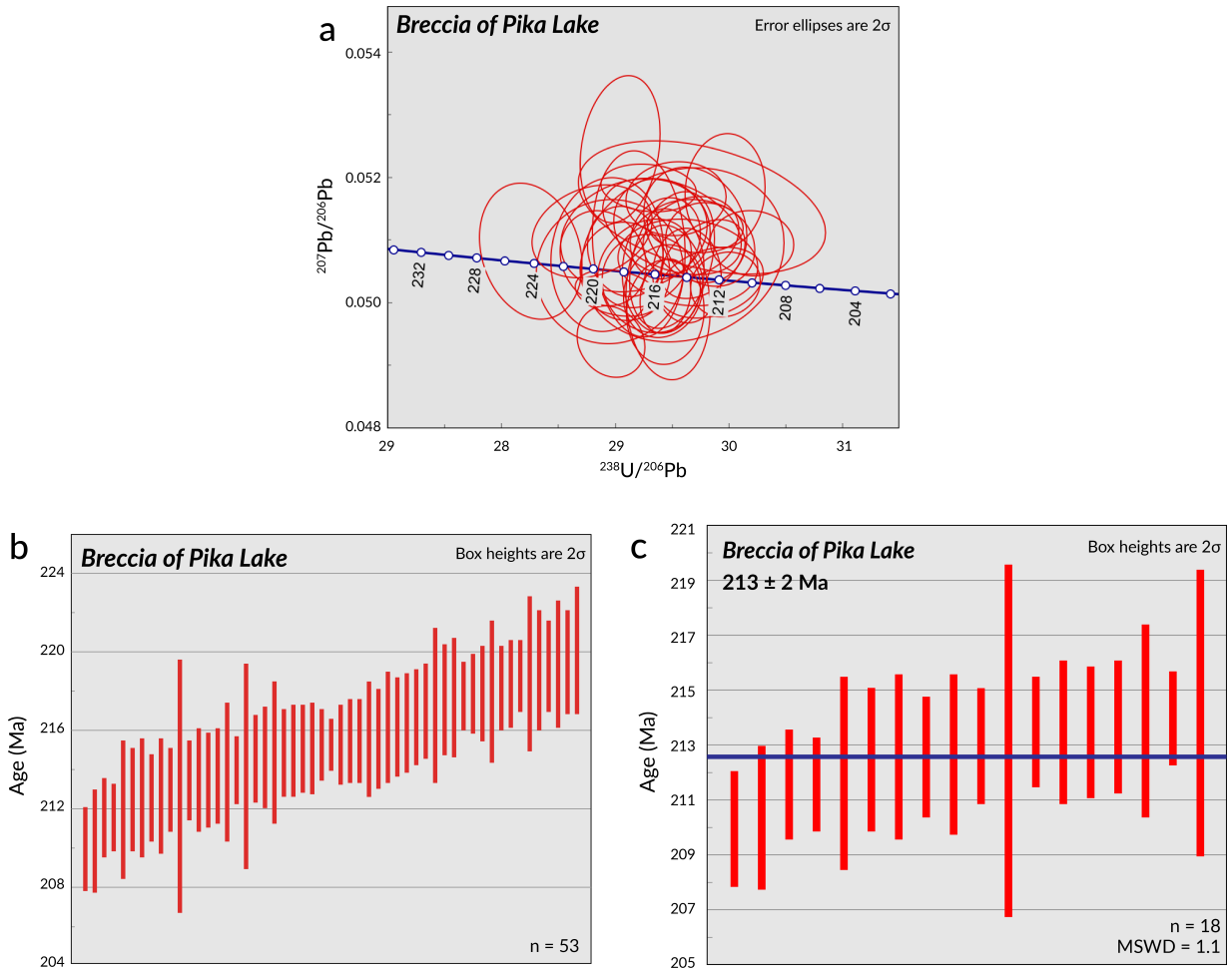

Figure 38: (a) Concordia diagram of all coherent zircons from a sample of the breccia of Pika Lake. (b) Plot of all zircons from a sample of the breccia of Pika Lake. (c) Weighted mean average of the youngest population of zircons from a sample of the breccia of Pika Lake. MSWD = mean square of weighted deviates. n = number of crystals analyzed.

4.2 GEOCHRONOLOGY OF JURASSIC ROCKS

The westernmost volcanic strata in the Mount Morrison pendant were emplaced in the Middle Jurassic epoch. A sample of the tuff of Deer Lakes (DLT, Table 5, Appendix A) was taken from the lower half of the sequence in Deer Lakes basin (Fig. 2). This unit is concordant with dacitic to rhyolitic volcanic strata between the Jurassic-Cretaceous fault and the western intrusive boundary of the pendant. The youngest coherent population of zircon crystals returned a weighted mean average of 170 ± 2 Ma with an MSWD of 0.9 (Fig. 39).

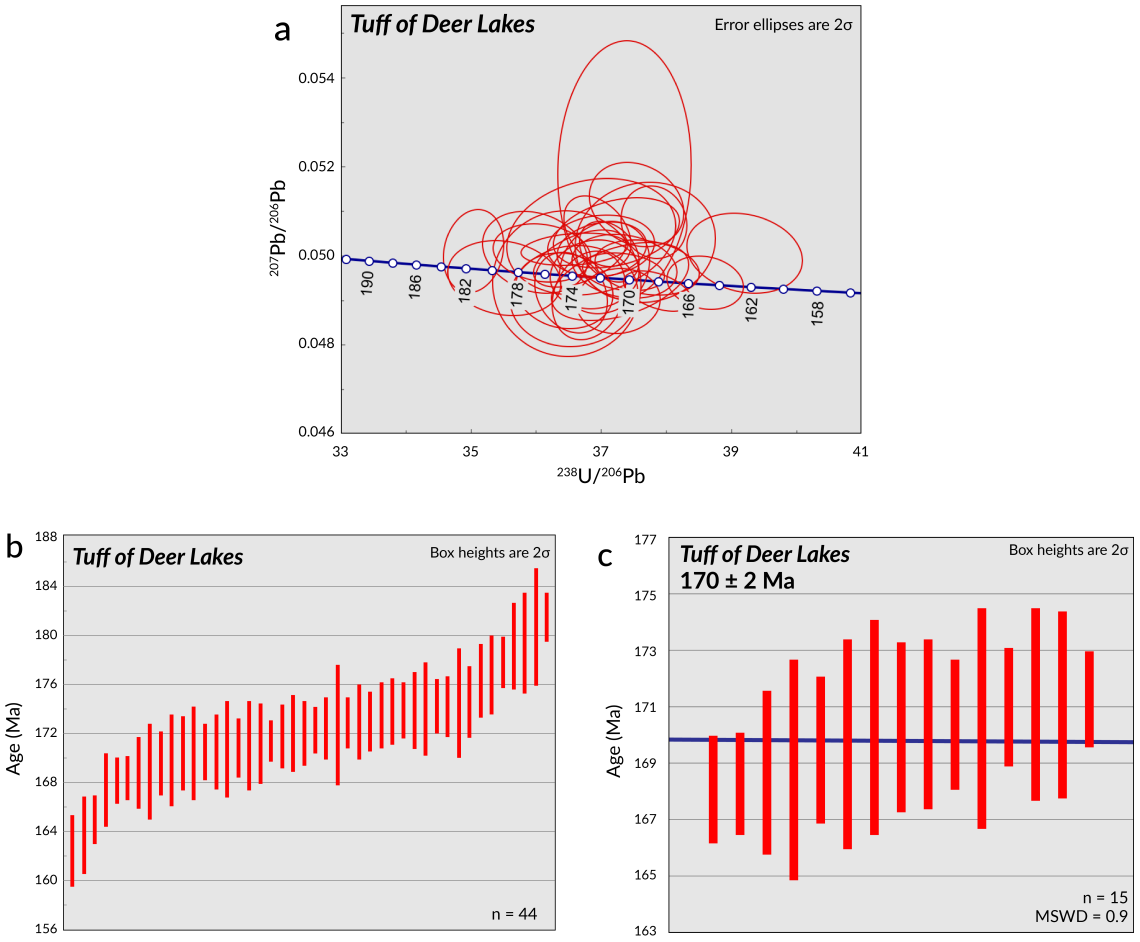

Figure 39: (a) Concordia diagram of all zircons from a sample of the tuff of Deer Lakes. (b) Plot of all zircons from a sample of the tuff of Deer Lakes. (c) Weighted mean average of the youngest population of zircons from a sample of the tuff of Deer Lakes. MSWD = mean square of weighted deviates. n = number of crystals analyzed.

4.3 GEOCHRONOLOGY OF CRETACEOUS ROCKS

Samples were taken from the two thickest units in the Cretaceous block: the rhyolite of Purple Lake (PLR, Table 6, Appendix A) and the andesite of Mammoth Crest (MCA, Table 7, Appendix A). The rhyolite of Purple Lake is zircon rich. A coherent group of 24 zircons from a sample of the rhyolite collected from the Duck Lake area returned a weighted mean average age of 101 ± 1 Ma, with an MSWD of 1.8 (Fig. 40).

The andesite of Mammoth Crest is zircon poor. Only 14 crystals were obtained from a 10-kg sample. The population with the lowest MSWD includes six zircons between 99 and 106 Ma, with a weighted mean average age of 101 ± 2 Ma (Fig. 41). A less coherent population of six zircons ranges from 210 to 228 Ma. Finally, there are two zircons at 198-202 Ma. The secondary population is interpreted as either sample contamination, which did not appear to play a role in other analyses (Tables 2-7), or xenocryst inheritance from assimilated wall rock. It is possible that dikes of the andesite of Mammoth Crest cut through Late Triassic rocks, such as the 216 ± 2 Ma tuff of Skelton Lake, and thereby entrained zircons on their way to the surface.

The granodiorite mass of Lee Lake mass intrudes all three volcanic blocks in the southern part of the pendant (Fig. 2). Although geochronology has yet to be done on this pluton, it cuts across the 101 ± 2 Ma andesite of Mammoth Crest and the 101 ± 1 Ma rhyolite of Purple Lake (101 ± 2 Ma), thus establishing its maximum age as ca. 101 Ma. This relation is consistent with the correlation of the Lee Lake mass with the Cretaceous Round Valley Peak Granodiorite immediately southeast (Rinehart and Ross, 1964).

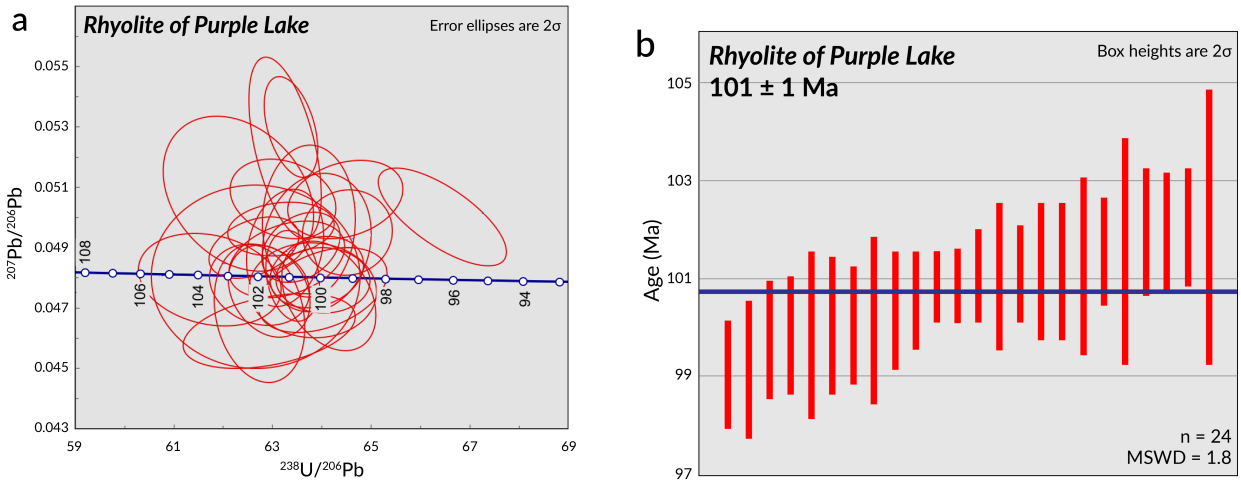

Figure 40: (a) Concordia diagram of all zircons from a sample of the rhyolite of Purple Lake. (b) Weighted mean average of the dominant population of zircons from a sample of the rhyolite of Purple Lake. MSWD = mean square of weighted deviates. n = number of crystals analyzed.

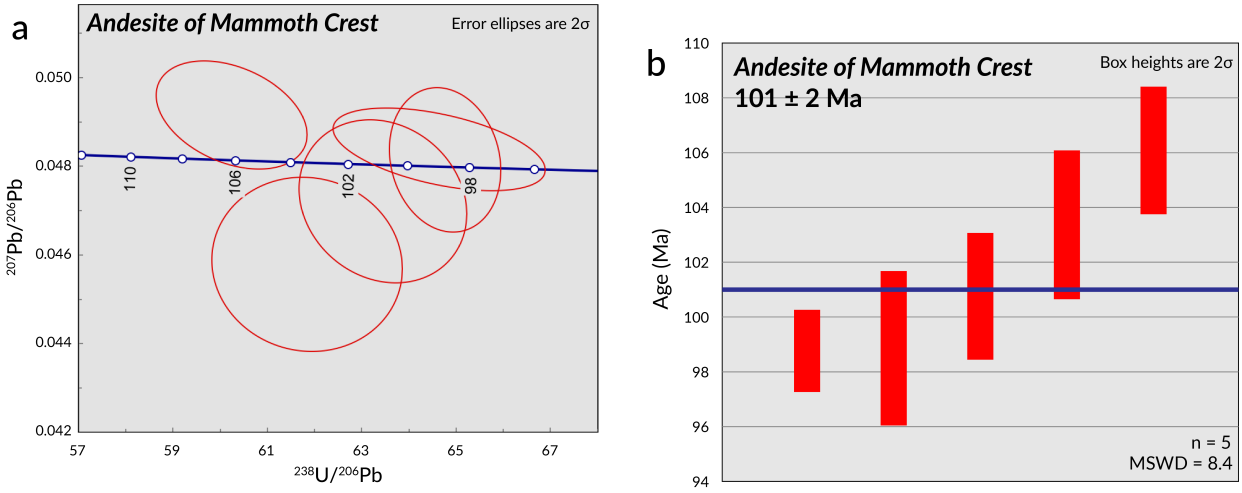

Figure 41: (a) Concordia diagram of all Cretaceous zircons from a sample of the andesite of Mammoth Crest. (b) Weighted mean average of Cretaceous zircons from a sample of the andesite of Mammoth Crest. MSWD = mean square of weighted deviates. n = number of crystals analyzed.

5. GEOCHEMISTRY

Major and trace element geochemistry analyses were performed on bulk-rock samples of six major volcanic units in the Mount Morrison pendant. Analytical data are presented in Appendix B. Several observations indicate that extensive regional fluid-rock interaction has altered the geochemistry of Mount Morrison pendant rocks (Rougvie et al., 2013). The effects of metasomatism must therefore be considered. Hydrothermal fluids promote leaching of mobile elements, which changes the original signature of the rock in a way that is difficult to measure (Pirajno, 1992; Otieno, 2016). Immobile elements, characterized by high ionic potential and resistance to fluid leaching, are therefore favored for analysis because they tend to remain conservative when subjected to hydrothermal fluids. Data from major alkali elements (e.g. K, Na, Ca) and other large-ion lithophile elements (e.g. Rb, Sr, and Ba) must be treated with caution due to the tendency of these elements toward mobilization during fluid-rock interaction (Pirajno, 1992; Barth et al., 2011; Otieno, 2016). High field strength elements (HFSE) and other elements with high ionic potential, including P, Ti, Nb, Ta, Zr, Hf, Y, Yb, La, Lu, Ta, Eu, and Tb are regarded as highly immobile elements in metavolcanic rocks (Verma et al., 2005; Franzson et al., 2008) and are considered the most reliable elements for this study. Elements with high ionic charge, such as P_2O_5, TiO_2, Al_2O_3 and Fe_2O_3, are used to distinguish the calc-alkaline trend. Co was used as a binding agent in the mill, so it is excluded from the discussion. Major element concentrations are given in weight per cent, abbreviated as % in the following text. Trace element concentrations are given in parts per million (ppm).

Only discrimination diagrams that rely on immobile elements are used for analysis. This study uses plots specifically designed for hydrothermally altered metavolcanic rocks. Tectonic setting is determined through Pearce (1983, 1984) diagrams. Ratios of Zr/Ti and Nb/Y are

plotted against SiO_2 and against one another to determine composition per Winchester and Floyd (1977). Each unit was sampled from only one location, so this study lacks redundancy. It cannot be ruled out that geochemical trends may be a product of analytical error and therefore not truly reflective of the original petrology of these rocks.

5.1 GEOCHEMISTRY OF TRIASSIC ROCKS

A clast sample from the monolithic facies of the breccia of Mammoth Rock (MRB, Tables 8-9, Appendix B) was analyzed. The breccia of Mammoth Rock has the lowest SiO_2 content (48.6%) in the suite, yet carries the signature of a rhyodacitic lava for nearly all other immobile elements. Bleaching of the matrix indicates mobilization of iron and explains the low Fe_2O_3 concentration of 3.9%. However, P_2O_5 and TiO_2 concentrations are also low – closer to concentrations in dacitic to rhyolitic rocks in the suite (Figs. 42, 43). The depletion of SiO_2 may be a consequence of extreme hydrothermal alteration, as the polymictic breccia is in fault contact with the Paleozoic Mount Baldwin Marble. Using the Winchester and Floyd (1977) discrimination diagram of Nb/Y against Zr/Ti (Fig. 50), the breccia plots as a rhyolite. This supports the original interpretation of Rinehart and Ross (1964) as well as petrographic evidence that the clasts are devitrified, high-silica glass.

A sample of the porphyritic facies of the dacite of Arrowhead Lake (ALD, Tables 8-9, Appendix B) has 68.5% SiO_2. It plots as a rhyodacite on Winchester and Floyd (1977) diagrams comparing Zr/Ti and Nb/Y to SiO_2 (Figs. 48, 49, 50). The unit displays LREE enrichment, negative Ta and Nb anomalies, and a positive Sr anomaly (Figs. 51, 52).

Barth (pers. comm., 2017) reported an SiO_2 value of 72.4% for the tuff of Skelton Lake. The sample has similar P_2O_5 and TiO_2 concentrations to the other two rhyolites, the Jurassic tuff of Deer Lakes and the Cretaceous rhyolite of Purple Lake (Figs. 42, 43).

The clasts of the breccia of Pika Lake (PLB, Tables 8-9, Appendix B) have a remarkably low silica content of 50.0% considering the abundance of zircon crystals, a mineral more commonly found in felsic rocks. Because a whole-rock sample was analyzed, it is likely that the matrix contains abundant detrital zircon grains. The breccia of Pika Lake contains the highest concentrations of P_2O_5 (0.38%) and TiO_2 (1.09%) of all rocks in the suite (Figs. 42, 43). The sample shows LREE enrichment and slight depletion of Hf and Zr (Figs. 51, 52). The rock plots as a basaltic andesite on the Winchester and Floyd (1977) Zr/Ti versus Nb/Y discrimination diagram (Fig. 50).

5.2 GEOCHEMISTRY OF JURASSIC ROCKS

The tuff of Deer Lakes (DLT, Tables 8-9, Appendix B) contains 74.1% SiO_2 and plots as a rhyolite on Winchester and Floyd (1977) diagrams comparing SiO_2 to Nb/Y and Zr/Ti (Figs. 48, 49). It is similar to the Triassic tuff of Skelton Lake and Cretaceous rhyolite of Purple Lake in TiO_2, P_2O_5, MgO, Fe_2O_3*, and Al_2O_3 content (Figs. 42-46). The unit displays LREE enrichment (Fig. 51).

5.3 GEOCHEMISTRY OF CRETACEOUS ROCKS

The rhyolite of Purple Lake (PLR, Tables 8-9, Appendix B) contains 74.0% SiO_2 and plots as a rhyolite on the Winchester and Floyd (1977) diagram of Zr/Ti versus SiO_2 (Fig. 49). A high concentration of Nb relative to Zr accounts for its classification as a trachyrhyolite on

Winchester and Floyd (1977) diagrams that use those elements (Figs. 48, 50). The sample is LREE enriched (Fig. 51).

The andesite of Mammoth Crest (MCA, Tables 8-9, Appendix B) has 53.4% SiO_2, which is slightly lower than the 58.4% value reported by Rinehart and Ross (1964), who originally classified the rock as a dark alkali trachyte based on major alkali element abundance. Using immobile elements, the rock plots as an andesite on Winchester and Floyd (1977) diagrams for Nb/Y versus SiO_2, Zr/Ti versus SiO_2, and Zr/Ti versus Nb/Y (Figs. 48, 49, 50). The andesite of Mammoth Crest has negative Hf and Zr anomalies (Fig. 52). A weakly negative Eu anomaly (Fig. 51), in spite of hydrothermal leaching, may reflect the limited fractionation of plagioclase.

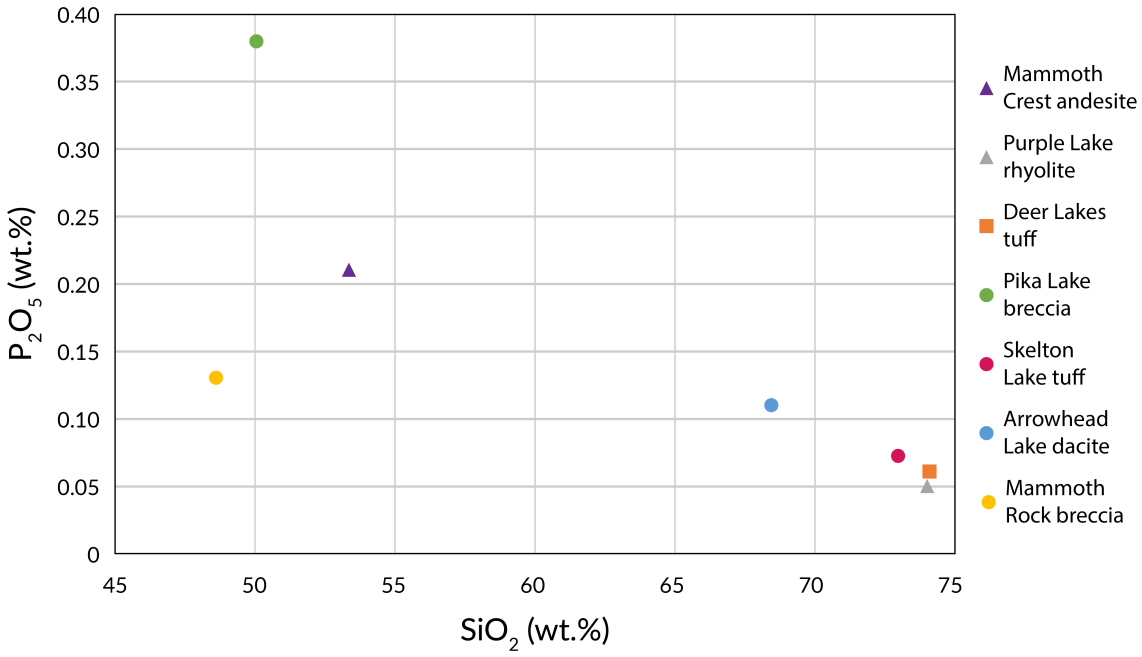

Figure 42: Plot of P_2O_5 against SiO2 for Mesozoic volcanic rocks of the Mount Morrison pendant. Data for the tuff of Skelton Lake from Barth (pers. comm., 2017).

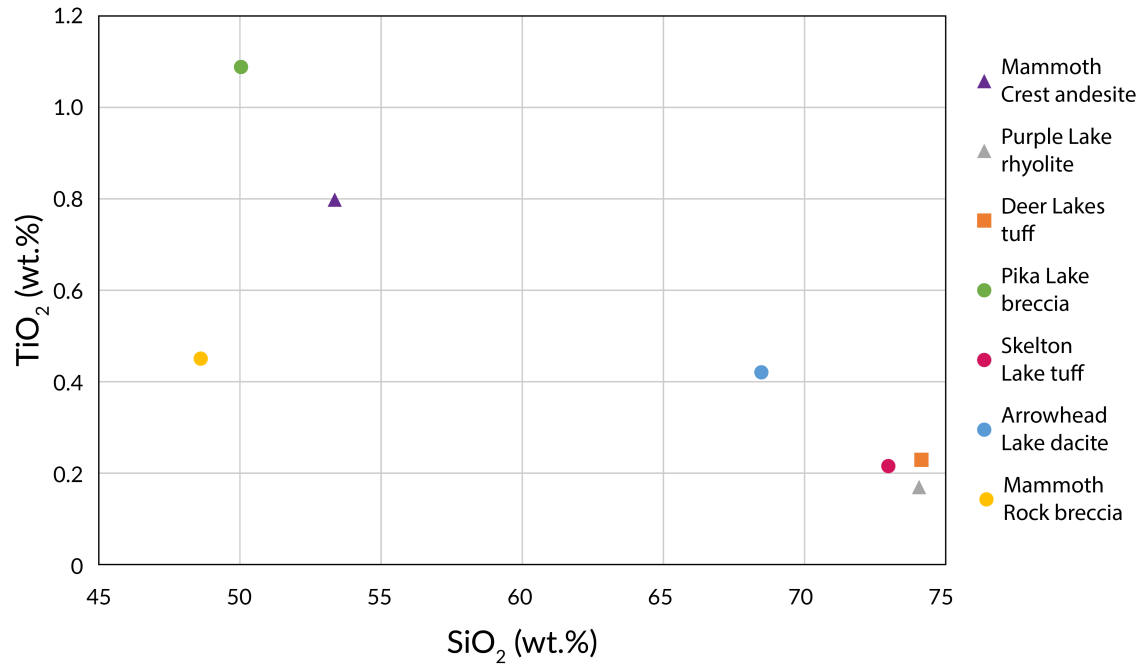

Figure 43: Plot of TiO_2 against SiO_2 for Mesozoic volcanic rocks of the Mount Morrison pendant. Data for the tuff of Skelton Lake from Barth (pers. comm. 2017).

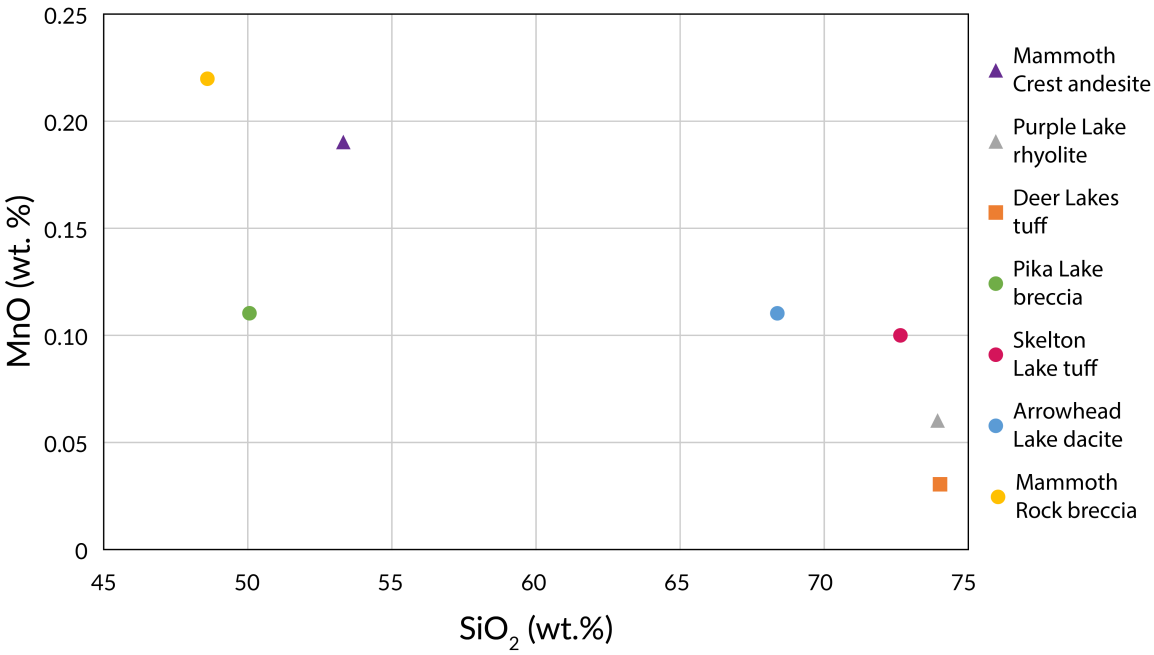

Figure 44: Plot of MnO against SiO_2 for Mesozoic volcanic rocks of the Mount Morrison pendant. Data for the tuff of Skelton Lake from Barth (pers. comm. 2017).

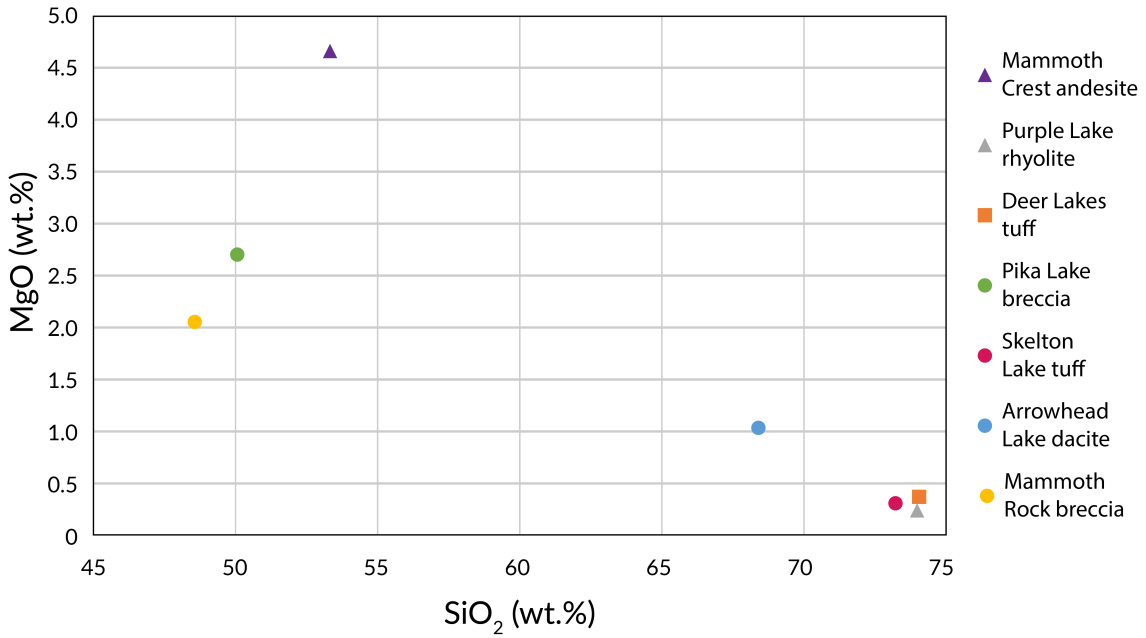

Figure 45: Plot of MgO against SiO_2 for Mesozoic volcanic rocks of the Mount Morrison pendant. Data for the tuff of Skelton Lake from Barth (pers. comm. 2017).

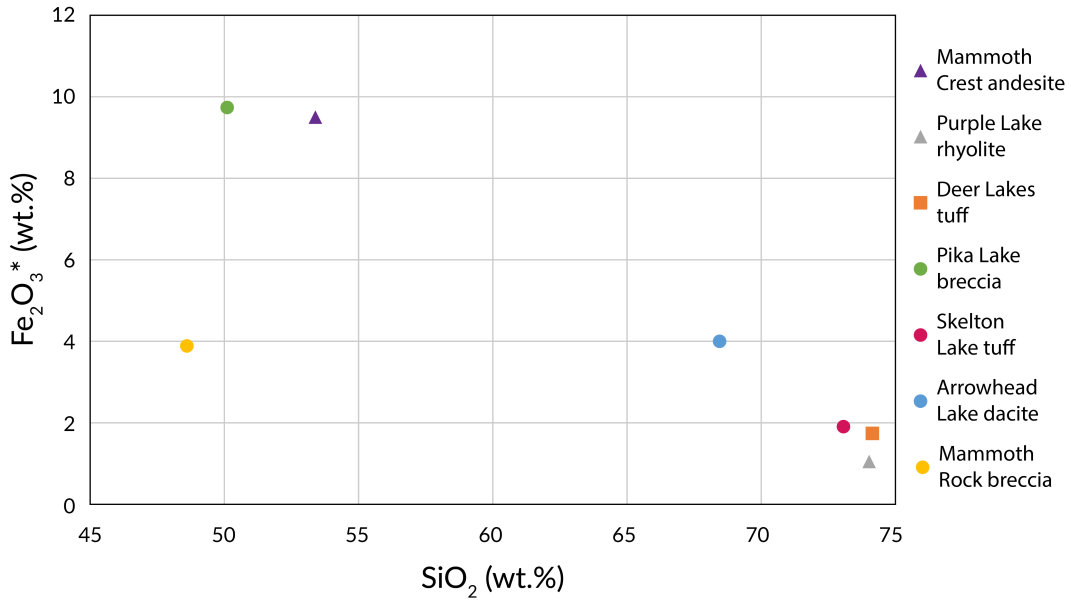

Figure 46: Plot of Fe_2O_3* against SiO_2 for Mesozoic volcanic rocks of the Mount Morrison pendant. Data for the tuff of Skelton Lake from Barth (pers. comm. 2017).

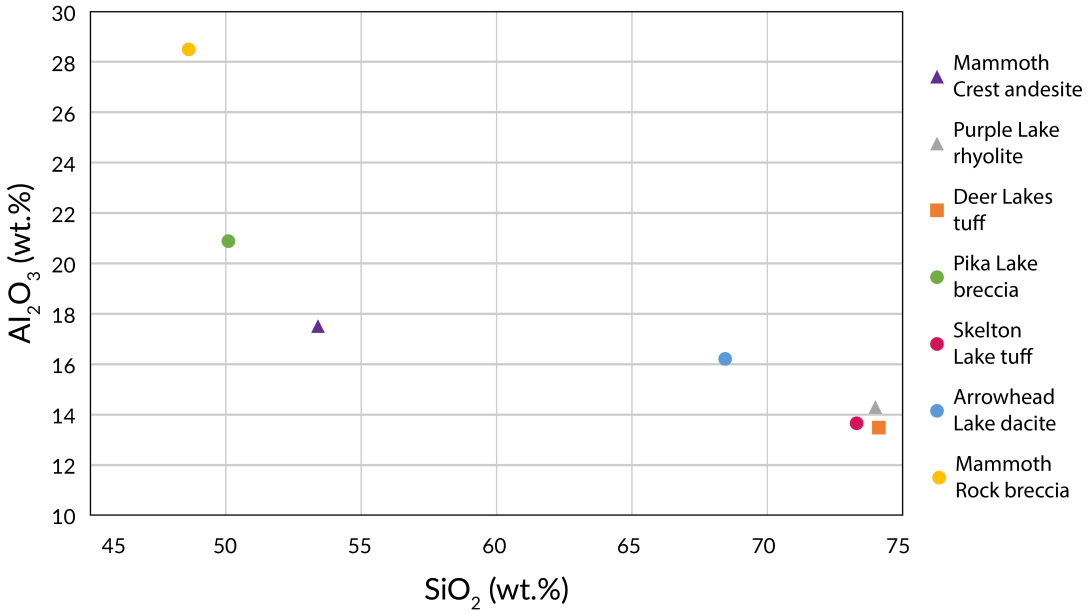

Figure 47: Plot of Al_2O_3 against SiO_2 for Mesozoic volcanic rocks of the Mount Morrison pendant. Data for the tuff of Skelton Lake from Barth (pers. comm. 2017).

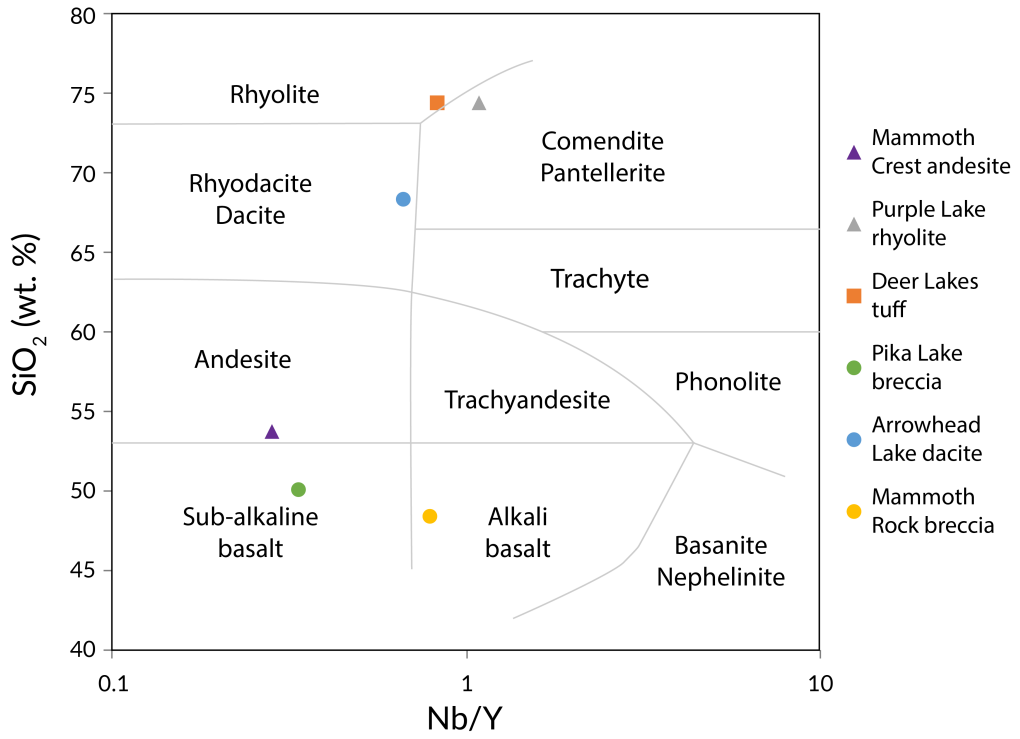

Figure 48: Classification of Mount Morrison volcanic rocks by comparing Nb/Y against SiO_2 per Winchester and Floyd (1977).

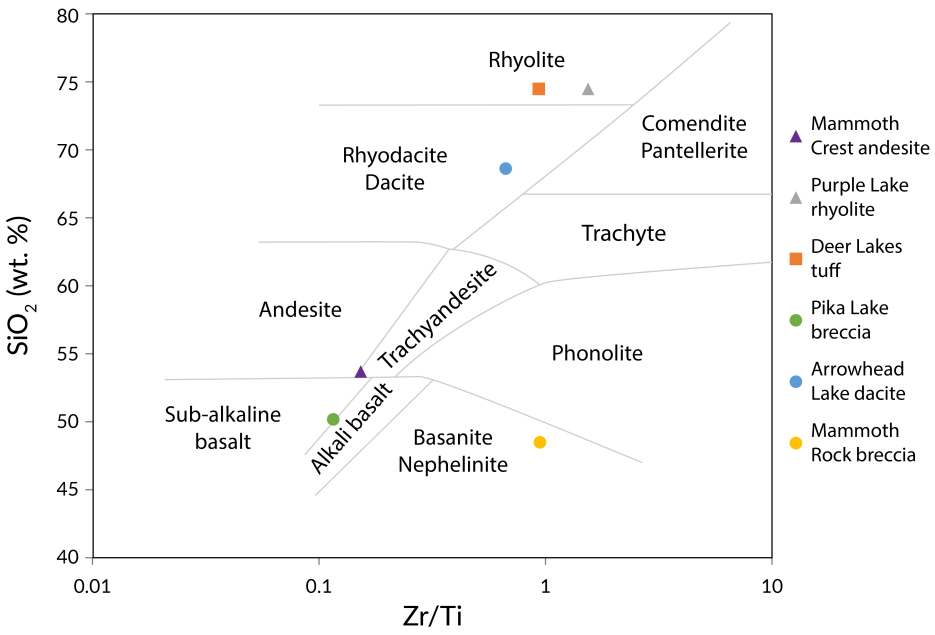

Figure 49: Classification of Mount Morrison volcanic rocks by comparing Zr/Ti with SiO_2 per Winchester and Floyd (1977).

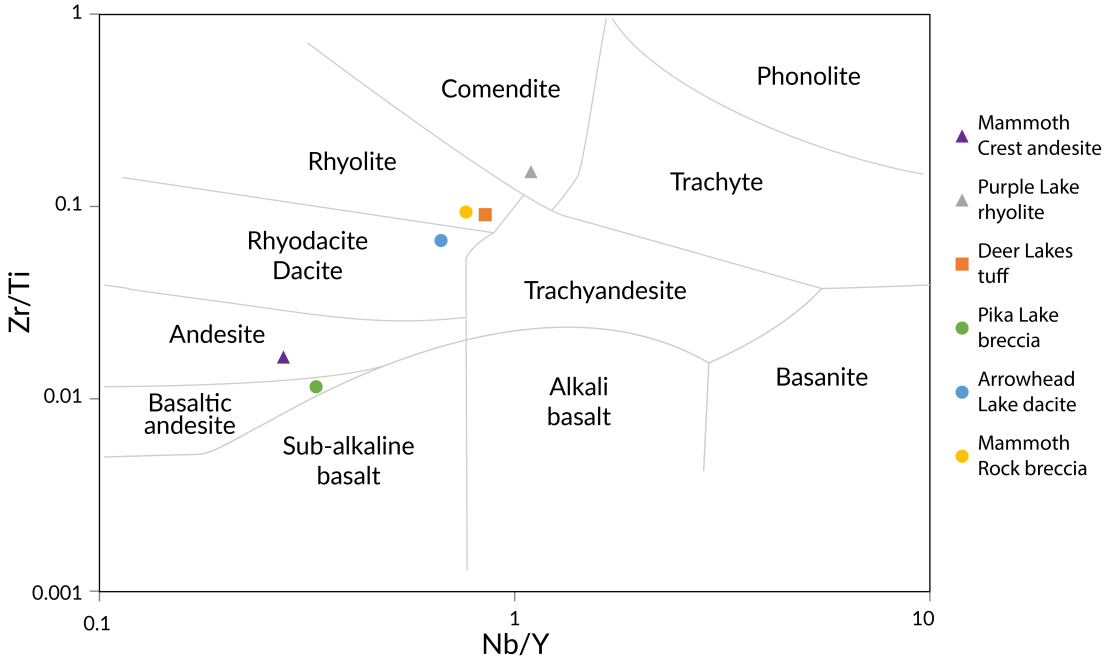

Figure 50: Classification of Mount Morrison volcanic rocks by comparing Nb/Y with Zr/Ti (Winchester and Floyd, 1977).

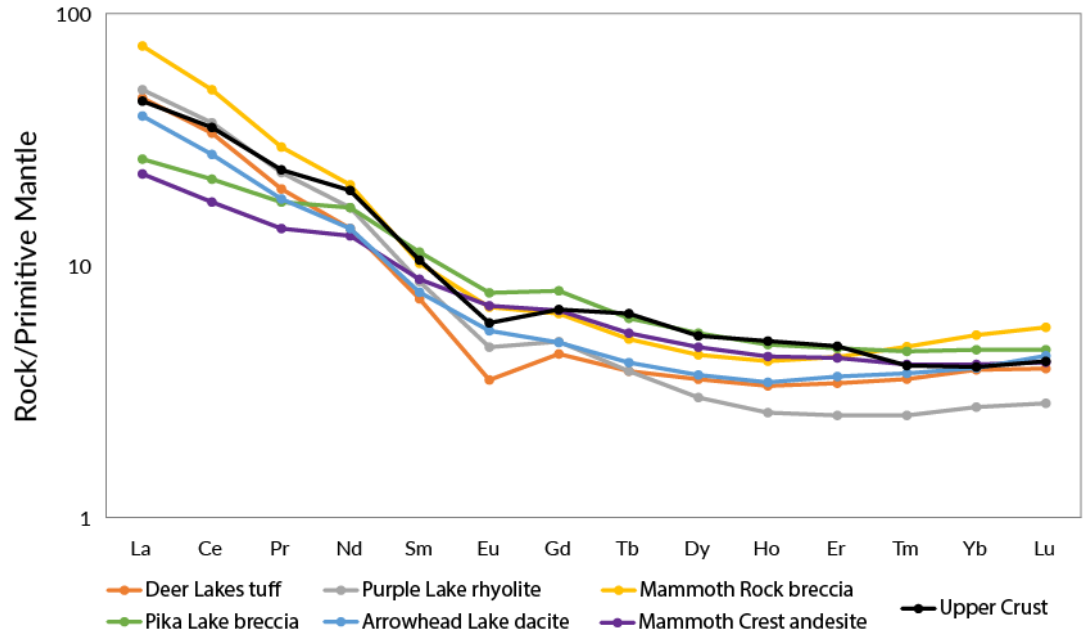

Figure 51: Spider diagram of rare earth elements for volcanic rocks of the Mount Morrison pendant normalized to primitive mantle (Sun and McDonough, 1989). Average upper crust composition from Rudnick (2003).

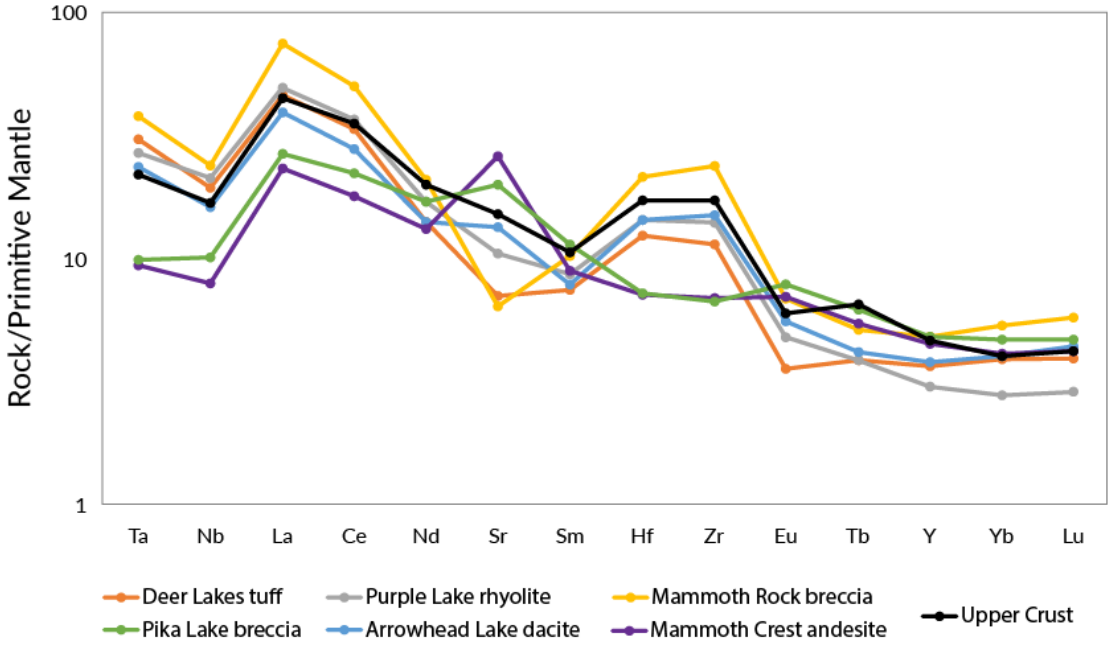

Figure 52: Spider diagram of selected trace elements normalized to primitive mantle (Sun and McDonough, 1989) for volcanic rocks of the Mount Morrison pendant. Average upper crust composition from Rudnick (2003).

6. STRUCTURAL GEOLOGY

Mesozoic volcanic rocks of the east-central Sierra Nevada, including those of the Mount Morrison pendant, were intruded by Cretaceous plutons and thus subjected to albite-epidote-hornfels-grade contact metamorphism and structural deformation in the form of dextral shear (Bentley, 2004; Whitesides, 2011). At least two episodes of deformation affected Triassic and Jurassic rocks, whereas one episode took place after the emplacement of Early Cretaceous volcanic rocks (Sharp et al., 2000). Original volcanic strata were thinned by 50% (Sharp et al., 2000) and tilted steeply to the southwest, and most units exhibit a penetrative slaty cleavage that generally aligns with inferred bedding planes (Tobisch et al., 2000).

Mesozoic beds strike between 300-330° throughout the Mount Morrison pendant (Fig. 53) with slight variances due to pluton-induced deformation. The average strike is akin to, though slightly more westward than, that of similar-aged rocks in the Ritter Range and Saddlebag Lake pendants (e.g. Huber and Rinehart, 1965; Tobisch and Fiske, 1982).

Within the Mount Morrison pendant, faults juxtapose three blocks of independent age and structural history. The youngest (Cretaceous) and least-deformed rocks are found in the central block, bound by the Triassic block on the east and the Jurassic block on the west (Fig. 2). Triassic rocks have steep (70-90°) southwestward cleavage and moderately developed foliation that aligns with bedding planes (Fig. 53). The trend applies to all Triassic units except the breccia of Mammoth Rock, which is nonfoliated and contains sandstone beds inclined only 25-30° SW despite aligning with the regional strike (Fig. 53). Bedding is subvertical in the overlying dacite of Arrowhead Lake and so it appears that such gentle dips occur solely in the breccia of Mammoth Rock, and that an angular unconformity exists between the two units.

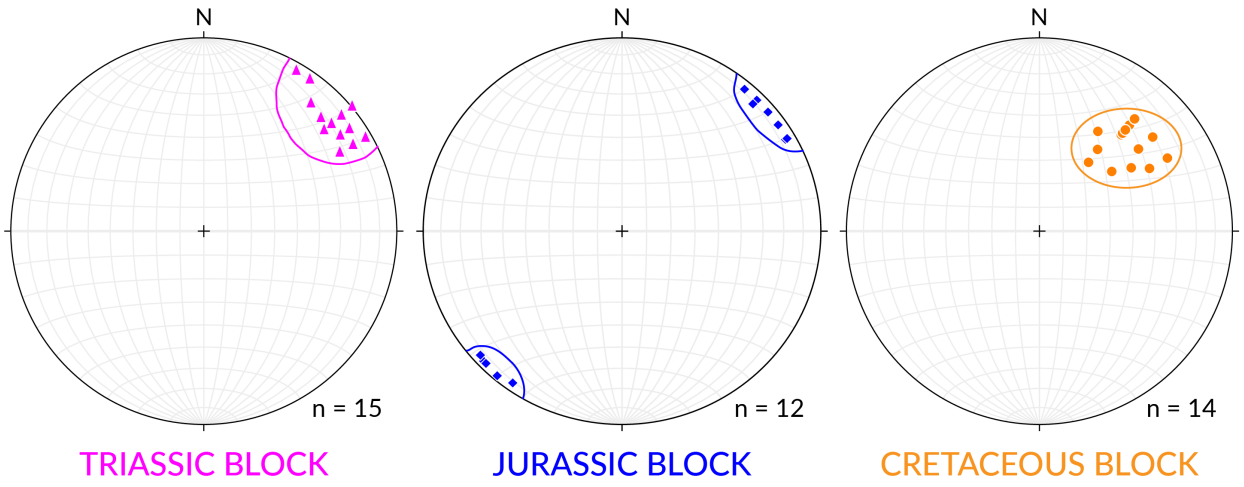

Figure 53: Stereographic projection of poles to cleavage planes for Triassic, Jurassic, and Cretaceous rocks in the Mount Morrison pendant.

Jurassic rocks exhibit the strongest deformation pattern, with closely spaced phyllitic to schistose cleavage and abundant secondary mica. The average dip is vertical (Fig. 53). Breccia facies show varying degrees of strain, with greater than 10:1 clast elongation observed in strata closest to the fault with the Cretaceous block (Fig. 54). Highly strained volcanic rocks grade into quartz schist and then to hornfels within 100 meters of the contact with the Cretaceous Mono Creek Granite. This gradation is characteristic of the Sierra Crest shear zone (Bentley, 2004). Quartz boudins within the deformation zone show evidence of dextral shear (Fig. 55).



Figure 54: Saussuritized dacite breccia of the Jurassic Deer Lakes sequence with highly strained and saussuritized clasts due to proximity to fault zone with the Cretaceous block. Compare with Figure 24d. Hammer is 33 cm long.

In the North Fork Fish Creek area (Fig. 2), Jurassic beds and underlying Triassic beds are rotated to a strike of 270-290°. This shows that both blocks were locally disturbed together as a package as a result of emplacement of the Cretaceous Lee Lake Mass of the Round Valley Peak Granodiorite (Figs. 2 and 13). Similar local disturbances are also observed elsewhere in eastern Sierran pendants due to plutonic intrusions (Bentley, 2004).

The Cretaceous block is characterized by moderate (45-65°) dips (Fig. 53) and minimal deformation. These rocks are notably less deformed than their older counterparts. Away from fault zones, there is little to no evidence of ductile strain, and a weak slaty cleavage is developed along bedding planes. Local folds are likely the result of slumping or loading due to eruption of the andesite of Mammoth Crest. Strata within 10-30 meters of the bounding faults have highly

elongated clasts and are overprinted by the quartz-epidote-piemontite metamorphic mineral assemblage.

Fault contacts between tectonic blocks (Fig. 2) are identified as broad (50-100 meter-wide) zones of brittle and ductile deformation. In Deer Lakes basin, the fault zone is an 80-100-meter-wide zone containing strong shear fabrics and large, elongate lenses of quartz-epidote-piemontite rock (Fig. 56). On the ridgeline immediately southeast of Duck Lake, ductile fabric is overprinted by brittle faulting. The Triassic-Cretaceous fault zone, along which the Skelton tuff and shales of the Triassic Duck Lake sequence are highly sheared, coincides with an approximately 500-m^2 block of planar-laminated, non-folded Cretaceous shale that has an anomalously low dip of 15-25° SW (Fig. 57).



Figure 55: Quartz boudins in the Jurassic Deer Lakes sequence indicating dextral shear motion. Photo was taken within 100 meters of the contact with the Cretaceous Mono Creek Granite. Hammer is 33 cm long.

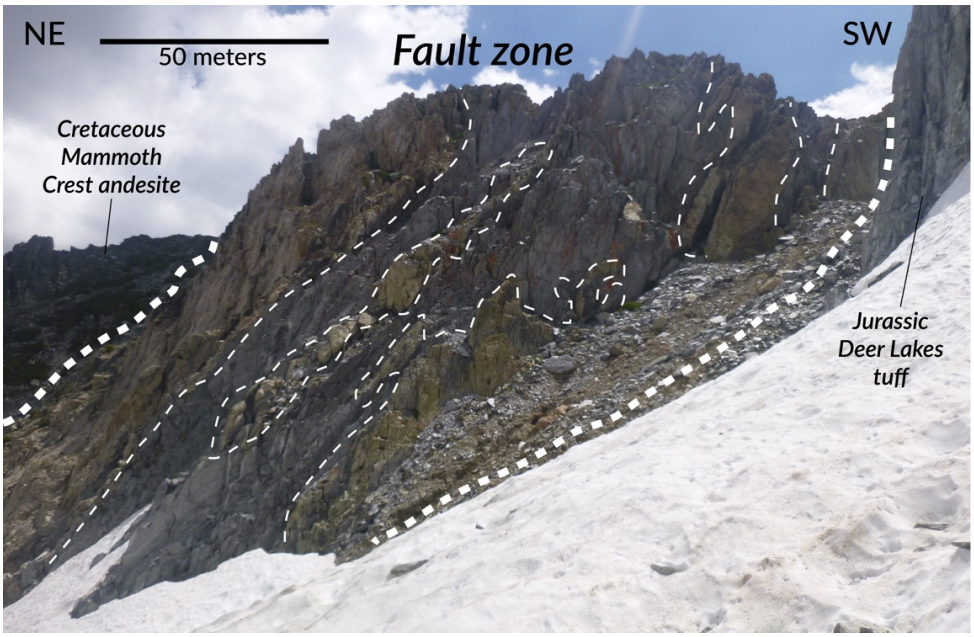

Figure 56: Looking northeast at the Jurassic-Cretaceous fault zone in Deer Lakes basin, showing of boudins of quartz-epidote-piemontite rocks (white dashed outline) within highly sheared rocks of the Jurassic Deer Lakes sequence. Thicker white dashed lines show the extent of the fault zone.

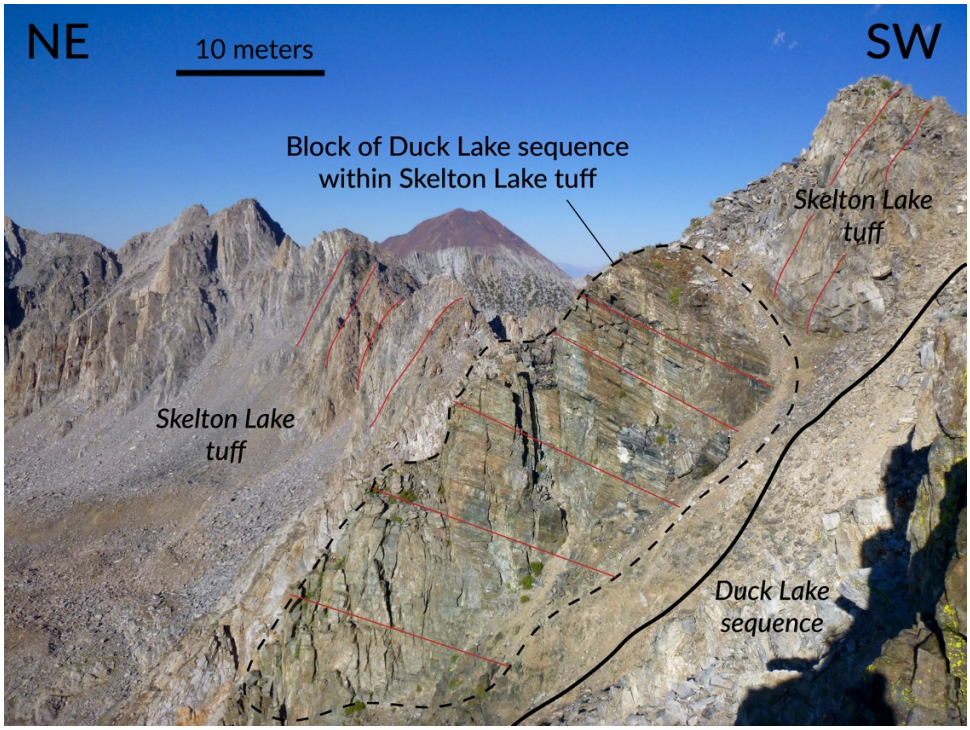

Figure 57: Looking northeast at a block of anomalously shallow-dipping sedimentary rocks of Duck Lake succession (center) on the ridgeline south of Pika Lake. Red lines show bedding.

7. DISCUSSION AND INTERPRETATIONS

New ages obtained in this study offer significant insight into the geologic evolution of this part of the east-central Sierra Nevada. Geochronologic data delineate distinct ages for each of the three tectonic blocks, which represent three distinct phases of Sierran arc activity juxtaposed against one another by faults. The eruptive and depositional history of each block is shown schematically in Figure 3, showing blocks separated by faults. The age distribution of Mesozoic Mount Morrison pendant rocks corresponds well with the overall Sierran arc tempo (Fig. 58). Areal extent of the Mount Morrison pendant volcanic rocks (Fig. 59) draw further attention to the contribution of Triassic volcanism in the growth of the Sierran arc.

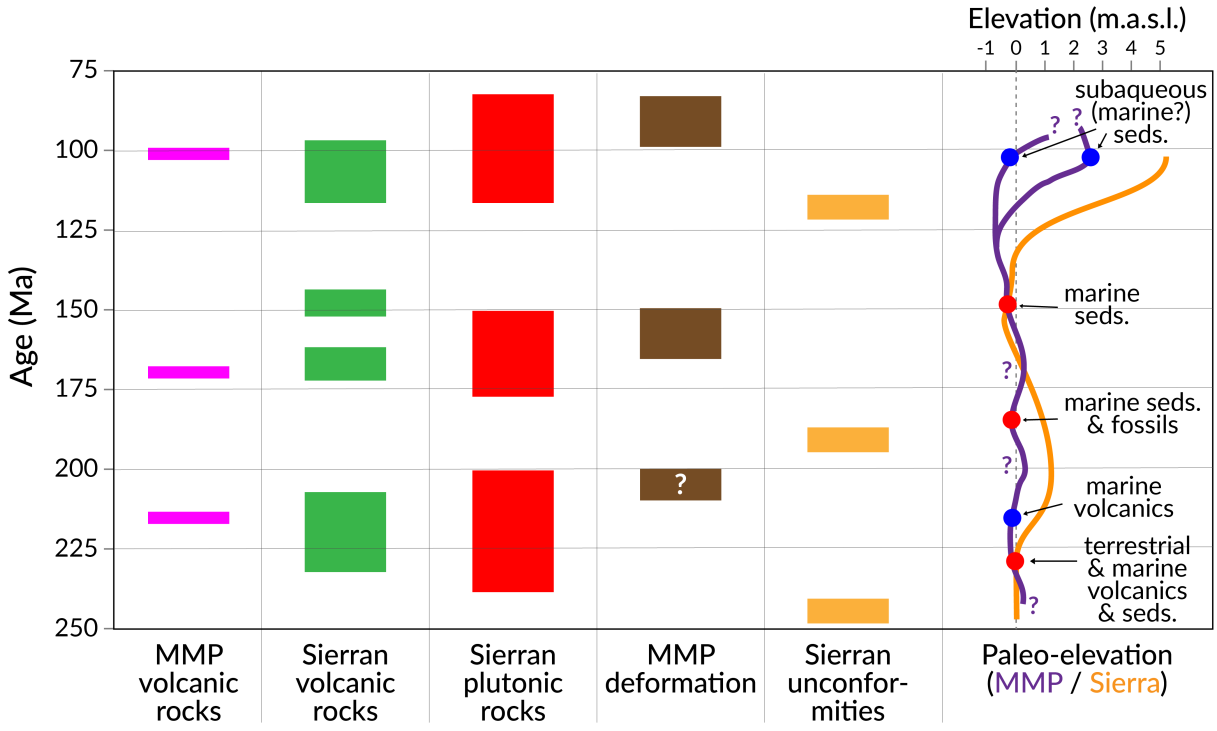

Figure 58: Summary diagram comparing volcanic and structural patterns in the Mount Morrison pendant (MMP) against overall Sierran arc trends from Cao and Paterson (2016). Blue circles are MMP rocks; red circles are other Sierran arc rocks from Paterson et al. (2014). The paleo-elevation curves are based on MMP facies (purple line) and Sierran facies (orange line) from Paterson et al. (2014).

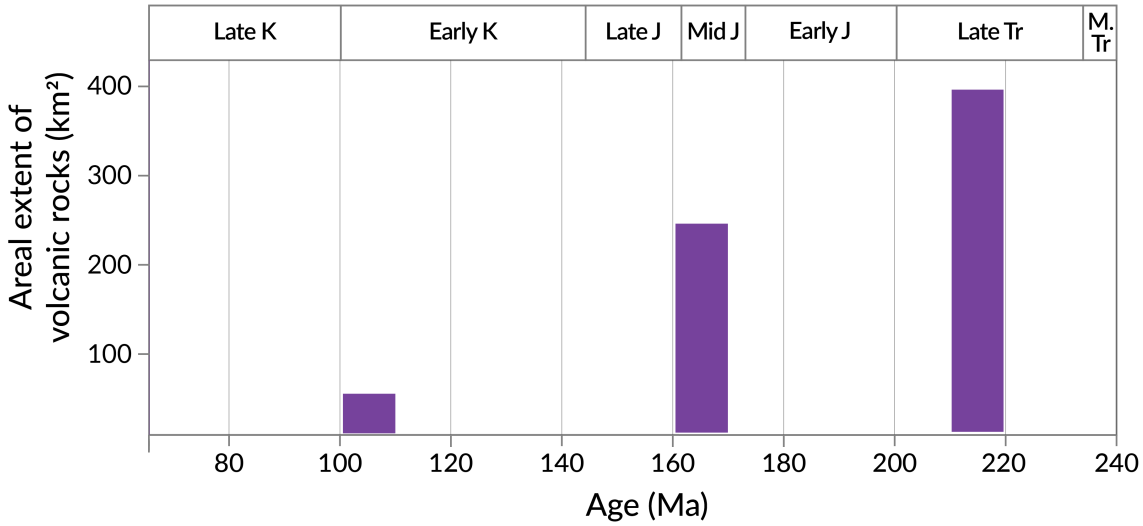

Figure 59: Areal extent of Mount Morrison pendant volcanic material according to age.

7.1 FACIES INTERPRETATIONS

The Triassic block contains a 3-km-thick sequence of dominantly felsic tuffaceous material with local deposits of subaqueous breccia. The breccia of Mammoth Rock (217 ± 2 Ma) is the earliest record of volcanism at this latitude and was emplaced in a series of subaqueous eruptions, as evidenced by clast textures. First, the polymictic breccia formed when basaltic lava extruded through the seafloor, incorporating subrounded clasts of shale, limestone, and sandstone (Rinehart and Ross, 1964). This is shown by the presence of both volcanic and sedimentary clasts in the basal polymictic unit. Almost 200 meters of monomictic basalt breccia were emplaced above the polymictic facies along a sharp contact. Cuspate, fluid, and jigsaw basalt clasts provide evidence for subaqueous eruption (Fisher, 1984; Batiza and White, 2000). Emplacement of the monomictic breccia facies was episodic, as shown by the presence of laminated sandstone interbedded with the massive breccia (Fig. 4).

The emplacement of the breccia of Mammoth Rock was followed by the deposition of a thick succession of dacitic tuffs and volcaniclastic rocks associated with the dacite of Arrowhead Lake. The porphyry facies of the dacite of Arrowhead Lake (216 ± 2 Ma) intruded these tuffaceous rocks and spread out as a sill beneath the tuff of Skelton Lake (216 ± 2 Ma). Intimate field relations between these units suggest that the tuff of Skelton Lake was still fluid when the porphyry body was emplaced (Fig. 21).

The tuff of Skelton Lake includes chaotic breccia facies up to 300 meters thick in the North Fork Fish Creek area as well as a 1.2-km-thick, monotonous, crystal-rich tuff that extends to the far northwest edge of the pendant (Figs. 2, 3). The breccia represents a proximal facies because large lithic clasts cannot travel as far as finer particles (Lipman, 1984). The monotonous, crystal-rich facies is too thick to be an extra-caldera deposit and so it is interpreted as caldera fill. The clasts have a different (more mafic) composition than the enclosing rhyolite tuff, and may be either fragments of the collapsed roof or wall, or fragments of wall rock erupted from a ring vent. The tuff of Skelton Lake is interpreted as an intra-caldera ignimbrite based on its thickness, volume, texture, and composition. The current lateral, along-strike extent of this unit is ~13 km, and the maximum exposed thickness is ~1.2 km (Fig. 2). For a simplified, equant caldera shape with a constant depth of 1.2 km, the total erupted volume would be ~200 km^3. This number would vary greatly depending on caldera geometry, and should be considered a rudimentary estimate.

Shortly after the emplacement of the tuff of Skelton Lake, the porphyry facies of the dacite of Arrowhead Lake (216 ± 2 Ma) intruded the entire volcanic sequence as an extensive hypabyssal body. The interpretation of a caldera sequence for the pyroclastic rocks of the Arrowhead Lake and Skelton Lake sequences is supported by the presence of several caldera

features (Lipman, 1984) including a thick intra-caldera ignimbrite (tuff facies of the tuff of Skelton Lake), collapse or wall-rock facies (breccia facies of the tuff of Skelton Lake) and a hypabyssal intrusion (intrusive dacite of Arrowhead Lake).

The continental arc signatures of the dacite of Arrowhead Lake and the tuff of Skelton Lake demonstrate that, by about 216 Ma, the arc was being emplaced through evolved continental crust. The onset of the Late Triassic high-flux magmatic episode is evidenced by the nearby 226-218 Ma Scheelite Intrusive Suite (Barth et al., 2011). Following the eruption of the tuff of Skelton Lake, the breccia of Pika Lake (213 ± 2 Ma) was emplaced as a local deposit, similar in eruptive style but different in composition to the breccia of Mammoth Rock. The presence of internally fractured, quench-fragmented basaltic andesite clasts filled with injections of fine-grained silicate material (Fig. 23) suggests that the breccia of Pika Lake had a subaqueous eruptive setting (Fisher, 1984; Batiza and White, 2000).

The Jurassic block contains a sequence of dominantly rhyolitic volcanic rocks including ignimbrites, laminated tuffs, tuff breccias, and dacite lava breccias. The sequence was emplaced through a series of many eruptions, as evidenced by the lenticular geometry of units. Laminated tuffs were emplaced by ash fall, as shown by grain size and sorting. Tuff breccias were emplaced by pyroclastic flows, as they are poorly sorted and contain ragged pumice fragments flattened along strike. A U-Pb zircon age of 170 ± 2 Ma for the tuff of Deer Lakes places it within the second pulse of Sierran arc volcanism. The Jurassic block is the most metamorphosed and highly strained. The rocks have strongly developed slaty to phyllitic foliation that parallels the intrusive contact with Mono Creek Granite.

In the Cretaceous block, sedimentary rocks are interlayered with minor rhyolite tuffs and two prominent volcanic facies, the rhyolite of Purple Lake (101 ± 1 Ma) and the andesite of

Mammoth Crest (101 ± 2 Ma). These units, and the underlying rhyolite tuff interbeds, represent intermediate to felsic activity in a volcanic field adjacent to the 99-101 Ma Cretaceous Minarets caldera (Fiske and Tobisch, 1994; McNulty et al., 1996). The rhyolite of Purple Lake tapers drastically from southeast to northwest (Fig. 25). The high-silica flow is notable for massive texture and lack of phenocrysts. In the absence of flow banding, marginal breccia, tephra deposits, and other dome facies, the rhyolite of Purple Lake is interpreted as a lava flow with a source in the southeast part of the pendant. The andesite of Mammoth Crest directly overlies the rhyolite of Purple Lake at Purple Lake, and intrudes the fine-grained sedimentary rocks of the Duck Lake succession, forming a sill between calc-silicate strata. In the vicinity of Purple Lake, thin-bedded shale and limestone are locally deformed and enclosed by the andesite (Fig. 29). At its far northwestern extent, the andesite body constitutes a tabular, concordant body overlying 40-80 meters of fine-grained sedimentary rocks. Therefore, this unit is interpreted as a shallow intrusion that cut through part of its sedimentary cover and spread out as a sill or laccolith. Where the unit has a thickness of ~400 meters (Fig. 26), the top of the unit is truncated by the fault with Jurassic rocks. Even considering tectonic thinning, this thickness is generally considered too great for a single andesite lava flow (Stevens, 2002) but is within reason for a laccolith or sill (e.g. Ruppel, 1972).

The Duck Lake succession records the depositional environment of the latest Early Cretaceous Sierran arc ~30 km south of the Minarets caldera. Interstratified sandstone, shale, and conglomerate in the lower part of the succession are composed of reworked tuffaceous material. The uppermost strata, which are interbedded with the 101 ± 1 Ma rhyolite of Purple Lake and the 101 ± 2 Ma andesite of Mammoth Crest, consist of finely laminated shale and limestone. Although these are common Triassic and Jurassic rock types of the Ritter Range pendant (Fiske

and Tobisch, 1978), examples from the Cretaceous period are largely absent. It is interesting to consider that Fiske and Tobisch (1994) documented "laminated tuffs of probable caldera lake origin" overlying the Cretaceous Minarets caldera fill. The 110-meter-thick sequence of finely laminated shale and limestone is not definitively marine in origin, as this study found no fossils to make the determination. The current lateral extent of these calc-silicate rocks is ~6 km, but the unit is truncated on either side by faults and intrusions (Fig. 2). Therefore, the present-day dimensions of thickness and lateral extent are within reason for a lake setting. Increase in thickness (from 50 to 140 m) to the southeast could represent distance from the paleo-shoreline, or it could represent the slope of a paleo-topographic ridge.

7.2 GEOCHEMISTRY INTERPRETATIONS

The entire analyzed suite of Mount Morrison pendant volcanic rocks was emplaced in a continental, calc-alkaline arc setting, as shown by immobile-element-based discrimination diagrams (Figs. 60-65) of Wood (1980), Pearce (1983), and Pearce et al. (1984). All rocks roughly follow the REE trend for average continental crust and display the LREE-enriched signature of continental arc rocks (Fig. 51).

The breccia of Mammoth Rock is the only unit that does not follow the linear trends of TiO_2 and P_2O_5 against SiO_2 (Figs. 42, 43), but this appears to be due to anomalously low SiO_2 content. Otherwise, the breccia correlates with the felsic rocks in its geochemical signature and petrography. It is hypothesized that abnormally high fluid-rock interaction, as suggested by pervasive mineralization in that section of the pendant (Rinehart and Ross, 1964), was the mechanism for SiO_2 mobilization. The breccia is interpreted as a rhyolite based on the Winchester and Floyd (1977) discrimination diagram that compares Nb/Y to Zr/Ti (Fig. 50)

The mafic breccia of Pika Lake is depleted in HREEs and slightly more enriched in LREEs than average continental crust (Fig. 51; Rudnick, 2003). Although the breccia plots as a continental arc lava, it has a slightly more primitive signature than the dacite of Arrowhead Lake and the tuff of Skelton Lake, and follows the overall trend of the andesite of Mammoth Crest (Figs. 60-65).

The Jurassic tuff of Deer Lakes has a comparable geochemical signature to other felsic tuffs in the Mount Morrison pendant (Table 1) as well as Jurassic rhyolites in the Ritter Range pendant (Barth et al., in press). The tuff of Deer Lakes has the LREE-depleted, HFSE-enriched signature of an evolved crustal source (Figs 51, 52), and plots as a continental, calc-alkaline arc lava on Pearce (1983) discrimination diagrams (Figs. 60-65).

The two Cretaceous units demonstrate a bimodal geochemical distribution, with the andesite of Mammoth Crest being more mafic than the rhyolite of Purple Lake. Although both rocks plot as continental arc lavas on Pearce (1983) discrimination diagrams, the andesite's signature is closer to a primitive mantle source (Figs. 60-65) and overall trends closely follow that of the mafic breccia of Pika Lake. The SiO_2 content of these two mafic units is therefore representative of the original composition, indicating that hydrothermal alteration did not affect these units as much as the breccia of Mammoth Rock. The rhyolite of Purple Lake is the most felsic rock in the Mount Morrison volcanic suite, with a high concentration of SiO_2 and low amounts of PO_2 and TiO_2, (Figs. 42, 43, 51). The rhyolite has a similar REE trend to that of average continental crust (Fig. 50; Rudnick, 2003).

The Mount Morrison volcanic suite plots entirely within the parameters for an active continental margin setting according to the Pearce (1983) diagram using Th, Ta, and Yb (Fig. 60). Likewise, all rocks plot within the continental arc setting on the Pearce (1983)

discrimination diagram based on Zr/Y versus Zr (Fig. 62). All samples are classified as arc lavas according to the Pearce (1981) diagram of Ti versus Zr (Fig. 61). Furthermore, all samples have major- and trace-elemental signatures of continental arc rocks. All rocks plot on a calc-alkaline trend using the Wood (1980) ternary diagram of Hf, Th, and SiO_2 (Figs. 65). Considering these discrimination diagrams together, rocks of the Mount Morrison pendant demonstrate that this part of the Sierran arc was emplaced through evolved continental crust.

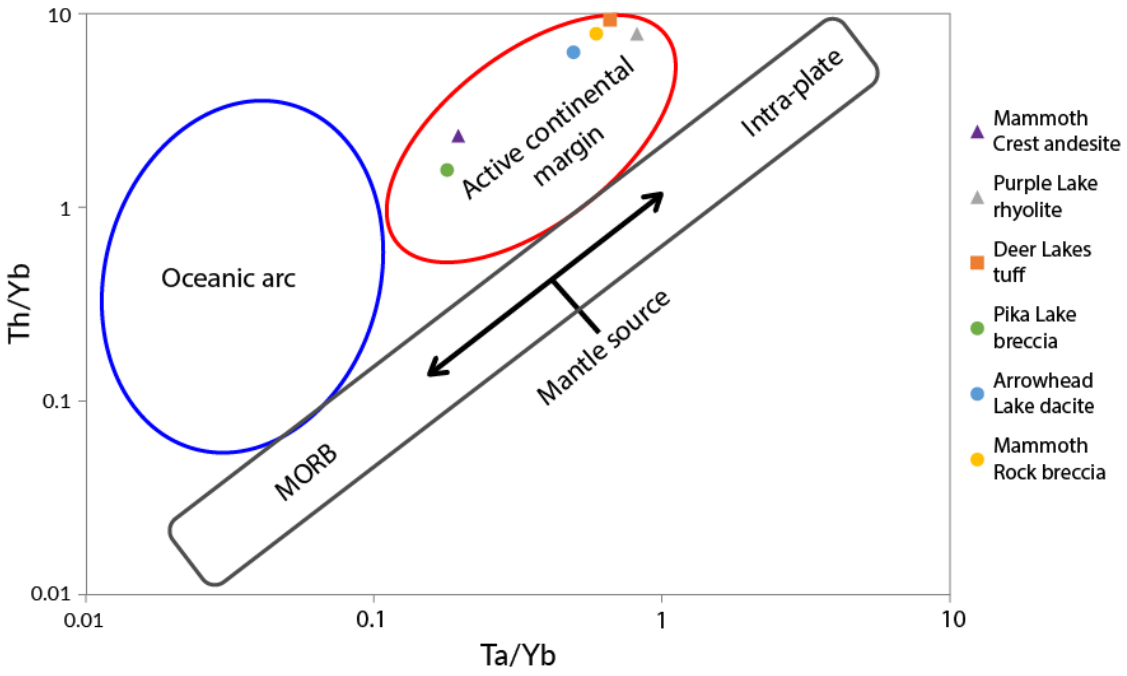

Figure 60: Discrimination of tectonic setting for volcanic rocks of the Mount Morrison pendant using Th/Yb against Ta/Yb (Pearce, 1983).

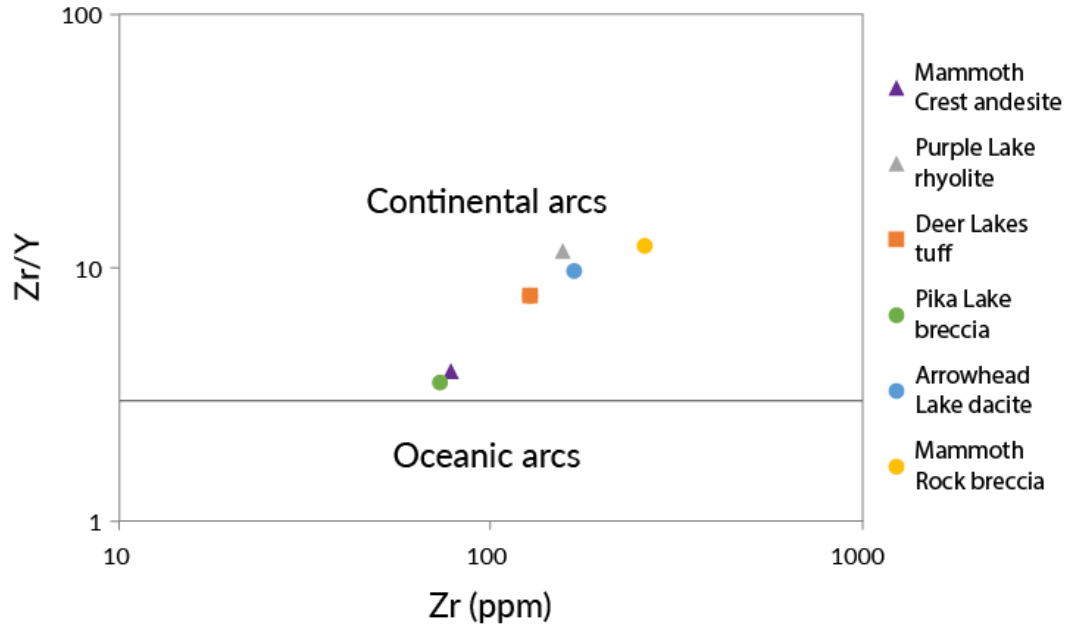

Figure 61: Discrimination of arc type for volcanic rocks of the Mount Morrison pendant using Zr/Y against Zr (Pearce, 1983).

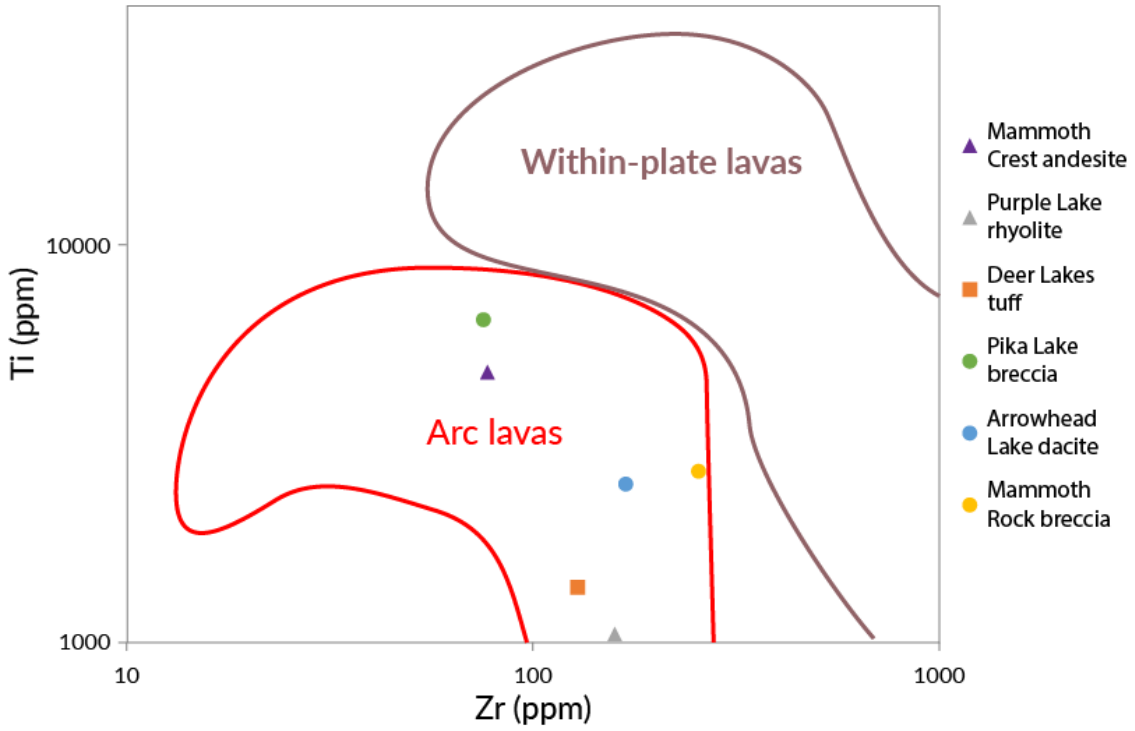

Figure 62: Discrimination of tectonic setting for volcanic rocks of the Mount Morrison pendant using Ti against Zr (Pearce, 1983).

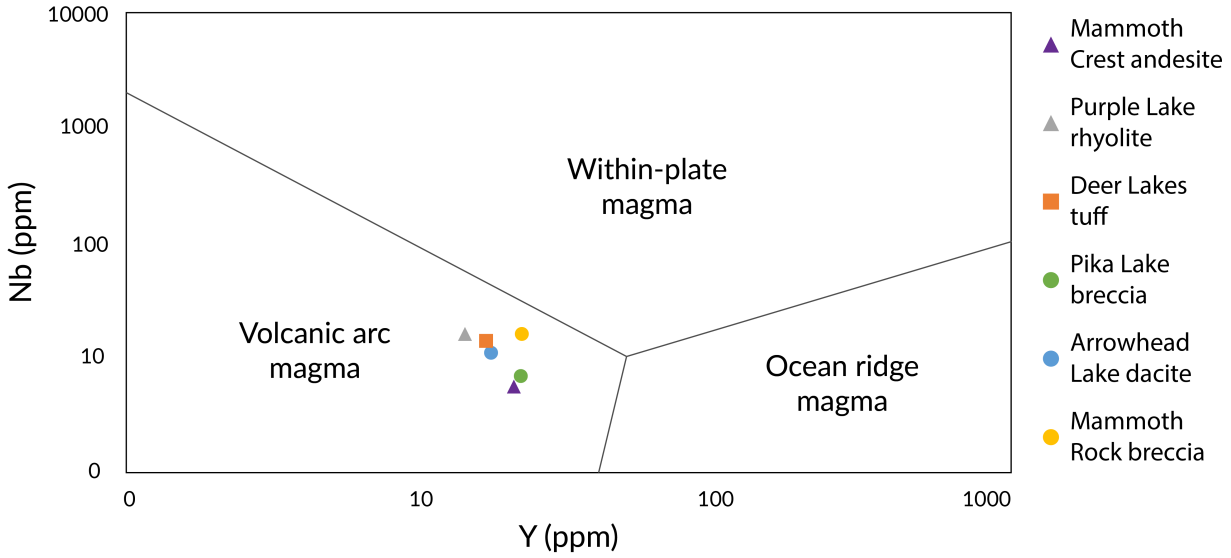

Figure 63: Discrimination of tectonic setting for volcanic rocks of the Mount Morrison pendant using Nb against Y (Pearce et al., 1984).

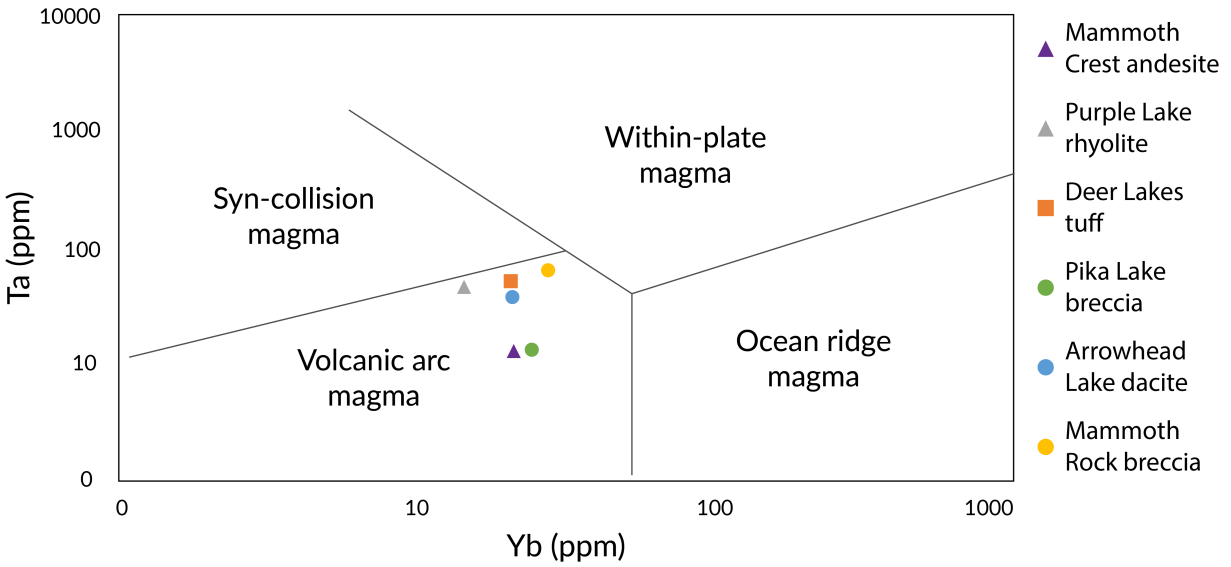

Figure 64: Discrimination of tectonic setting for volcanic rocks of the Mount Morrison pendant using Ta against Yb (Pearce et al., 1984).

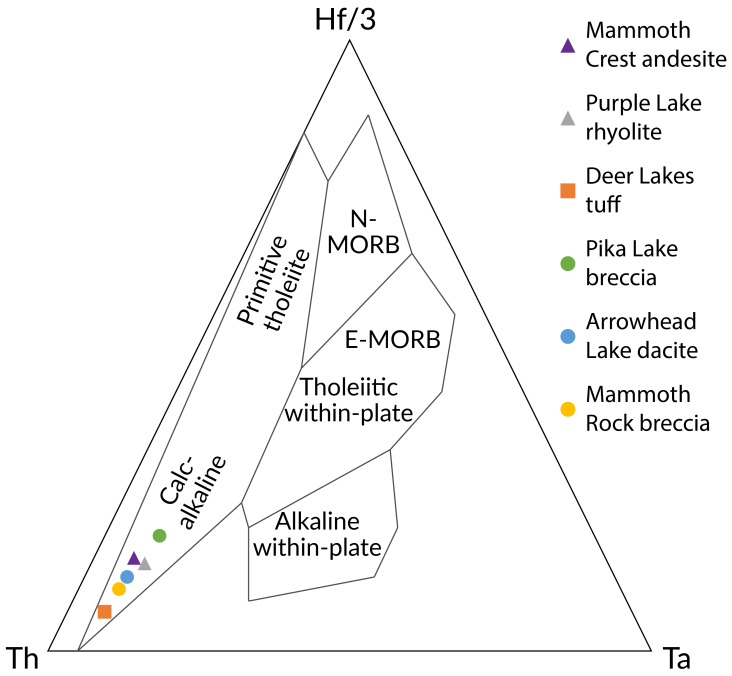

Figure 65: Ternary diagram for discrimination of tectonic setting for Mesozoic volcanic rocks of the Mount Morrison pendant using Hf, Th, and Ta (Wood, 1980).

7.3 STRUCTURAL GEOLOGY INTERPRETATIONS

The high-angle fault between Paleozoic and Mesozoic rocks in the Mount Morrison pendant is exposed at Mammoth Rock and in the North Fork Fish Creek area (Fig. 2). It is expressed at both locations as a 15-20-meter-wide zone of severely altered, fine-grained material. A period of uplift and erosion between the Pennsylvanian period and the Triassic period, documented elsewhere across the region (Russell and Nokleberg, 1977; Miller et al., 1992; Saleeby, 2011), is evidenced by the difference in structural fabric between highly folded Paleozoic rocks and steeply west-dipping Mesozoic rocks. At Mammoth Rock, the Triassic breccia of Mammoth Rock is juxtaposed against Pennsylvanian Mount Baldwin Marble. In the North Fork Fish Creek area (Figs. 2, 13), the fault divides the steeply west-dipping Triassic dacite of Arrowhead Lake (breccia and tuff facies) and isoclinally folded Pennsylvanian rocks

(Lake Dorothy Hornfels and Bloody Mountain Formation). The fault is recognized here as a 20-m-wide zone of hydrothermal alteration affecting the lowermost strata of the Triassic dacite of Arrowhead Lake. In the 10-km distance between the exposures at Mammoth Rock and the North Fork Fish Creek area, the fault is intruded by the Cretaceous Lee Lake granodiorite (Fig. 2).

The pattern of generally steep foliation in Triassic and Jurassic strata juxtaposed against more moderate (45-65°) foliation in Cretaceous units (Fig. 54) is observed both in the Mount Morrison pendant and 30 km to the northwest in the Ritter Range pendant (Fiske and Tobisch, 1994; Bentley, 2004). This angular discordance shows that Triassic and Jurassic blocks underwent at least one episode of deformation and translation prior to emplacement of Cretaceous rocks. Because metamorphism and deformation are broadly similar between the Mount Morrison pendant and the Ritter Range pendant, studies of the latter are used to make inferences regarding the deformational history of the former.

In the Ritter Range pendant, duplex thrusting of Late Triassic to Early Triassic rocks between 164 and 105 Ma produced cryptic, bedding-parallel faults and rotated blocks up to 45° (Tobisch et al., 2000, Barth et al., in press). Detailed mapping coupled with U-Pb zircon geochronology delineated five discrete structural blocks (Tobisch et al., 2000). Late Cretaceous deformation due to downward wall-rock flow during pluton emplacement is constrained to 98-90 Ma and accounts for additional tilting (Tobisch et al., 2000). Strike-slip partitioning created parallel structures as the Sierra Crest shear zone became active around 95 Ma (Tobisch et al., 1986; Sharp et al., 2000). Horizontal lineations on vertical shear surfaces demonstrate strain partitioning in a transpressional tectonic system (Tobisch et al., 2000). Structures that formed during crustal contraction during the Jurassic period were later displaced by the Sierra Crest shear zone. Tabular shear zones developed synchronously with the Late Cretaceous high-flux

magmatic event in response to increased crustal contraction (Tikoff and de Saint Blanquat, 1997; Sharp et al., 2000). Emplacement of Cretaceous granites was contemporaneous with the formation of ductile shear zones as the arc transitioned to a dextral transpressional regime.

Although this study did not measure lineations on slip surfaces, the timing and orientation of structural fabrics in the Mount Morrison pendant are broadly consistent with those of the Ritter Range pendant, and can be explained by a combination of Jurassic contraction and Cretaceous dextral transpressional shear along the axis of the arc with minor(?) influence from pluton emplacement dynamics. Jurassic and Triassic blocks were evidently rotated and cut by thrust faults prior to emplacement of Cretaceous rocks. Following the emplacement of Cretaceous rocks, the regional tectonic regime changed to oblique dextral transpression, which resulted in deformation of all Mesozoic rocks in addition to regional strike-slip strain partitioning. Studies of Sierran shear zones indicate that dextral displacement may have exceeded 20 km (Tobisch et al., 1986; Green and Schweickert, 1995). Based on this model, the rocks of the Mount Morrison pendant may be related to similar-aged plutonic and volcanic rocks in the Pine Creek pendant approximately 20 km to the southeast along the range axis. Future work correlating volcanic rocks between pendants thus depends not only on geochronology and geochemistry, but on tectonic reconstruction.

7.4 IMPLICATIONS FOR SIERRAN ARC TEMPO

The age distribution of Mount Morrison pendant rocks corresponds with pulses of Sierran arc volcanism recorded across the Sierra Nevada (Cao and Paterson, 2016). Figure 58 shows data from the Mount Morrison pendant compared to overall Sierran arc trends (Paterson et al., 2014; Cao and Paterson, 2016). Triassic rocks of the Mount Morrison pendant were emplaced within

the time frame of the first pulse of Sierran arc magmatism. Subaqueous textures in the breccia of Mammoth Rock, the breccia of Pika Lake, and the breccia of the dacite of Arrowhead Lake indicate that the arc was in a subaqueous setting. This agrees with observations of shallow marine rocks from the Late Triassic Sierran arc (Roberts, 2013; Paterson et al., 2014; Barth et al., in press).

The Jurassic block (i.e. the Deer Lakes sequence) corresponds to the beginning of the second Sierran arc magmatic pulse. Of the two minor volcanic pulses recorded in the Jurassic Sierra Nevada, the Deer Lakes sequence falls into the first (170-160 Ma). Lack of sedimentary structures within the Deer Lakes sequence prevent interpretation of paleogeographic setting.

Cretaceous rocks of the Mount Morrison pendant were emplaced during the midst of the third and final Sierran arc magmatic pulse. Compared to Sierran volcanic rocks, the Cretaceous block lines up with the end of major volcanic activity along the arc. Subaqueous sedimentary rocks suggest that the arc may have still been in a submarine setting at the end of the Early Cretaceous, or else that the Cretaceous block records lacustrine deposition. Subaqueous Cretaceous rocks are present in the Ritter Range pendant, and were interpreted as laminated tuffs deposited in a lake that formed within the Minarets caldera (Fiske and Tobisch, 1994). Subaqueous rocks in the Mount Morrison may therefore demonstrate one of two things: that the volcanic record of the Cretaceous Sierran arc is biased toward inverted topography of lake basins, or that the arc was still in a submarine setting at the end of the Early Cretaceous.

Following the thermochronologic modeling of McPhillips and Brandon (2012), the Sierra Nevada stood 5 km high at 100 Ma. However, this end-member-based method of inverse modeling merely simulates the exhumation of the range, and does not account for strain related to transpressional arc tectonics. The youngest marine rocks previously documented in the Sierra

Nevada are ~145 Ma (Fig. 58; Paterson et al., 2014), thereby providing a constraint on the elevation of the arc at the end of the Middle Jurassic magmatic pulse. The presence of subaqueous rocks (i.e. Duck Lake succession) in the Cretaceous block of the Mount Morrison pendant suggests either the presence of a large lake in the Late Cretaceous, or that the arc may not have emerged into the terrestrial realm until after ca. 100 Ma. Paleo-elevation curves on Figure 58 show the implications of each interpretation in comparison to a current model (Cao and Paterson, 2016) that was developed without knowledge of Cretaceous subaqueous rocks in the Mount Morrison pendant. Volcanic and sedimentary facies of the Mount Morrison pendant largely fit into the Cao and Paterson (2016) model, unless the subaqueous Cretaceous sedimentary rocks are taken to be marine in origin (Fig. 58).

8. CONCLUSIONS

The Mount Morrison pendant contains Mesozoic volcanic rocks from all three pulses of Sierran arc magmatism. Late Triassic (ca. 216 Ma) volcanism entailed the emplacement of voluminous dacitic to rhyolitic tuffs (tuff of Skelton Lake and tuffs associated with the dacite of Arrowhead Lake) and an extensive hypabyssal sill (intrusive dacite of Arrowhead Lake). Cuspate and jigsaw clast textures observed in the volcanic breccias (breccia of Mammoth Rock and breccia of Pika Lake) suggest that Triassic strata were emplaced in a subaqueous setting. Dacitic to rhyolitic pyroclastic rocks were emplaced through evolved continental crust in the Middle Jurassic (ca. 170 Ma). These rocks make up the Deer Lakes sequence and are today the westernmost exposure of volcanic strata in the Mount Morrison pendant. Growth of plutons during the Late Triassic and Middle Jurassic magmatic episodes was contemporaneous with the rotation and translation of Triassic and Jurassic rocks due to dextral transpressional motion along

the Sierra Crest shear zone. Around 101 Ma, massive volcanic flows (andesite of Mammoth Crest and rhyolite of Purple Lake) were emplaced in a subaqueous volcanic field. The andesite produced local folding in the intercalated shale and limestone layers. The final stage of batholith emplacement, during the Late Cretaceous, generated a third and final episode of magmatism and deformation, and as a result, Cretaceous rocks dip much less steeply and are much less deformed than Jurassic and Triassic rocks.

Geochronology of the Mount Morrison pendant corresponds with periods of high magmatic flux along the arc, bolstering the idea that such pulses are responsible for the majority of volcanic rocks in the Sierra Nevada. Immobile-element geochemistry shows that the entire suite was emplaced through evolved continental crust in a continental arc setting. high strain in Jurassic rocks obscures primary textures and prevents such interpretation. Volcanic textures in Triassic and Cretaceous rocks demonstrate a subaqueous setting. The present exposure of the Mount Morrison pendant demonstrates the episodic nature of Sierran arc magmatism.

REFERENCES

Barth, A., A. Feilen, S. Yager, S. Douglas, J. Wooden, N. Riggs, and J. Walker, 2012, Petrogenetic connections between ash-flow tuffs and a granodioritic to granitic intrusive suite in the Sierra Nevada arc, California: *Geosphere*, v. 8, no. 2, p. 1-15.

Barth, A., J. Walker, J. Wooden, N. Riggs, and R. Schweickert, 2011, Birth of the Sierra Nevada magmatic arc: Early Mesozoic plutonism and volcanism in the east-central Sierra Nevada of California: *Geosphere*, v. 7, no. 4, p. 877-897.

Barth, A., J. Wooden, C. Jacobson, and R. Economos, 2013, Detrital zircon as a proxy for tracking the magmatic arc system: The California arc example: *Geology*, v. 41, no. 2, p. 223-226.

Barth, A., J. Wooden, N. Riggs, J. Walker, and C. Jacobson, 2015, Marine volcaniclastic record of subduction inception and early Sierran arc evolution, Ritter Range pendant, California: *Geological Society of America Abstracts and Programs*, v. 47, n. 7, p. 579.

Barth, A., J. Wooden, R. Fiske, N. Riggs, J. Walker, K. Tani, R. Hanson, and C. Jacobson, in press, Marine volcaniclastic record of subduction inception and early arc evolution in the eastern Ritter Range pendant, east-central Sierra Nevada, California.

Batiza, R., and J. White, 2000, Submarine lavas and hyaloclastite, *in* Sigurdsson, H., B. Houghton, S. McNutt, H. Rymer, and J. Stix, eds, *Encyclopedia of Volcanoes: Academic Press*, p. 361-381.

Bentley, S., 2013, Rock fabric analysis of the Sierra Crest shear zone system, California: Implications for crustal-scale transpressional shear zones: M.S. Thesis, University of Maryland, College Park, 172 p.

Brook, C. A., 1977, Stratigraphy and structure of the Saddlebag Lake roof pendant, Sierra Nevada, California: *Geological Society of America Bulletin*, v. 88, p. 321–334.

Busby-Spera, C., 1985, Large-volume rhyolite ash-flow eruptions and submarine caldera collapse in the lower Mesozoic Sierra Nevada, California: *Journal of Geophysical Research*, v. 89, p. 8417-8427.

Cao, W., and S. Paterson, 2016, A mass balance and isostasy model: Exploring the interplay between magmatism, deformation and surface erosion in continental arcs using central Sierra Nevada as a case study, *Geochemistry, Geophysics, Geosystems*, v. 17.

Cassel, E., S. Graham, C. Chamberlain, and C. Henry, 2012, Early Cenozoic topography, morphology, and tectonics of the northern Sierra Nevada and western Basin and Range: *Geosphere*, v. 8, n. 2, p. 229-249.

de Silva, S., N. Riggs, and A. Barth, 2015, Quickening the pulse: fractal tempos in continental magmatism: *Elements*, v. 11, p. 113-118.

Davidson, A., 1995, A review of the Grenville orogeny in its North American type area: *Journal of Australian Geology & Geophysics*, v. 16, p. 3-24.

Douglas, S., N. Riggs, A. Barth, and J. Walker, 2010, The breccia of Frog Lakes: reconstructing Triassic volcanism in the east-central Sierra Nevada, California: *Geological Society of America Abstracts and Programs*, v. 42, n. 5, p. 296.

Ducea, M., 2001, The California arc: Thick granitic batholiths, eclogitic residues, lithospheric-scale thrusting, and magmatic flare-ups: *GSA Today*, v. 11, p. 4-10.

Fisher, R., 1984, Submarine volcaniclastic rocks *in* Kokelaar, B. and M. Howells, eds, Marginal basin geology: Volcanic and associated sedimentary and tectonic processes in modern and ancient marginal basins: *Special Publication, Geological Society of London*, v. 16, p. 5-27.

Fiske, R., and O. Tobisch, 1978, Paleogeographic significance of the volcanic rocks of the Ritter Range pendant, central Sierra Nevada, California: *Mesozoic Paleogeography of the Western United States*, issue 2, v. 209-221.

Fiske, R., and O. Tobisch, 1994, Middle Cretaceous ash-flow tuff and caldera-collapse deposit in the Minarets caldera, east-central Sierra Nevada, California: *Geological Society of America Bulletin*, v. 106, p. 582-593.

Gehrels, G., 2000, Introduction to detrital zircon studies of Paleozoic and Triassic strata in western Nevada and northern California, *in* Soreghan, M.J., and Gehrels, G.E., eds., Paleozoic and Triassic Paleogeography and Tectonics of Western Nevada and Northern California: *Geological Society of America Special Paper 347*, p. 1-17.

Gioncada, A., O. Gonzalez-Ferran, M. Lezzerini, R. Mazzuoli, M. Bisson, and S. Rapu, 2010, The volcanic rocks of Easter Island (Chile) and their use for the Moai sculptures: *European Journal of Mineralogy*, v. 22, p. 855-867.

Hanson, B., S. Sorensen, M. Barton, and R. Fiske, 1993, Long-Term Evolution of Fluid-Rock Interactions in Magmatic Arcs: Evidence from the Ritter Range Pendant, Sierra Nevada, California, and Numerical Modeling, *Journal of Petrology,* v. 34, n. 1, p. 23-6.

Huber, N., and C. Rinehart, 1965, Geologic map of the Devils Postpiles quadrangle, Sierra Nevada, California, Map GQ-437: *U.S. Geological Survey*, Reston, Virginia.

Jones, E., and J. Rougvie, 2004, Structural and metamorphic history in the vicinity of Purple Lake, Mount Morrison roof pendant, California: *Geological Society of America Abstracts and Programs*, v. 36, n. 3, p. 42.

Kokelaar, P., and C. Busby, 1992, Subaqueous explosive eruption and welding of pyroclastic density deposits: *Science*, v. 259, p. 196-201.

Kylander-Clark, A., B. Hacker, and J. Cottle, 2013, Laser-ablation split-stream ICP petrochronology: *Chemical Geology*, v. 345, p. 99-112.

McNulty, B., W. Tong, and O. Tobisch, 1996, Assembly of a dike-fed magma chamber: The Jackass Lakes pluton, central Sierra Nevada, California, *Geological Society of America Bulletin*, v. 108, n. 8, p. 926-940.

McPhillips, D. and M. Brandon, 2012, Topographic evolution of the Sierra Nevada measured directly by inversion of low-temperature thermochronology: *American Journal of Science*, v. 312, p. 90-116.

Miller, E., M. Miller, C. Stevens, J. Wright, and R. Madrid, 1992, Latest Precambrian to latest Devonian time; Development of a continental margin: *The Cordilleran Orogen: Conterminous U.S.: The Geology of North America*, v. G-3, p. 57-106.

Mullen, E., 1983, MnO/TiO2/P2O5: A minor element discriminant for basaltic rocks of oceanic environments and its implications for petrogenesis: *Earth and Planetary Science Letters*, v. 62 i. 1, 53-62.

Nokleberg, W., and R. Kistler, 1980, Paleozoic and Mesozoic deformations in the central Sierra Nevada, California: *United States Geological Survey Professional Paper 1145*.

Nyman, M., and K. Karlstrom, 1997, Pluton emplacement processes and tectonic setting of the 1.42 Ga Signal batholith, SW USA: important role of crustal anisotropy during regional shortening: *Precambrian Research*, v. 82, i. 3-4, p. 237-263.

Otieno,V. 2016, Assessing hydrothermal alteration effects on bulk-rock geochemistry: A case example of Well OW-910 at Olkaria geothermal field, Kenya: *African Rift Geothermal Conference Abstract*.

Paterson, S.R., Memeti, V., Anderson, L., Cao, W., Lackey, J.S., Putirka, K.D., Miller, R.B., Miller, J.S., Mundil, R., 2014, Day 6: overview of arc processes and tempos. In: Memeti, V., Paterson, S.R., Putirka, K.D. (Eds.), *Formation of the Sierra Nevada Batholith: Magmatic and Tectonic Processes and Their Tempos*, p. 87–116.

Paterson, S., and M. Ducea, 2015, Arc magmatic tempos: Gathering the evidence: *Elements*, v. 11, p. 91-98.

Pearce, J., 1983, Role of the sub-continental lithosphere in magma genesis at active continental margins: p. 230-249 in Hawkesworth, C.J. and Norry, M.J., eds., *Continental Basalts and Mantle Xenoliths*, Shiva Publishing Ltd., Cambridge, Mass., 272 p.

Pearce, J., N. Harris, and A. Tindle, Trace element discrimination diagrams for the tectonic interpretation of granitic rocks: *Journal of petrology*, v. 25, i. 4, p. 956-983.

Pirajno, F., 1992, *Hydrothermal Mineral Deposits.* John Wiley and Sons, Sydney, 709 p.

Poage, M., and C. Chamberlain, 2002, Stable isotopic evidence for a Pre-Middle Miocene rain shadow in the western Basin and Range:Implications for the paleotopography of the Sierra Nevada: *Tectonics*, v. 21, p. 1-10.

Rinehart, C., and D. Ross, 1964, Geology and Mineral Deposits of the Mount Morrison Quadrangle, Sierra Nevada, California: *Geological Survey Professional Paper 385*, v. 106.

Roberts, S., 2013, Breccia of Frog Lakes: Reconstructing Triassic volcanism and subduction initiation in the east-central Sierra Nevada, California: M.S. Thesis, Indiana University, Bloomington, 57 p.

Rougvie, J., S. Sorensen, M. Barton, and R. Skoza, 2013, Low-T alteration of volcanoplutonic rocks: Processing fluids in the uppermost subduction factory: *Geological Society of America Abstracts and Programs*, v. 45, n. 7, p. 276.

Rudnick, 2003, Composition of the continental crust, v. 3, p. 1-64 in *Treatise on Geochemistry*, eds. Holland, D., and K. Turekian, Elsevier Publishing, Oxford.

Ruppel, E., 1972, Geology of pre-Tertiary rocks in the northern part of Yellowstone National Park, Wyoming: *Geological Survey Professional Paper*, n. 729, 65 p.

Russell, S., and W. Nokleberg, 1977, Superimposition and timing of deformations in the Mount Morrison roof pendant and in the central Sierra Nevada, California: *Geologic Society of America Bulletin*, v. 88, i. 3, p. 334-345.

Saleeby, J., and G. Dunne, 2015, Temporal and tectonic relations of Early Mesozoic arc magmatism, southern Sierra Nevada, California: *Geological Society of America Special Papers*, v. 513.

Schweickert, R., and M. Lahren, 1993, Tectonics of the east-central Sierra Nevada: Saddlebag Lake and northern Ritter Range pendants *in* Lahren, M., J. Trexler, and C. Spinosa, eds., *Crustal Evolution of the Great Basin and Sierra Nevada*: University of Nevada, Reno NV, p. 313-351.

Schweickert, R., and M. Lahren, 1999, Triassic caldera at Tioga Pass, Yosemite National Park, California: Structural relationships and significance: *Geological Society of America Bulletin*, v. 111, no. 11, p. 1714-1722.

Schweickert, R., and M. Lahren, 2006, Geologic evolution of Saddlebag Lake pendant, eastern Sierra Nevada, California: Tectonic implications, *in* Girty, G., and Cooper, J.D., eds., Using stratigraphy, sedimentology, and geochemistry to unravel the geologic history of the southwestern Cordillera: *Pacific Section: Society for Sedimentary Geology*, p. 27-56.

Sharp, W., O. Tobisch, and P. Renne, 2000, Development of Cretaceous transpressional cleavage synchronous with batholith emplacement, central Sierra Nevada, California: *Geological Society of America Bulletin*, v. 112, i. 7, p. 1059–1066.

Sorensen, S., G. Dunne, R. Hanson, M. Barton, J. Becker, O. Tobisch, and R Fiske, 1998, From Jurassic shores to Cretaceous plutons: Geochemical evidence for paleoalteration environments of metavolcanic rocks, eastern California *Geological Society of America Bulletin*, v. 110, n. 3, p. 326-343.

Sruoga, P., M. Japas, F. Salani, and L. Kleiman, 2013, La Peligrosa caldera: A key event during the Jurassic ignimbrite flare-up in southern Patagonia, Argentina: *Journal of Volcanology and Geothermal Research*, v. 269. P. 44-56.

Stern, R., 2004, Subduction initiation: spontaneous and induced: *Earth and Planetary Science Letters*, v. 226, p. 275–292.

Steven, T., and P. Lipman, 1976, Calderas of the San Juan volcanic field, southwestern Colorado: *U.S. Geological Survey Professional Paper 95*, 35 pp.

Stevens, C., P. Stone, G. Dunne, D. Greene, J. Walker, and B. Swanson, 1997, Paleozoic and Mesozoic evolution of East-Central California: *Geological Society of America*, p. 119-154.

Stevens, M., 2012, Emplacement of the large andesite lava flow in the Oturere Stream valley, Tongariro Volcano, from airborne interferometric radar: *New Zealand Journal of Geology and Geophysics*, v. 43, i. 3, p. 387-394.

Sun, S., and W. McDonough, 1989, Chemical and isotopic systematics of oceanic basalts: Implications for mantle composition and processes: *Geological Society, London, Special*

Publications, v. 42, p. 313-345.

Tikoff, B., and M. de Saint Blanquat, 1997, Transpressional shearing and strike-slip partitioning in the Late Cretaceous Sierra Nevada magmatic arc, California: *Tectonics*, v. 16, i. 3, p. 442-459.

Tobisch, O., and R. Fiske, 1982, Repeated parallel deformation in part of the eastern Sierra Nevada, California and its implications for dating structural events: Journal of Structural Geology, v. 4, i. 2, p. 177-195.

Tobisch, O., J. Saleeby, and R. Fiske, 1986, Structural history of continental volcanic arc rocks, eastern Sierra Nevada, California: A case for extensional tectonics: *Tectonics*, v. 5, n. 1, p. 65-94.

Tobisch, O., R. Fiske, J. Saleeby, E. Holt, and S. Sorensen, 2000, Steep tilting of metavolcanic rocks by multiple mechanisms, central Sierra Nevada, California: *Geological Society of America Bulletin*, v. 112, n. 7, p. 1043-1058.

Whitesides, J., 2011, Rock fabric analysis of the Sierra Crest shear zone system, California: Implications for crustal-scale transpressional shear zones: B.Sc. Thesis, University of Maryland, College Park, 172 p.

Winchester, J., and P. Floyd, 1977, Geochemical discrimination of different magma series and their differentiation products using immobile elements: *Chemical geology* v. 20 p. 325-343.

Wood, David A. "The application of a Th Hf Ta diagram to problems of tectonomagmatic classification and to establishing the nature of crustal contamination of basaltic lavas of the British Tertiary Volcanic Province: *Earth and Planetary Science Letters*, v. 50, i. 1, p. 11-30.

Zimmer, B., N. Riggs, and G. Carrasco-Nunez, 2010, Evolution of tuff ring dome complex: the case study of Cerro Pinto, eastern Transmexican Volcanic Belt: *Bulletin of Volcanology*, v. 72, i. 10, p. 1223-1240

APPENDIX A

Sample	$^{207}Pb/^{235}U$	207/235 2σ error	$^{206}Pb/^{238}U$	206/238 2σ error	Error correlation 7/35-6/38	$^{207}Pb/^{206}Pb$	206/207 2σ error	Error correlation 6/38-6/7
MRB-73	0.238	0.0025	0.0338	0.00038	0.153	0.0509	0.00034	0.153
MRB-58	0.234	0.0027	0.0339	0.00034	0.017	0.0504	0.00030	0.017
MRB-35	0.239	0.0028	0.0340	0.00025	-0.070	0.0510	0.00043	-0.070
MRB-21	0.236	0.0042	0.0340	0.00024	0.200	0.0505	0.00094	0.200
MRB-17	0.266	0.0033	0.0341	0.00036	0.469	0.0566	0.00110	0.469
MRB-44	0.241	0.0022	0.0341	0.00032	0.410	0.0511	0.00021	0.410
MRB-53	0.254	0.0037	0.0343	0.00024	0.317	0.0533	0.00071	0.317
MRB-30	0.246	0.0022	0.0344	0.00016	-0.074	0.0518	0.00047	-0.074
MRB-3	0.247	0.0037	0.0346	0.00023	0.065	0.0521	0.00070	0.065
MRB-41	0.242	0.0031	0.0346	0.00051	0.455	0.0507	0.00024	0.455
MRB-39	0.249	0.0028	0.0348	0.00028	0.077	0.0518	0.00045	0.077
MRB-64	0.249	0.0053	0.0350	0.00060	0.180	0.0513	0.00076	0.180
MRB-55	0.246	0.0033	0.0352	0.00039	-0.151	0.0507	0.00037	-0.151
MRB-38	0.250	0.0012	0.0353	0.00014	0.445	0.0513	0.00019	0.445
MRB-59	0.250	0.0027	0.0356	0.00023	0.039	0.0510	0.00036	0.039
MRB-45	0.253	0.0032	0.0356	0.00041	0.303	0.0516	0.00033	0.303
MRB-16	0.248	0.0020	0.0356	0.00026	0.425	0.0505	0.00043	0.425
MRB-8	0.253	0.0032	0.0357	0.00025	0.035	0.0515	0.00062	0.035
MRB-5	0.251	0.0063	0.0357	0.00045	-0.296	0.0509	0.00095	-0.296
MRB-14	0.263	0.0042	0.0358	0.00049	-0.049	0.0524	0.00080	-0.049
MRB-28	0.261	0.0037	0.0358	0.00035	0.351	0.0527	0.00058	0.351
MRB-6	0.252	0.0028	0.0359	0.00035	-0.071	0.0512	0.00039	-0.071
MRB-42	0.254	0.0039	0.0359	0.00045	-0.142	0.0508	0.00051	-0.142
MRB-34	0.252	0.0030	0.0359	0.00025	0.126	0.0509	0.00052	0.126
MRB-36	0.253	0.0028	0.0360	0.00047	0.267	0.0506	0.00046	0.267
MRB-43	0.275	0.0057	0.0361	0.00026	-0.030	0.0553	0.00120	-0.030
MRB-25	0.268	0.0057	0.0361	0.00047	0.100	0.0539	0.00130	0.100
MRB-37	0.251	0.0056	0.0362	0.00038	0.169	0.0504	0.00110	0.169
MRB-13	0.255	0.0047	0.0362	0.00035	-0.021	0.0507	0.00076	-0.021
MRB-24	0.249	0.0046	0.0362	0.00028	-0.077	0.0498	0.00078	-0.077
MRB-29	0.256	0.0042	0.0363	0.00034	0.308	0.0508	0.00069	0.308
MRB-11	0.257	0.0038	0.0363	0.00032	0.656	0.0514	0.00097	0.656
MRB-32	0.257	0.0035	0.0363	0.00038	0.297	0.0514	0.00070	0.297

Table 2a (continued on next page): U-Pb analytical data for 49 zircon samples of the breccia of Mammoth Rock (MRB).

Sample	207Pb/235U	207/235 2σ error	206Pb /238U	206/238 2σ error	Error correlation 7/35-6/38	207Pb/206Pb	206/207 2σ error	Error correlation 6/38-6/7
MRB-33	0.263	0.0024	0.0364	0.00045	0.371	0.0524	0.00050	0.371
MRB-15	0.261	0.0020	0.0364	0.00043	0.018	0.0512	0.00079	0.018
MRB-4	0.255	0.0047	0.0365	0.00063	-0.012	0.0507	0.00045	-0.012
MRB-2	0.254	0.0052	0.0366	0.00038	-0.315	0.0510	0.00050	-0.315
MRB-23	0.258	0.0023	0.0367	0.00020	0.245	0.0507	0.00039	0.245
MRB-27	0.283	0.0052	0.0367	0.00062	0.204	0.0558	0.00064	0.204
MRB-67	0.277	0.0071	0.0368	0.00039	0.221	0.0547	0.00120	0.221
MRB-60	0.258	0.0082	0.0368	0.00083	-0.116	0.0507	0.00092	-0.116
MRB-52	0.282	0.0083	0.0369	0.00026	-0.289	0.0553	0.00130	-0.289
MRB-46	0.265	0.0025	0.0369	0.00025	0.401	0.0517	0.00056	0.401
MRB-22	0.349	0.0097	0.0488	0.00044	0.242	0.0518	0.00120	-0.388
MRB-26	2.034	0.0510	0.1830	0.00270	-0.388	0.0798	0.00190	0.046
MRB-62	2.755	0.0390	0.2277	0.00170	0.046	0.0874	0.00110	0.167
MRB-69	2.703	0.0320	0.2277	0.00290	0.167	0.0863	0.00071	0.111
MRB-9	3.040	0.0310	0.2439	0.00230	-0.834	0.0906	0.00045	-0.207
MRB-61	3.114	0.0420	0.2471	0.00240	-0.207	0.0914	0.00054	-0.180
MRB-18	6.780	0.1000	0.3755	0.00360	-0.180	0.1307	0.00039	0.060

Table 2a (continued from previous page): U-Pb analytical data for 49 zircon samples of the breccia of Mammoth Rock (MRB).

Sample	Age (Ma) $^{207}Pb/^{235}U$	207/235 age 2σ error	Age (Ma) $^{206}Pb/^{238}U$	206/238 age 2σ error	Age (Ma) $^{206}Pb/^{207}Pb$	concor-dance filter	Pb (ppm)	U (ppm)	Th (ppm)
MRB-73	216	2.1	214	2.3	235	0.99	1034.0	275.9	26.6
MRB-58	214	2.2	215	2.1	214	1.01	903.0	266.2	25.9
MRB-35	217	2.3	216	1.6	238	0.99	649.0	246.2	23.7
MRB-21	216	3.9	216	1.5	216	1.00	162.0	48.9	4.9
MRB-17	240	2.6	216	2.3	474	0.90	179.8	83.7	9.5
MRB-44	219	1.8	216	2.0	246	0.99	1561.0	1173.0	113.6
MRB-53	230	3.0	218	1.5	340	0.95	1083.0	499.7	50.7
MRB-30	224	1.8	218	1.0	276	0.97	1009.0	334.3	34.0
MRB-3	224	3.0	219	1.4	288	0.98	1105.0	343.4	36.5
MRB-41	220	2.6	219	3.2	226	0.99	1250.0	482.0	47.7
MRB-39	226	2.2	220	1.7	275	0.98	843.0	311.0	30.6
MRB-64	225	4.4	222	3.7	254	0.98	340.0	154.0	15.1
MRB-55	224	2.7	223	2.5	233	1.00	1029.0	318.0	31.6
MRB-38	226	1.0	223	0.9	253	0.99	1435.0	490.0	48.9
MRB-59	226	2.2	225	1.4	239	1.00	956.0	224.9	22.8
MRB-45	229	2.6	226	2.6	268	0.99	292.0	116.9	11.4
MRB-16	225	1.6	226	1.6	217	1.00	859.0	213.9	22.5
MRB-8	229	2.6	226	1.6	263	0.99	431.0	169.9	18.9
MRB-5	227	5.1	226	2.8	236	1.00	263.0	80.0	9.0
MRB-14	237	3.4	227	3.0	314	0.96	207.6	99.7	11.0
MRB-28	236	3.0	227	2.2	315	0.96	307.0	93.2	9.8
MRB-6	228	2.3	227	2.2	248	1.00	934.0	323.2	35.4
MRB-42	229	3.1	228	2.8	231	0.99	431.1	230.5	23.9
MRB-34	228	2.4	228	1.6	236	1.00	468.8	137.6	13.8
MRB-36	229	2.3	228	2.9	221	1.00	446.0	162.2	16.6
MRB-43	246	4.5	228	1.6	420	0.93	591.0	335.0	34.9
MRB-25	241	4.6	229	2.9	363	0.95	617.0	246.5	28.4
MRB-37	227	4.6	229	2.4	210	1.01	210.0	67.2	6.7
MRB-13	230	3.8	229	2.2	237	1.00	216.0	78.2	8.7
MRB-24	226	3.8	229	1.8	182	1.02	401.8	133.6	14.1
MRB-29	232	3.4	230	2.1	231	0.99	241.8	116.5	12.1
MRB-11	232	3.1	230	2.0	255	0.99	338.0	101.7	11.5
MRB-32	232	2.8	230	2.3	256	0.99	501.0	207.0	21.3

Table 2b (continued on next page): U-Pb age data for 49 zircon samples of the breccia of Mammoth Rock (MRB).

Sample	Age (Ma) 207Pb/235U	207/235 age 2σ error	Age (Ma) 206Pb/238U	206/238 age 2σ error	Age (Ma) 206Pb/207Pb	concor-dance filter	Pb (ppm)	U (ppm)	Th (ppm)
MRB-33	237	2.0	230	2.8	300	0.97	806.0	382.0	40.5
MRB-15	235	1.6	231	2.6	247	0.98	294.0	122.0	12.8
MRB-4	230	3.8	231	3.9	227	1.00	630.0	320.0	41.0
MRB-2	230	4.2	232	2.4	240	1.01	147.7	37.2	4.2
MRB-23	233	1.8	232	1.3	227	1.00	544.2	232.9	25.9
MRB-27	253	4.1	233	3.9	443	0.92	457.0	194.0	21.8
MRB-67	248	5.6	233	2.4	396	0.94	294.0	108.0	12.0
MRB-60	233	6.6	233	5.2	224	1.00	356.0	99.5	10.4
MRB-52	252	6.5	234	1.6	423	0.93	331.9	119.4	13.8
MRB-46	238	2.0	234	1.5	270	0.98	203.4	75.4	7.9
MRB-22	304	7.3	307	2.7	272	1.01	164.7	116.5	16.4
MRB-26	1126	17.0	1084	15.0	1189	0.91	62.0	35.4	19.0
MRB-62	1343	11.0	1322	8.7	1368	0.97	46.9	37.2	21.5
MRB-69	1329	8.9	1323	15.0	1345	0.98	122.5	48.8	29.5
MRB-9	1420	8.7	1407	12.0	1439	0.98	268.5	47.9	34.4
MRB-61	1436	10.0	1424	13.0	1454	0.98	167.7	88.2	58.4
MRB-18	2087	11.0	2055	17.0	2108	0.98	55.0	72.7	73.7

Table 2b (continued from previous page): U-Pb age data for 49 zircon samples of the breccia of Mammoth Rock (MRB).

Sample	$^{207}Pb/^{235}U$	207/235 2σ error	$^{206}Pb/^{238}U$	206/238 2σ error	Error correlation 7/35-6/38	$^{207}Pb/^{206}Pb$	206/207 2σ error	Error correlation 6/38-6/7
ALD-17	0.237	0.0037	0.0319	0.00037	0.191	0.0532	0.00081	0.481
ALD-35	0.230	0.0023	0.0322	0.00047	0.849	0.0515	0.00037	0.706
ALD-26	0.230	0.0029	0.0328	0.00042	0.606	0.0504	0.00046	0.422
ALD-11	0.230	0.0056	0.0335	0.00059	0.641	0.0500	0.00096	0.206
ALD-9	0.237	0.0026	0.0338	0.00028	0.426	0.0503	0.00051	0.292
ALD-32	0.239	0.0041	0.0338	0.00031	0.884	0.0513	0.00045	-0.469
ALD-29	0.238	0.0054	0.0338	0.00037	0.891	0.0506	0.00048	-0.546
ALD-3	0.240	0.0030	0.0340	0.00027	0.746	0.0510	0.00043	-0.052
ALD-18	0.237	0.0018	0.0341	0.00026	0.430	0.0508	0.00038	0.345
ALD-13	0.239	0.0041	0.0342	0.00032	0.808	0.0507	0.00066	-0.367
ALD-21	0.240	0.0049	0.0342	0.00047	0.885	0.0510	0.00043	-0.414
ALD-12	0.246	0.0039	0.0342	0.00045	0.695	0.0520	0.00055	-0.117
ALD-14	0.238	0.0035	0.0343	0.00022	0.550	0.0507	0.00067	-0.163
ALD-30	0.244	0.0046	0.0343	0.00033	0.671	0.0513	0.00042	0.069
ALD-24	0.242	0.0064	0.0344	0.00090	0.924	0.0510	0.00063	-0.037
ALD-20	0.249	0.0045	0.0345	0.00045	0.548	0.0525	0.00049	0.189
ALD-33	0.242	0.0035	0.0345	0.00040	0.800	0.0509	0.00040	-0.087
ALD-7	0.243	0.0054	0.0346	0.00059	0.886	0.0506	0.00045	-0.256
ALD-6	0.253	0.0060	0.0346	0.00043	0.556	0.0530	0.00093	0.114
ALD-39	0.238	0.0031	0.0346	0.00040	0.521	0.0498	0.00053	0.200
ALD-40	0.239	0.0040	0.0346	0.00042	0.720	0.0502	0.00059	0.229
ALD-8	0.243	0.0049	0.0347	0.00040	0.512	0.0509	0.00091	0.191
ALD-4	0.245	0.0025	0.0347	0.00038	0.575	0.0510	0.00057	0.611
ALD-34	0.241	0.0046	0.0347	0.00072	0.664	0.0510	0.00079	0.369
ALD-19	0.239	0.0026	0.0347	0.00041	0.449	0.0501	0.00063	0.564
ALD-2	0.242	0.0050	0.0348	0.00043	0.647	0.0500	0.00055	-0.145
ALD-27	0.251	0.0043	0.0350	0.00037	0.208	0.0523	0.00094	0.399
ALD-38	0.251	0.0044	0.0351	0.00032	0.674	0.0517	0.00066	-0.105
ALD-28	0.248	0.0032	0.0351	0.00029	0.629	0.0511	0.00044	-0.110
ALD-5	0.247	0.0042	0.0351	0.00034	0.747	0.0510	0.00064	-0.398
ALD-10	0.263	0.0064	0.0351	0.00056	0.608	0.0540	0.00110	-0.104
ALD-15	0.245	0.0020	0.0351	0.00025	0.568	0.0505	0.00038	0.279
ALD-22	0.254	0.0061	0.0353	0.00059	0.489	0.0520	0.00069	0.150
ALD-23	0.252	0.0030	0.0355	0.00037	0.781	0.0517	0.00020	0.218
ALD-24	0.263	0.0091	0.0355	0.00050	0.498	0.0530	0.00160	0.023
ALD-25	0.249	0.0032	0.0356	0.00032	0.591	0.0506	0.00052	0.119
ALD-26	0.261	0.0023	0.0368	0.00053	0.570	0.0511	0.00064	0.498
ALD-27	0.255	0.0058	0.0368	0.00049	0.862	0.0510	0.00063	-0.413
ALD-28	0.259	0.0044	0.0369	0.00032	0.705	0.0505	0.00060	-0.225
ALD-29	0.290	0.0085	0.0392	0.00038	0.178	0.0533	0.00140	-0.014

Table 3a: U-Pb analytical data for 40 zircon samples of the dacite of Arrowhead Lake (ALD).

Sample	Age (Ma) $^{207}Pb/^{235}U$	207/235 age 2σ error	Age (Ma) $^{206}Pb/^{238}U$	206/238 age 2σ error	Age (Ma) $^{206}Pb/^{207}Pb$	concor-dance filter	Pb (ppm)	U (ppm)	Th (ppm)
ALD-17	216	3.0	202	2.3	360	0.94	14.6	330.0	185.4
ALD-35	210	1.9	204	2.9	263	0.97	45.5	932.0	446.6
ALD-26	210	2.4	208	2.6	215	0.99	28.5	464.0	273.7
ALD-11	210	4.6	212	3.7	195	1.01	8.8	295.0	85.0
ALD-9	216	2.1	214	1.7	209	0.99	18.8	416.0	178.9
ALD-32	219	3.7	214	1.9	253	0.98	25.2	735.0	256.3
ALD-29	217	4.4	214	2.3	223	0.99	25.1	467.0	235.9
ALD-3	218	2.5	216	1.7	242	0.99	41.7	1152.0	420.0
ALD-18	216	1.5	216	1.6	229	1.00	24.7	798.0	252.0
ALD-13	217	3.4	217	2.0	224	1.00	23.4	432.0	222.2
ALD-21	218	4.0	217	2.9	242	0.99	52.2	592.0	515.0
ALD-12	223	3.2	217	2.8	283	0.97	21.0	511.0	197.2
ALD-14	217	2.8	217	1.3	227	1.00	14.2	443.0	147.0
ALD-30	222	3.7	217	2.1	253	0.98	14.8	355.0	141.0
ALD-24	220	5.3	218	5.6	240	0.99	29.4	386.0	297.0
ALD-20	226	3.7	218	2.8	314	0.97	11.6	348.0	109.7
ALD-33	220	2.9	219	2.5	234	0.99	49.9	714.0	471.0
ALD-7	221	4.4	219	3.7	220	0.99	27.1	480.0	254.0
ALD-6	229	4.8	220	2.7	327	0.96	21.1	438.0	199.5
ALD-39	217	2.5	220	2.5	186	1.01	16.9	300.0	156.7
ALD-40	218	3.3	220	2.6	204	1.01	23.5	441.6	223.5
ALD-8	221	4.0	220	2.5	232	1.00	19.6	464.0	194.5
ALD-4	223	2.0	220	2.4	238	0.99	13.1	396.0	119.4
ALD-34	219	3.8	220	4.5	238	1.00	10.1	330.0	97.5
ALD-19	218	2.2	220	2.5	199	1.01	10.9	340.0	101.2
ALD-2	220	4.1	220	2.7	196	1.00	16.9	373.6	160.4
ALD-27	228	3.5	221	2.3	295	0.97	122.3	1178.0	1305.0
ALD-38	228	3.5	222	2.0	271	0.98	15.6	409.0	139.3
ALD-28	225	2.6	222	1.8	244	0.99	39.5	793.0	402.1
ALD-5	224	3.4	223	2.1	240	0.99	16.1	300.0	164.0
ALD-10	237	5.1	223	3.5	371	0.94	21.8	375.6	199.8
ALD-15	223	1.6	223	1.6	217	1.00	25.8	537.0	251.0
ALD-22	230	4.9	224	3.7	286	0.97	33.7	585.0	332.0
ALD-23	228	2.5	225	2.3	273.3	0.99	54.7	1090.0	496.0
ALD-24	237	7.3	225	3.1	324	0.95	11.9	191.7	117.9
ALD-25	226	2.6	226	2.0	222	1.00	21.9	503.0	191.0
ALD-26	235	1.8	233	3.3	244	0.99	16.8	380.9	161.8
ALD-27	231	4.7	233	3.0	241	1.01	17.6	391.6	177.8
ALD-28	234	3.6	234	2.0	219	1.00	18.1	534.0	184.0
ALD-29	258	6.7	248	2.3	340	0.96	20.2	326.4	215.0

Table 3b: U-Pb age data for 40 zircon samples of the dacite of Arrowhead Lake (ALD).

Sample	$^{207}Pb/^{235}U$	207/235 2σ error	$^{206}Pb/^{238}U$	206/238 2σ error	Error correlation 6/38-7/35	$^{206}Pb/^{207}Pb$	206/207 2σ error
PLB-16	0.233	0.0031	0.0331	0.00033	0.779	0.0513	0.00039
PLB-67	0.240	0.0046	0.0332	0.00041	0.716	0.0523	0.00060
PLB-15	0.238	0.0040	0.0334	0.00032	0.520	0.0519	0.00075
PLB-12	0.231	0.0026	0.0334	0.00028	0.671	0.0503	0.00047
PLB-69	0.260	0.0095	0.0334	0.00057	0.787	0.0563	0.00180
PLB-25	0.233	0.0031	0.0335	0.00042	0.748	0.0508	0.00054
PLB-63	0.242	0.0053	0.0335	0.00048	0.860	0.0521	0.00073
PLB-30	0.235	0.0038	0.0335	0.00036	0.752	0.0511	0.00060
PLB-22	0.261	0.0100	0.0335	0.00046	0.587	0.0571	0.00190
PLB-28	0.235	0.0026	0.0336	0.00034	0.543	0.0509	0.00067
PLB-11	0.239	0.0094	0.0336	0.00100	0.918	0.0515	0.00092
PLB-8	0.254	0.0037	0.0337	0.00032	0.673	0.0546	0.00061
PLB-2	0.238	0.0050	0.0337	0.00042	0.731	0.0508	0.00069
PLB-54	0.238	0.0033	0.0337	0.00039	0.876	0.0508	0.00036
PLB-6	0.237	0.0033	0.0337	0.00039	0.689	0.0511	0.00059
PLB-19	0.236	0.0050	0.0337	0.00057	0.855	0.0508	0.00059
PLB-9	0.235	0.0035	0.0338	0.00028	0.572	0.0505	0.00068
PLB-49	0.237	0.0073	0.0338	0.00083	0.697	0.0507	0.00081
PLB-56	0.244	0.0038	0.0339	0.00035	0.637	0.0524	0.00078
PLB-31	0.241	0.0036	0.0339	0.00041	0.780	0.0518	0.00053
PLB-36	0.239	0.0058	0.0339	0.00057	0.881	0.0517	0.00071
PLB-18	0.237	0.0041	0.0339	0.00035	0.277	0.0509	0.00085
PLB-3	0.244	0.0040	0.0339	0.00037	0.476	0.0521	0.00081
PLB-21	0.234	0.0055	0.0339	0.00035	0.518	0.0504	0.00095
PLB-27	0.229	0.0047	0.0339	0.00037	0.508	0.0492	0.00082
PLB-29	0.239	0.0030	0.0340	0.00029	0.570	0.0516	0.00066
PLB-24	0.235	0.0025	0.0340	0.00021	0.436	0.0502	0.00049
PLB-14	0.234	0.0038	0.0340	0.00032	0.543	0.0501	0.00073
PLB-17	0.237	0.0044	0.0340	0.00034	0.506	0.0512	0.00086
PLB-44	0.235	0.0034	0.0340	0.00033	0.564	0.0499	0.00063
PLB-45	0.248	0.0063	0.0340	0.00047	0.544	0.0531	0.00120
PLB-37	0.240	0.0043	0.0340	0.00040	0.739	0.0515	0.00056
PLB-51	0.252	0.0049	0.0341	0.00045	0.721	0.0532	0.00074

Table 4a (continued on next page): U-Pb analytical data for 58 zircon samples of the breccia of Pika Lake (PLB).

Sample	207Pb/235U	207/235 2σ error	206Pb/238U	206/238 2σ error	Error correlation 6/38-7/35	206Pb/207Pb	206/207 2σ error
PLB-33	0.237	0.0043	0.0341	0.00041	0.714	0.0505	0.00059
PLB-60	0.244	0.0034	0.0341	0.00040	0.906	0.0517	0.00031
PLB-10	0.239	0.0033	0.0342	0.00039	0.609	0.0506	0.00058
PLB-61	0.241	0.0066	0.0342	0.00039	0.507	0.0512	0.00140
PLB-43	0.242	0.0051	0.0343	0.00062	0.740	0.0508	0.00072
PLB-59	0.251	0.0063	0.0343	0.00045	0.754	0.0528	0.00083
PLB-65	0.259	0.0080	0.0344	0.00049	0.652	0.0544	0.00130
PLB-38	0.254	0.0039	0.0344	0.00028	0.580	0.0536	0.00061
PLB-1	0.241	0.0038	0.0344	0.00032	0.680	0.0511	0.00070
PLB-20	0.239	0.0041	0.0344	0.00038	0.674	0.0513	0.00069
PLB-55	0.259	0.0056	0.0344	0.00057	0.553	0.0543	0.00110
PLB-57	0.249	0.0047	0.0344	0.00034	0.322	0.0518	0.00090
PLB-66	0.238	0.0032	0.0345	0.00036	0.901	0.0502	0.00036
PLB-23	0.235	0.0032	0.0345	0.00029	0.726	0.0498	0.00053
PLB-71	0.241	0.0062	0.0345	0.00063	0.692	0.0503	0.00090
PLB-42	0.242	0.0056	0.0346	0.00048	0.526	0.0504	0.00096
PLB-32	0.242	0.0042	0.0346	0.00037	0.719	0.0508	0.00058
PLB-50	0.259	0.0046	0.0346	0.00051	0.689	0.0544	0.00061
PLB-40	0.272	0.0065	0.0346	0.00041	0.554	0.0574	0.00110
PLB-68	0.245	0.0041	0.0347	0.00052	0.728	0.0509	0.00049
PLB-47	0.255	0.0037	0.0350	0.00039	0.382	0.0528	0.00088
PLB-34	0.256	0.0050	0.0351	0.00040	0.558	0.0529	0.00092
PLB-70	0.271	0.0048	0.0352	0.00053	0.624	0.0561	0.00086
PLB-26	0.248	0.0059	0.0354	0.00046	0.695	0.0509	0.00091
PLB-48	0.303	0.0046	0.0381	0.00034	0.073	0.0571	0.00093
PLB-5	0.368	0.0047	0.0481	0.00043	0.915	0.0553	0.00032

Table 4a (continued from previous page): U-Pb analytical data for 58 zircon samples of the breccia of Pika Lake (PLB).

Sample	Age (Ma) $^{207}Pb/^{235}U$	207/235 age 2σ error	Age (Ma) $^{206}Pb/^{238}U$	206/238 age 2σ error	Age (Ma) $^{206}Pb/^{207}Pb$	206/207 age 2σ error	concor-dance filter	Pb (ppm)	U (ppm)	Th (ppm)
PLB-16	212	2.6	210	2.1	252	18	0.99	75.6	975.0	725.0
PLB-67	219	3.8	210	2.6	296	26	0.96	19.0	393.0	164.9
PLB-15	217	3.3	212	2.0	278	33	0.98	15.2	350.0	135.1
PLB-12	211	2.1	212	1.7	206	22	1.00	15.6	426.8	144.6
PLB-69	235	7.6	212	3.5	454	69	0.90	6.1	165.4	49.5
PLB-25	212	2.5	213	2.6	230	24	1.00	22.1	512.4	209.3
PLB-63	220	4.4	213	3.0	287	32	0.97	15.6	356.0	140.7
PLB-30	215	3.2	213	2.2	244	27	0.99	33.0	689.0	310.5
PLB-22	236	8.1	213	2.9	482	72	0.90	6.5	148.2	56.1
PLB-28	214	2.1	213	2.1	234	30	0.99	20.9	374.0	194.8
PLB-11	217	7.7	213	6.4	267	39	0.98	25.7	411.0	245.0
PLB-8	229	3.0	214	2.0	395	25	0.93	53.8	683.0	485.0
PLB-2	217	4.1	214	2.6	237	33	0.99	16.1	297.3	149.4
PLB-54	217	2.7	214	2.4	234	16	0.99	62.4	1132.0	580.0
PLB-6	216	2.7	214	2.4	245	26	0.99	14.4	312.3	134.7
PLB-19	215	4.1	214	3.5	231	27	1.00	12.3	260.0	111.9
PLB-9	214	2.9	214	1.7	229	27	1.00	14.1	314.0	128.1
PLB-49	215	6.0	214	5.2	224	37	0.99	8.6	268.0	81.1
PLB-56	222	3.1	215	2.2	308	33	0.97	16.0	344.0	145.2
PLB-31	219	3.0	215	2.6	277	24	0.98	58.4	974.0	540.0
PLB-36	219	5.3	215	3.6	268	31	0.98	23.0	373.0	200.0
PLB-18	216	3.3	215	2.2	233	38	1.00	6.3	151.3	56.9
PLB-3	222	3.3	215	2.3	293	34	0.97	15.0	272.7	135.2
PLB-21	214	4.5	215	2.2	209	43	1.01	5.6	143.6	50.8
PLB-27	210	3.8	215	2.3	162	40	1.03	11.3	227.0	102.7
PLB-29	218	2.5	215	1.8	264	29	0.99	12.6	318.8	123.9
PLB-24	214	2.1	215	1.3	204	23	1.01	32.7	578.0	302.7
PLB-14	213	3.2	215	2.0	198	34	1.01	15.4	354.8	138.3
PLB-17	216	3.6	216	2.1	247	39	1.00	7.5	207.9	68.7
PLB-44	215	2.8	216	2.1	190	29	1.00	19.6	354.3	176.2
PLB-45	225	5.1	216	2.9	327	52	0.96	7.0	175.1	59.7
PLB-37	218	3.5	216	2.5	262	25	0.99	31.7	628.0	294.7
PLB-51	228	4.0	216	2.8	342	33	0.95	15.1	392.0	134.7

Table 4b (continued on next page): U-Pb age data for 58 zircon samples of the breccia of Pika Lake (PLB).

Sample	Age (Ma) $^{207}Pb/^{235}U$	207/235 age 2σ error	Age (Ma) $^{206}Pb/^{238}U$	206/238 age 2σ error	Age (Ma) $^{206}Pb/^{207}Pb$	206/207 age 2σ error	concor-dance filter	Pb (ppm)	U (ppm)	Th (ppm)
PLB-33	216	3.5	216	2.5	217	27	1.00	16.2	317.4	145.7
PLB-60	222	2.8	216	2.5	271	14	0.98	47.3	1444.0	447.0
PLB-10	217	2.7	217	2.4	222	26	1.00	16.5	374.0	147.1
PLB-61	219	5.4	217	2.4	240	62	0.99	3.3	88.8	28.8
PLB-43	220	4.2	217	3.9	239	30	0.99	9.8	234.0	87.4
PLB-59	227	5.1	218	2.8	317	35	0.96	10.7	259.2	89.8
PLB-65	233	6.4	218	3.0	382	50	0.93	31.5	677.1	271.9
PLB-38	230	3.2	218	1.7	359	27	0.95	17.4	307.5	152.3
PLB-1	219	3.1	218	2.0	242	32	0.99	9.6	275.9	83.9
PLB-20	218	3.4	218	2.4	251	31	1.00	8.3	234.3	75.8
PLB-55	234	4.5	218	3.6	377	46	0.93	12.1	213.0	105.0
PLB-57	226	3.8	218	2.1	288	35	0.97	8.1	213.7	71.2
PLB-66	217	2.6	218	2.2	205	17	1.01	83.8	1291.0	745.0
PLB-23	214	2.6	219	1.8	184	25	1.02	18.7	401.4	165.4
PLB-71	219	5.0	219	3.9	205	41	1.00	7.8	230.0	68.1
PLB-42	220	4.6	219	3.0	211	44	1.00	13.3	289.7	118.0
PLB-32	221	3.6	219	2.3	231	26	0.99	12.5	346.7	107.9
PLB-50	235	3.4	219	3.2	388	25	0.94	23.5	375.0	246.0
PLB-40	244	5.2	220	2.6	504	43	0.90	18.2	317.1	148.7
PLB-68	222	3.3	220	3.2	239	24	0.99	22.3	471.8	193.4
PLB-47	231	3.0	222	2.4	316	38	0.96	14.8	306.0	156.0
PLB-34	231	4.1	223	2.5	329	38	0.96	13.7	340.0	122.3
PLB-70	243	3.9	223	3.3	455	34	0.92	15.6	281.0	129.0
PLB-26	225	4.8	224	2.8	231	41	1.00	16.8	283.0	142.0
PLB-48	269	3.6	241	2.1	491	37	0.90	13.4	233.4	137.4
PLB-5	318	3.5	303	2.7	422	13	0.95	52.3	680.0	324.7

Table 4b (continued from previous page): U-Pb age data for 58 zircon samples of the breccia of Pika Lake (PLB).

Sample	$^{207}Pb/^{235}U$	207/235 2σ error	$^{206}Pb/^{238}U$	206/238 2σ error	Error correlation 6/38-7/35	$^{206}Pb/^{207}Pb$	206/207 2σ error
DLT-47	0.176	0.0045	0.0255	0.00047	0.826	0.0498	0.00083
DLT-7	0.193	0.0037	0.0257	0.0005	0.581	0.0540	0.00099
DLT-18	0.177	0.0030	0.0259	0.00032	0.818	0.0489	0.00042
DLT-21	0.180	0.0033	0.0263	0.00048	0.832	0.0486	0.00057
DLT-2	0.179	0.0029	0.0264	0.0003	0.913	0.0490	0.00029
DLT-20	0.185	0.0033	0.0265	0.00029	0.681	0.0502	0.00059
DLT-32	0.182	0.0040	0.0265	0.00046	0.893	0.0491	0.00049
DLT-17	0.184	0.0057	0.0265	0.00062	0.709	0.0499	0.00071
DLT-29	0.188	0.0045	0.0266	0.00042	0.784	0.0500	0.00075
DLT-23	0.182	0.0057	0.0267	0.00059	0.857	0.0488	0.00077
DLT-28	0.192	0.0096	0.0268	0.0006	0.414	0.0503	0.00260
DLT-42	0.184	0.0042	0.0268	0.00047	0.863	0.0501	0.00067
DLT-6	0.189	0.0050	0.0268	0.00047	0.605	0.0510	0.00090
DLT-35	0.183	0.0031	0.0268	0.00037	0.914	0.0494	0.00037
DLT-8	0.183	0.0039	0.0268	0.00062	0.790	0.0495	0.00083
DLT-31	0.181	0.0033	0.0268	0.00038	0.741	0.0491	0.00065
DLT-48	0.187	0.0039	0.0269	0.00057	0.816	0.0501	0.00070
DLT-45	0.195	0.0043	0.0269	0.00053	0.811	0.0527	0.00072
DLT-15	0.186	0.0032	0.0269	0.00027	0.792	0.0495	0.00066
DLT-27	0.185	0.0039	0.0270	0.00041	0.599	0.0495	0.00073
DLT-33	0.187	0.0031	0.0270	0.00041	0.799	0.0497	0.00047
DLT-49	0.187	0.0038	0.0270	0.00049	0.835	0.0500	0.00065
DLT-1	0.189	0.0038	0.0271	0.00031	0.805	0.0506	0.00064
DLT-12	0.185	0.0035	0.0271	0.00041	0.741	0.0492	0.00085
DLT-41	0.189	0.0061	0.0271	0.00078	0.765	0.0498	0.00097
DLT-46	0.193	0.0038	0.0272	0.00047	0.958	0.0513	0.00028
DLT-5	0.184	0.0034	0.0272	0.00034	0.486	0.0494	0.00079
DLT-22	0.183	0.0023	0.0272	0.00039	0.869	0.0486	0.00035
DLT-14	0.188	0.0026	0.0273	0.00043	0.759	0.0499	0.00043

Table 5a (continued on next page): U-Pb analytical data for 44 zircon samples of the tuff of Deer Lakes (DLT).

Sample	$^{207}Pb/^{235}U$	207/235 2σ error	$^{206}Pb/^{238}U$	206/238 2σ error	Error correlation 6/38-7/35	$^{206}Pb/^{207}Pb$	206/207 2σ error
DLT-38	0.184	0.0031	0.0273	0.00043	0.786	0.0488	0.00048
DLT-40	0.189	0.0034	0.0273	0.0005	0.948	0.0502	0.00035
DLT-11	0.182	0.0034	0.0273	0.00036	0.723	0.0484	0.00070
DLT-44	0.185	0.0052	0.0273	0.0006	0.740	0.0494	0.00080
DLT-4	0.197	0.0050	0.0274	0.0004	0.832	0.0520	0.00085
DLT-3	0.186	0.0040	0.0274	0.00034	0.733	0.0497	0.00070
DLT-24	0.187	0.0070	0.0274	0.0007	0.693	0.0500	0.00120
DLT-43	0.186	0.0043	0.0275	0.00046	0.794	0.0493	0.00070
DLT-30	0.191	0.0041	0.0277	0.00047	0.873	0.0494	0.00063
DLT-34	0.192	0.0050	0.0278	0.00051	0.826	0.0508	0.00097
DLT-19	0.215	0.0034	0.0280	0.00034	0.407	0.0550	0.00084
DLT-10	0.192	0.0050	0.0282	0.00056	0.849	0.0497	0.00071
DLT-26	0.190	0.0055	0.0282	0.00065	0.962	0.0490	0.00039
DLT-36	0.198	0.0078	0.0284	0.00076	0.840	0.0510	0.00110
DLT-16	0.197	0.0034	0.0285	0.00031	0.495	0.0501	0.00074
DLT-25	0.247	0.0067	0.0354	0.00068	0.885	0.0505	0.00061

Table 5a (continued from previous page): U-Pb analytical data for 44 zircon samples of the tuff of Deer Lakes (DLT).

Sample	Age (Ma) $^{207}Pb/^{235}U$	207/235 age 2σ error	Age (Ma) $^{206}Pb/^{238}U$	206/238 age 2σ error	Age (Ma) $^{206}Pb/^{207}Pb$	206/207 age 2σ error	concor-dance filter	Pb (ppm)	U (ppm)	Th (ppm)
DLT-47	165	3.9	162	2.9	181	39	0.99	14.4	306.0	165.9
DLT-7	179	3.2	164	3.1	368	41	0.91	35.5	691.0	377.9
DLT-18	165	2.6	165	2.0	141	20	1.00	100.9	826.0	1349.0
DLT-21	168	2.8	167	3.0	128	27	1.00	42.2	575.0	555.0
DLT-2	167	2.5	168	1.9	145	14	1.00	82.7	1395	991.0
DLT-20	172	2.8	168	1.8	201	27	0.98	73.3	947.0	862.0
DLT-32	170	3.5	169	2.9	151	24	0.99	35.4	413.0	422.0
DLT-17	172	4.9	169	3.9	188	32	0.98	32.2	586.0	427.8
DLT-29	175	3.8	170	2.6	191	35	0.97	30.4	420.0	372.0
DLT-23	170	4.8	170	3.7	137	37	1.00	28.6	311.0	337.0
DLT-28	178	8.2	170	3.8	180	110	0.96	1.4	26.4	16.0
DLT-42	171	3.6	170	3.0	197	31	0.99	15.0	274.7	178.4
DLT-6	176	4.2	170	3.0	235	39	0.91	42.3	793.0	459.0
DLT-35	171	2.7	170	2.3	168	18	1.00	43.4	848.0	517.0
DLT-8	170	3.4	171	3.9	167	39	1.00	31.3	335.0	355.0
DLT-31	169	2.8	171	2.4	150	31	1.01	40.1	521.0	479.3
DLT-48	174	3.4	171	3.6	198	33	0.98	21.0	294.0	239.0
DLT-45	181	3.7	171	3.3	315	31	0.95	63.8	988.0	714.0
DLT-15	173	2.8	171	1.7	167	31	0.99	21.5	355.8	251.6
DLT-27	172	3.3	172	2.6	168	34	1.00	13.4	306.7	158.6
DLT-33	174	2.8	172	2.6	181	22	0.99	33.6	444.0	392.0
DLT-49	174	3.2	172	3.1	197	29	0.99	24.8	360.0	288.0
DLT-1	176	3.2	172	1.9	222	29	0.98	19.1	336.3	214.4
DLT-12	173	3.0	172	2.5	154	40	1.00	10.0	151.6	106.6
DLT-41	175	5.2	173	4.9	184	45	0.98	17.2	261.0	209.0
DLT-46	179	3.3	173	3.0	253	12	0.96	101.3	2458	1201
DLT-5	172	2.9	173	2.1	164	37	1.01	25.3	369.2	288.4
DLT-22	170	2.0	173	2.4	126	17	1.02	133.7	1406	1627
DLT-14	175	2.3	173	2.7	187	20	0.99	25.1	730.0	271.0

Table 5b (continued on next page): U-Pb age data for 44 zircon samples of the tuff of Deer Lakes (DLT).

Sample	Age (Ma) $^{207}Pb/^{235}U$	207/235 age 2σ error	Age (Ma) $^{206}Pb/^{238}U$	206/238 age 2σ error	Age (Ma) $^{206}Pb/^{207}Pb$	206/207 age 2σ error	concor-dance filter	Pb (ppm)	U (ppm)	Th (ppm)
DLT-38	172	2.6	174	2.7	138	23	1.01	38.0	507.0	437.0
DLT-40	176	2.9	174	3.1	201	16	0.99	77.3	1805.0	876.0
DLT-11	170	2.9	174	2.3	118	34	1.03	13.2	313.7	145.5
DLT-44	172	4.4	174	3.8	163	37	1.01	30.2	493.0	348.0
DLT-4	182	4.2	174	2.5	282	37	0.95	22.7	309.8	248.0
DLT-3	173	3.4	174	2.2	179	33	1.01	40.8	391.0	457.0
DLT-24	174	6.0	174	4.4	190	53	1.00	15.6	188.0	186.0
DLT-43	173	3.7	175	2.9	158	34	1.01	23.1	399.7	254.4
DLT-30	178	3.5	176	3.0	167	30	0.99	17.3	359.0	189.3
DLT-34	178	4.3	177	3.2	226	43	0.99	58.8	852.0	710.0
DLT-19	198	2.8	178	2.1	417	37	0.90	49.6	955.0	564.0
DLT-10	178	4.3	179	3.5	183	34	1.00	37.5	448.0	394.0
DLT-26	177	4.4	179	4.1	146	19	1.01	39.2	592.0	435.0
DLT-36	184	6.6	181	4.8	243	52	0.98	19.5	238.8	229.0
DLT-16	183	2.9	181	2.0	196	33	0.99	56.9	815.0	620.0
DLT-25	224	5.5	224	4.3	223	27	1.00	21.0	410.0	185.0

Table 5b (continued from previous page): U-Pb age data for 44 zircon samples of the tuff of Deer Lakes (DLT).

Sample	$^{207}Pb/^{235}U$	207/235 2σ error	$^{206}Pb/^{238}U$	206/238 2σ error	Error correlation 7/35 vs 6/38	$^{207}Pb/^{206}Pb$	206/207 2σ error	Error correlation 6/38 vs 6/7
PLR-10	0.104	0.0041	0.0151	0.00024	0.885	0.0499	0.0014	-0.745
PLR-1	0.106	0.0027	0.0155	0.00018	0.416	0.0494	0.0011	0.037
PLR-39	0.108	0.0024	0.0155	0.00023	0.418	0.0508	0.0013	0.174
PLR-38	0.102	0.0038	0.0156	0.00019	0.621	0.0472	0.0014	-0.398
PLR-35	0.103	0.0023	0.0156	0.00019	0.565	0.0470	0.0010	0.111
PLR-28	0.103	0.0024	0.0156	0.00026	0.312	0.0479	0.0013	0.319
PLR-17	0.106	0.0041	0.0157	0.00022	0.229	0.0491	0.0018	0.140
PLR-31	0.104	0.0022	0.0157	0.00019	0.375	0.0478	0.0011	0.126
PLR-8	0.103	0.0033	0.0157	0.00026	0.542	0.0478	0.0015	0.008
PLR-32	0.108	0.0046	0.0157	0.00019	0.261	0.0494	0.0021	0.206
PLR-6	0.106	0.0020	0.0157	0.00016	0.209	0.0491	0.0009	0.263
PLR-26	0.105	0.0029	0.0158	0.00011	0.432	0.0479	0.0011	-0.187
PLR-3	0.115	0.0034	0.0158	0.00011	0.616	0.0528	0.0014	-0.446
PLR-27	0.114	0.0060	0.0158	0.00015	0.654	0.0522	0.0025	-0.577
PLR-18	0.106	0.0023	0.0158	0.00024	0.369	0.0483	0.0009	0.315
PLR-15	0.107	0.0034	0.0158	0.00016	0.095	0.0484	0.0012	0.234
PLR-21	0.110	0.0031	0.0158	0.00022	0.674	0.0503	0.0010	-0.212
PLR-20	0.108	0.0020	0.0158	0.00022	0.622	0.0499	0.0013	-0.104
PLR-29	0.112	0.0056	0.0158	0.00029	-0.015	0.0493	0.0015	0.355
PLR-9	0.104	0.0032	0.0159	0.00017	0.563	0.0477	0.0012	-0.218
PLR-2	0.101	0.0025	0.0159	0.00036	0.579	0.0462	0.0010	0.411
PLR-37	0.105	0.0030	0.0159	0.00021	0.606	0.0476	0.0011	-0.165
PLR-16	0.103	0.0045	0.0159	0.00019	0.457	0.0471	0.0019	-0.165
PLR-11	0.108	0.0018	0.0160	0.00019	0.330	0.0492	0.0013	0.272
PLR-23	0.106	0.0062	0.0160	0.00044	0.474	0.0484	0.0025	0.107
PLR-12	0.112	0.0057	0.0161	0.00032	0.629	0.0503	0.0015	-0.358
PLR-40	0.107	0.0038	0.0162	0.00031	0.695	0.0466	0.0014	-0.325
PLR-5	0.121	0.0065	0.0169	0.00027	-0.322	0.0518	0.0032	0.570

Table 6a: U-Pb analytical data for 27 zircon samples of the rhyolite of Purple Lake (PLR).

Sample	Age (Ma) $^{207}Pb/^{235}U$	207/235 age 2σ error	Age (Ma) $^{206}Pb/^{238}U$	206/238 age 2σ error	Age (Ma) $^{206}Pb/^{207}Pb$	concor-dance filter	Pb (ppm)	U (ppm)	Th (ppm)
PLR-10	100	3.8	96	1.5	186	0.96	7.4	277.0	157.3
PLR-1	102	2.5	99	1.1	166	0.97	7.9	201.0	173.0
PLR-39	104	2.2	99	1.4	230	0.95	4.0	121.6	82.7
PLR-38	99	3.5	100	1.2	63	1.01	7.4	191.8	153.2
PLR-35	100	2.1	100	1.2	53	1.00	11.2	248.7	239.4
PLR-28	99	2.2	100	1.7	96	1.01	14.9	265.1	320.0
PLR-17	102	3.8	100	1.4	151	0.98	8.1	190.9	174.4
PLR-31	101	2.0	100	1.2	88	1.00	11.9	242.7	258.7
PLR-8	99	3.1	100	1.7	88	1.01	16.9	320.0	364.0
PLR-32	104	4.2	100	1.2	162	0.97	5.9	134.0	127.0
PLR-6	103	1.8	101	1.0	149	0.98	11.0	257.5	249.0
PLR-26	101	2.6	101	0.7	97	1.00	11.2	256.9	242.0
PLR-3	111	3.1	101	0.7	315	0.91	19.1	367.6	402.3
PLR-27	110	5.5	101	1.0	280	0.92	13.8	247.2	284.0
PLR-18	102	2.2	101	1.5	110	0.99	15.4	298.6	312.1
PLR-15	103	3.1	101	1.0	115	0.98	9.3	204.5	194.0
PLR-21	106	2.8	101	1.4	207	0.95	13.0	253.9	266.4
PLR-20	104	1.8	101	1.4	187	0.97	9.8	218.8	209.1
PLR-29	108	5.1	101	1.8	196	0.94	2.0	71.6	40.9
PLR-9	101	3.0	102	1.1	85	1.01	8.5	204.3	177.3
PLR-2	98	2.3	102	2.3	17	1.04	10.1	214.3	210.6
PLR-37	101	2.7	102	1.3	81	1.01	8.5	179.1	169.8
PLR-16	99	4.2	102	1.2	63	1.03	2.0	77.5	42.1
PLR-11	104	1.7	102	1.2	155	0.98	11.8	234.9	246.7
PLR-23	102	5.7	102	2.8	120	1.00	3.7	94.0	77.0
PLR-12	108	5.2	103	2.0	204	0.95	7.1	150.0	150.0
PLR-40	103	3.5	104	2.0	38	1.00	8.9	186.0	179.0
PLR-5	116	5.9	108	1.7	260	0.93	2.4	61.4	41.6

Table 6b: U-Pb age data for 27 zircon samples of the rhyolite of Purple Lake (PLR).

Sample	^{207}Pb / ^{235}U	207/235 2σ error	^{206}Pb / ^{238}U	206/238 2σ error	Error Correlation 6/38-7/35	^{206}Pb / ^{207}Pb	206/207 2σ error
MCA-2	0.103	0.0034	0.0154	0.00023	0.569	0.0477	0.00120
MCA-12	0.103	0.0040	0.0155	0.00044	0.936	0.0488	0.00062
MCA-15	0.103	0.0043	0.0158	0.00036	0.662	0.0472	0.00190
MCA-13	0.102	0.0046	0.0162	0.00043	0.629	0.0461	0.00160
MCA-11	0.113	0.0039	0.0166	0.00036	0.839	0.0496	0.00079
MCA-1	0.240	0.0049	0.0312	0.00062	0.856	0.0558	0.00047
MCA-14	0.223	0.0052	0.0318	0.00079	0.888	0.0504	0.00069
MCA-7	0.231	0.0030	0.0331	0.00035	0.475	0.0508	0.00072
MCA-3	0.228	0.0043	0.0331	0.00051	0.901	0.0503	0.00040
MCA-8	0.230	0.0046	0.0332	0.00053	0.627	0.0507	0.00085
MCA-9	0.229	0.0043	0.0338	0.00046	0.488	0.0495	0.00087
MCA-6	0.249	0.0050	0.0341	0.00050	0.694	0.0525	0.00074
MCA-10	0.252	0.0065	0.0359	0.00091	0.990	0.0506	0.00042
MCA-4	4.252	0.0710	0.2963	0.00420	0.942	0.1042	0.00056

Table 7a: U-Pb analytical data for 14 zircon samples of the andesite of Mammoth Crest (MCA).

Sample	Age (Ma) ^{207}Pb / ^{235}U	207/235 age 2σ error	Age (Ma) ^{206}Pb / ^{238}U	206/238 age 2σ error	Age (Ma) ^{206}Pb / ^{207}Pb	206/207 age 2σ error	concor-dance filter	Pb (ppm)	U (ppm)	Th (ppm)
MCA-2	99	3.2	99	1.5	88	54	1.00	8.9	195.7	193.7
MCA-12	100	3.7	99	2.8	104	5.8	0.99	14.7	486.0	347.0
MCA-15	99	4.0	101	2.3	108	2.8	1.02	5.3	131.3	108.2
MCA-13	99	4.3	103	2.7	106	4.6	1.05	3.4	99.1	70.5
MCA-11	108	3.6	106	2.3	100	2.3	0.98	19.3	452.0	422.0
MCA-1	218	4.0	198	3.9	443	19	0.91	74.6	2030.0	743.0
MCA-14	205	4.3	202	4.9	203	6.1	0.99	11.8	285.0	128.3
MCA-7	211	2.5	210	2.2	227	33	0.99	16.5	288.4	168.1
MCA-3	208	3.5	210	3.2	209	19	1.01	43.3	744.0	440.0
MCA-8	210	3.8	211	3.3	225	39	1.00	10.6	186.0	106.6
MCA-9	209	3.5	214	2.9	171	40	1.02	8.2	224.6	77.4
MCA-6	226	4.1	216	3.1	305	32	0.96	21.9	416.0	208.6
MCA-10	228	5.3	228	5.6	227	6.7	1.00	37.0	1016.0	375.0
MCA-4	1684	14.0	1673	21.0	1700	9.8	0.99	88.0	264.3	104.5

Table 7b: U-Pb age data for 14 zircon samples of the andesite of Mammoth Crest (MCA).

APPENDIX B

	MRB	ALD	PLB	DLT	MCA	PCR
SiO_2 (wt.%)	48.64	68.45	50.06	74.13	53.37	74.03
TiO_2 (wt.%)	0.45	0.42	1.09	0.23	0.8	0.17
Al_2O_3 (wt.%)	28.6	16.31	20.94	13.53	17.59	14.37
Fe_2O_3* (wt.%)	3.88	4.03	9.77	1.76	9.54	1.08
MnO (wt.%)	0.22	0.11	0.11	0.03	0.19	0.06
MgO (wt.%)	2.05	1.04	2.7	0.37	4.66	0.25
CaO (wt.%)	1.08	1.7	6.24	0.53	8.03	0.93
Na_2O (wt.%)	0.3	3.11	4.72	4.2	3.87	4.13
K_2O (wt.%)	10.28	3.04	2.83	4.6	0.97	4.06
P_2O_5 (wt.%)	0.13	0.11	0.38	0.06	0.21	0.05
LOI (wt.%)	3.93	1.47	1	0.41	0.6	0.66
Sum	95.63	98.32	98.84	99.44	99.23	99.13

Table 8: Analytical data for bulk-rock major element oxide geochemistry of Mount Morrison samples. Unit abbreviations: ALD = dacite of Arrowhead Lake, DLT = tuff of Deer Lakes, PLR = rhyolite of Purple Lake, MCA = andesite of Mammoth Crest, PLB = breccia of Pika Lake, MRB = breccia of Mammoth Rock.

	MRB	ALD	PLB	DLT	PLR	MCA
Sc (ppm)	6.57	9.03	29.47	3.90	2.64	30.06
σ	1.23%	3.02%	0.60%	12.42%	5.16%	4.05%
V (ppm)	46.69	68.23	319.50	18.39	2.90	237.72
σ	2.59%	0.67%	1.03%	2.73%	5.48%	0.74%
Cr (ppm)	1.042	2.269	7.348	1.622	1.709	27.643
σ	4.31%	4.98%	4.97%	9.71%	2.66%	0.44%
Co (ppm)	4.58	13.75	22.37	10.25	9.16	29.65
σ	1.07%	1.94%	1.08%	3.69%	2.27%	0.99%
Ni (ppm)	1.177	1.713	11.009	1.102	0.868	17.586
σ	8.46%	3.36%	0.80%	13.88%	6.78%	1.01%
Rb (ppm)	495.5	144.1	165.9	147.6	117.3	28.7
σ	0.92%	0.74%	1.19%	1.16%	1.15%	1.33%
Sr (ppm)	135.2	282.3	421.6	147.6	220.7	551.2
σ	0.46%	1.39%	0.74%	0.94%	1.03%	0.85%
Y (ppm)	21.78	17.16	21.69	16.61	13.70	20.35
σ	0.43%	1.02%	0.86%	0.32%	1.81%	2.60%
Zr (ppm)	266.1	168.6	75.0	128.1	157.8	76.6
σ	0.55%	1.57%	0.92%	1.74%	0.98%	2.26%
Nb (ppm)	17.08	11.51	7.18	13.85	15.21	5.63
σ	1.36%	0.79%	1.50%	3.02%	1.97%	0.86%
Cs (ppm)	13.32	14.85	46.56	4.86	6.61	10.66
σ	1.13%	1.81%	2.03%	3.48%	1.00%	0.75%
Ba (ppm)	3122.1	1120.1	624.9	948.1	1471.0	611.2
σ	0.64%	1.11%	1.72%	2.22%	1.74%	1.32%
La (ppm)	51.43	27.12	18.22	32.02	34.33	15.93
σ	0.83%	1.09%	2.40%	0.80%	0.88%	1.23%
Ce (ppm)	88.96	49.37	39.39	59.67	65.72	31.86
σ	0.21%	0.76%	1.72%	0.48%	0.30%	0.91%
Pr (ppm)	8.797	5.480	5.319	6.006	6.970	4.185
σ	0.30%	0.65%	2.25%	1.15%	0.80%	2.59%

Table 9 (continued on next page): Analytical data for bulk-rock trace element geochemistry of Jurassic and Cretaceous samples. Unit abbreviations: ALD = dacite of Arrowhead Lake, DLT = tuff of Deer Lakes, PLR = rhyolite of Purple Lake, MCA = andesite of Mammoth Crest, PLB = breccia of Pika Lake, MRB = breccia of Mammoth Rock.

	MRB	ALD	PLB	DLT	PLR	MCA
Nd (ppm)	28.39	19.20	23.06	19.07	23.06	17.86
σ	0.78%	2.43%	1.55%	0.17%	0.90%	1.73%
Sm (ppm)	4.559	3.487	5.033	3.295	3.850	3.952
σ	2.15%	1.76%	0.89%	0.78%	3.78%	1.08%
Eu (ppm)	1.154	0.930	1.312	0.594	0.803	1.171
σ	1.83%	2.32%	1.64%	1.82%	2.05%	1.29%
Gd (ppm)	3.856	2.984	4.778	2.682	3.003	3.996
σ	0.25%	2.76%	1.18%	2.73%	0.78%	4.28%
Tb (ppm)	0.555	0.448	0.671	0.416	0.415	0.587
σ	2.03%	1.25%	2.01%	1.73%	4.13%	2.68%
Dy (ppm)	3.282	2.721	3.990	2.628	2.225	3.513
σ	2.34%	2.46%	2.07%	1.67%	2.27%	2.27%
Ho (ppm)	0.689	0.567	0.799	0.551	0.429	0.720
σ	2.80%	0.97%	1.37%	1.89%	2.53%	2.48%
Er (ppm)	2.097	1.743	2.281	1.650	1.233	2.071
σ	1.05%	1.94%	2.52%	2.00%	0.58%	1.36%
Tm (ppm)	0.355	0.277	0.340	0.264	0.189	0.302
σ	2.23%	1.42%	4.06%	1.99%	2.86%	1.94%
Yb (ppm)	2.630	1.952	2.304	1.921	1.364	2.008
σ	1.64%	2.36%	3.31%	0.61%	3.18%	0.78%
Lu (ppm)	0.424	0.325	0.346	0.290	0.212	0.308
σ	2.75%	1.85%	3.56%	2.94%	2.94%	1.74%
Hf (ppm)	6.614	4.435	2.213	3.816	4.422	2.212
σ	0.99%	0.96%	1.64%	4.03%	0.91%	2.32%
Ta (ppm)	1.562	0.965	0.404	1.256	1.104	0.386
σ	1.12%	1.02%	2.41%	1.02%	1.25%	5.50%
Pb (ppm)	30.66	12.24	24.63	12.49	24.76	17.68
σ	1.56%	2.07%	1.04%	1.03%	0.93%	0.24%
Th (ppm)	21.05	12.01	3.68	19.21	10.43	4.77
σ	1.09%	0.19%	1.23%	0.67%	1.41%	2.26%
U (ppm)	6.956	3.566	1.068	2.414	2.677	1.340
σ	0.76%	1.94%	0.56%	0.99%	2.10%	1.71%

Table 9 (continued from previous page): Analytical data for bulk-rock trace element geochemistry of Jurassic and Cretaceous samples. Unit abbreviations: ALD = dacite of Arrowhead Lake, DLT = tuff of Deer Lakes, PLR = rhyolite of Purple Lake, MCA = andesite of Mammoth Crest, PLB = breccia of Pika Lake, MRB = breccia of Mammoth Rock.